

**Pressure Drop, Heat Transfer, Critical Heat Flux,
and Flow Stability of Two-Phase Flow Boiling
of Water and Ethylene Glycol/Water Mixtures –
Final Report for Project “Efficient Cooling
in Engines with Nucleate Boiling”**

Energy Systems Division

About Argonne National Laboratory

Argonne is a U.S. Department of Energy laboratory managed by UChicago Argonne, LLC under contract DE-AC02-06CH11357. The Laboratory's main facility is outside Chicago, at 9700 South Cass Avenue, Argonne, Illinois 60439. For information about Argonne and its pioneering science and technology programs, see www.anl.gov.

Availability of This Report

This report is available, at no cost, at <http://www.osti.gov/bridge>. It is also available on paper to the U.S. Department of Energy and its contractors, for a processing fee, from:

U.S. Department of Energy

Office of Scientific and Technical Information

P.O. Box 62

Oak Ridge, TN 37831-0062

phone (865) 576-8401

fax (865) 576-5728

reports@adonis.osti.gov

Disclaimer

This report was prepared as an account of work sponsored by an agency of the United States Government. Neither the United States Government nor any agency thereof, nor UChicago Argonne, LLC, nor any of their employees or officers, makes any warranty, express or implied, or assumes any legal liability or responsibility for the accuracy, completeness, or usefulness of any information, apparatus, product, or process disclosed, or represents that its use would not infringe privately owned rights. Reference herein to any specific commercial product, process, or service by trade name, trademark, manufacturer, or otherwise, does not necessarily constitute or imply its endorsement, recommendation, or favoring by the United States Government or any agency thereof. The views and opinions of document authors expressed herein do not necessarily state or reflect those of the United States Government or any agency thereof, Argonne National Laboratory, or UChicago Argonne, LLC.

**Pressure Drop, Heat Transfer, Critical Heat Flux,
and Flow Stability of Two-Phase Flow Boiling
of Water and Ethylene Glycol/Water Mixtures –
Final Report for Project “Efficient Cooling
in Engines with Nucleate Boiling”**

by
W. Yu, D.M. France, and J.L. Routbort
Energy Systems Division, Argonne National Laboratory

December 2010

Table of Contents

Nomenclature	4
Abstract	7
1. Introduction.....	7
2. Experimental Apparatus.....	9
2.1. Description of Two-Phase Loop	9
2.2. Experimental Test Section	10
2.3. Instrumentation Calibration	11
2.4. Data Acquisition	11
2.5. Heat Loss Calibration	13
2.6. Single-Phase Heat Transfer Verification	14
3. Boiling Data Reduction.....	17
3.1. Ideal Mixture Assumption	17
3.2. Ethylene Glycol Molar Concentration and Mass Concentration	18
3.3. Vapor Mass Quality	19
3.4. Local Fluid Boiling Temperature.....	19
3.5. Local Boiling Heat Transfer Coefficient	20
3.6. Iteration Calculation Procedure	21
3.7. Fluid Thermophysical Properties	22
4. Boiling Experimental Results – Boiling Curve	24
4.1. Ranges of Experimental Parameters	24
4.2. Effect of System Pressure on Boiling Curve	24
4.3. Effect of Test Section Inlet Temperature on Boiling Curve	25
4.4. Effect of Ethylene Glycol Volume Concentration on Boiling Curve	26
4.5. Effect of Flow Direction on Boiling Curve	27
4.6. Effect of Mass Flux on Boiling Curve.....	28
4.6.1. Water Boiling – Three Flow-Boiling Regions.....	28
4.6.2. Ethylene Glycol/Water Mixture Boiling.....	29
4.6.3. Criteria for Nucleation-dominant Boiling.....	31
5. Boiling Experimental Results – Pressure Drop	32
5.1. Predictive Models for Two-Phase Pressure Drop in the Literature	32
5.1.1. Two-Phase Parameters.....	32
5.1.2. Two-Phase Pressure Drops	32
5.1.3. Slip Ratio Models	36
5.2. Effect of Slip Ratio on Experimental Two-Phase Friction Multiplier.....	36
5.3. Effect of Vapor Mass Quality on Experimental Two-Phase Friction Multiplier.....	38
5.4. Correlation of Experimental Two-Phase Friction Multiplier	39
6. Boiling Experimental Results – Heat Transfer Coefficient	42

6.1.	Predictive Models for Boiling Heat Transfer Coefficient in the Literature.....	42
6.2.	Boiling Heat Transfer Coefficient Comparison.....	47
6.2.1.	Water Boiling.....	47
6.2.2.	Ethylene Glycol/Water Mixture Boiling.....	52
6.3.	Correlation of Experimental Boiling Heat Transfer Coefficient	56
6.3.1.	General Considerations.....	56
6.3.2.	Equation for All Experimental Data	57
6.3.3.	Equation for Water Boiling.....	60
6.3.4.	Equation for Ethylene Glycol/Water Mixture Boiling.....	61
7.	Boiling Experimental Results – Critical Heat Flux and Flow Stability.....	64
7.1.	Predictive Models for Critical Heat Flux in the Literature	64
7.2.	Critical Heat Flux of Water Boiling.....	65
7.2.1.	Effect of Mass Flux on Critical Heat Flux.....	65
7.2.2.	Critical Heat Flux Comparison	66
7.3.	Flow Stability of Ethylene Glycol/Water Mixture Boiling.....	67
8.	Summary.....	69
	References.....	72

Nomenclature

A	area, m^2
Bo	boiling number, $Bo = \dot{q}'' / (Gi_{fg})$
Co	convection number, $Co = [(1-x)/x]^{0.8} (\rho_v / \rho_l)^{0.5}$
C_p	specific heat, J/kgK
D	mass diffusivity, m^2/s
d_i	inside diameter, m
d_o	outside diameter, m
E	voltage drop, V
f	friction factor
F	mass concentration
Fr	Froude number, $Fr = G^2 / (gd_i \rho^2)$
g	gravitational acceleration, m/s^2
G	mass flux, kg/m^2s
h	heat transfer coefficient, W/m^2K
i	enthalpy, J/kg
I	current, A
i_{fg}	latent heat of vaporization, J/kg
k	thermal conductivity, W/mK
L	length, m
m	mass, kg
\dot{m}	mass flowrate, kg/s
M	molecular mass, u
Nu	Nusselt number, $Nu = hd_i / k$
p	pressure, Pa
p_c	critical pressure, Pa
p_r	reduced pressure, $p_r = p / p_c$
Pr	Prandtl number, $Pr = C_p \mu / k$
q	heat, J
\dot{q}	heat transfer rate, W
\dot{q}''	heat flux, W/m^2
Q	volumetric flowrate, m^3/s
\dot{q}_{loss}	heat loss rate, W
R	specific gas constant, J/kgK
R_a	wall roughness, μm
Re	Reynolds number, $Re = Gd_i / \mu$
Re_l	liquid Reynolds number, $Re_l = G(1-x)d_i / \mu_l$
S	slip ratio

Sc	Schmidt number, $Sc = \mu/(\rho D)$
T	temperature, K
T_{amb}	ambient temperature, K
T'_w	outer surface wall temperature, K
v	velocity, m/s
V	volume concentration
We	Weber number, $We = G^2 d_i / (\rho \sigma)$
x	vapor mass quality
X	Lockhart-Martinelli parameter $X = \sqrt{(dp/dL)_l / (dp/dL)_v}$
X_{ll}	Lockhart-Martinelli parameter for laminar-liquid/laminar-vapor flow
X_{lt}	Lockhart-Martinelli parameter for laminar-liquid/turbulent-vapor flow
X_{tl}	Lockhart-Martinelli parameter for turbulent-liquid/laminar-vapor flow
X_{tt}	Lockhart-Martinelli parameter for turbulent-liquid/turbulent-vapor flow
Y	molar concentration
z	axial location, m
Z	compressibility factor, $Z = 0.98 \pm 1\%$

Greek symbols

α	cross-sectional void fraction
Δp	pressure drop, Pa
Δp_a	acceleration pressure drop, Pa
Δp_f	friction pressure drop, Pa
Δp_g	gravitation pressure drop, Pa
Δp_{sat}	pressure difference, Pa, $\Delta p_{sat} = p_w - p_{sat}$
Δq	heat input to a segment, J
ΔT_{sat}	wall superheat, K, $\Delta T_{sat} = T_w - T_{sat}$
ϕ_l	two-phase multiplier, $\phi_l = \sqrt{(\Delta p_f)_{TP} / (\Delta p_f)_l}$
κ	thermal diffusivity, m^2/s , $\kappa = k / (\rho C_p)$
μ	viscosity, kg/ms
ρ	density, kg/m^3
σ	surface tension, N/m

Subscripts

<i>bubble</i>	bubble point
<i>CHF</i>	critical heat flux
<i>dew</i>	dew point
<i>EG</i>	ethylene glycol
<i>exp</i>	experimental

<i>f</i>	fluid
<i>hor</i>	horizontal
<i>in</i>	inlet
<i>l</i>	liquid
<i>out</i>	outlet
<i>sat</i>	saturation
<i>SP</i>	single phase
<i>TP</i>	two phase
<i>v</i>	vapor
<i>ver</i>	vertical
<i>w</i>	wall
<i>W</i>	water

Pressure Drop, Heat Transfer, Critical Heat Flux, and Flow Stability of Two-Phase Flow Boiling of Water and Ethylene Glycol/Water Mixtures

– Final Report for Project “Efficient Cooling in Engines with Nucleate Boiling”

Wenhua Yu, David M. France, and Jules L. Routbort

Energy Systems Division, Argonne National Laboratory, 9700 South Cass Avenue, Argonne, IL 60439, USA

Abstract

Because of its order-of-magnitude higher heat transfer rates, there is interest in using controllable two-phase nucleate boiling instead of conventional single-phase forced convection in vehicular cooling systems to remove ever increasing heat loads and to eliminate potential hot spots in engines. However, the fundamental understanding of flow boiling mechanisms of a 50/50 ethylene glycol/water mixture under engineering application conditions is still limited. In addition, it is impractical to precisely maintain the volume concentration ratio of the ethylene glycol/water mixture coolant at 50/50. Therefore, any investigation into engine coolant characteristics should include a range of volume concentration ratios around the nominal 50/50 mark. In this study, the forced convective boiling heat transfer of distilled water and ethylene glycol/water mixtures with volume concentration ratios of 40/60, 50/50, and 60/40 in a 2.98-mm-inner-diameter circular tube has been investigated in both the horizontal flow and the vertical flow. The two-phase pressure drop, the forced convective boiling heat transfer coefficient, and the critical heat flux of the test fluids were determined experimentally over a range of the mass flux, the vapor mass quality, and the inlet subcooling through a new boiling data reduction procedure that allowed the analytical calculation of the fluid boiling temperatures along the experimental test section by applying the ideal mixture assumption and the equilibrium assumption along with Raoult’s law. Based on the experimental data, predictive methods for the two-phase pressure drop, the forced convective boiling heat transfer coefficient, and the critical heat flux under engine application conditions were developed. The results summarized in this final project report provide the necessary information for designing and implementing nucleate-boiling vehicular cooling systems.

1. Introduction

Thermal management in heavy vehicles is an essential concern in view of new environmental regulations and increased power and performance requirements. Thermal management affects such areas as engine performance, fuel economy, safety, reliability, engine and component lifetime, maintenance cost and schedule, materials, and more. Consequently, efficient thermal management has become critical to the design of large class 6–8 trucks when a primary concern is to remove the heat at high rates in small cooling systems that are lightweight and that have relatively small fluid inventories.

Currently, cooling systems in heavy vehicles are designed to use a 50/50 ethylene glycol/water (EG/W) mixture in the liquid state. Most of the heat is transferred in the radiator to the heat sink ambient air. The amount of the heat rejected in the radiator is limited by the current

radiator designs that are essentially optimal. In addition, precision cooling using the 50/50 EG/W liquid mixture is limited by the coolant liquid properties and the cooling system geometry. Because of its order-of-magnitude higher heat transfer rates, there is interest in using controllable two-phase nucleate boiling instead of conventional single-phase forced convection in vehicular cooling systems under certain conditions or in certain areas of the engine to remove ever increasing heat loads and to eliminate potential hot spots in engines [1-14].

Order-of-magnitude higher heat transfer rates can be achieved in nucleate-boiling cooling systems when compared with conventional, single-phase, forced-convective cooling systems. However, successful designs and applications of nucleate-boiling cooling systems for engine applications require that two critical phenomena, the critical heat flux (CHF) and flow instability, not be reached, by design or by circumstance. Therefore, a fundamental understanding of flow boiling mechanisms under engine application conditions is required to develop reliable and effective nucleate-boiling cooling systems. Cooling engine areas such as the head region often contain small metal masses that lead to small coolant channels. This geometry, in turn, leads to low mass flow rates that minimize pressure drops. Although significant research has been performed on the boiling heat transfer and the CHF phenomenon, the fundamental understanding of the two-phase flow and the heat transfer of a 50/50 EG/W mixture under engineering application conditions is still limited. In addition, it is impractical to precisely maintain the volume concentration ratio of the EG/W mixture coolant at 50/50. Therefore, any investigation into engine coolant characteristics should include a range of volume concentration ratios around the nominal 50/50 mark.

The objectives of this project are (a) to verify the feasibility of nucleate-boiling cooling systems; (b) to experimentally investigate the characteristics of the two-phase pressure drop, forced convective boiling heat transfer, and boiling limitation under conditions of small channels and low mass fluxes for distilled water and EG/W mixtures with volume concentration ratios of 40/60, 50/50, and 60/40 in both the horizontal flow and the vertical flow; and (c) to develop predictive methods for the two-phase pressure drop, the forced convective boiling heat transfer coefficient, and the CHF under engine application conditions.

2. Experimental Apparatus

2.1. Description of Two-Phase Loop

The experimental apparatus used in this study, a closed-loop system consisting mainly of two pumps, a hydraulic accumulator, a flowmeter set, a preheater, two similar experimental test sections (one for the horizontal flow and one for the vertical flow), and a condenser, was designed and fabricated to study the pressure drop, heat transfer, CHF, and flow stability of two-phase flow boiling of water and EG/W mixtures.

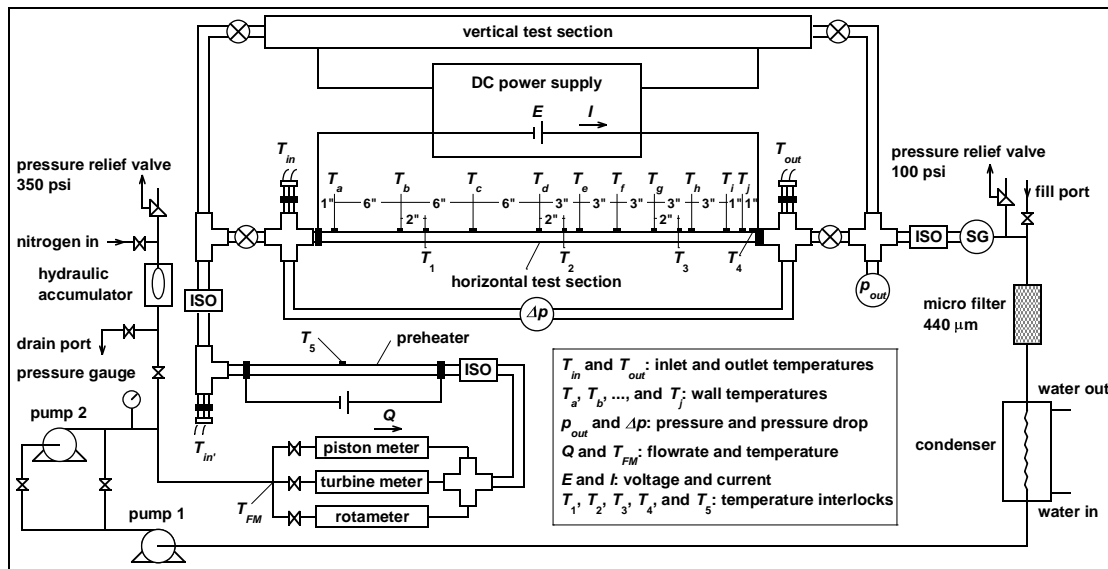


Figure 1. Schematic diagram of experimental apparatus

As shown in the schematic diagram of the experimental apparatus in Figure 1, the test fluid was pumped through the two-phase loop by two serially-arranged pumps (Micropump Corporation, Model 220-000) and was pressurized by a bladder-type hydraulic accumulator (Greer Hydraulics, Inc.) connected to a high-pressure nitrogen cylinder. The serially-arranged pumps driven by alternating current adjustable-frequency drivers (Dayton Electric Manufacturing Company, Model 1XC95) were used to minimize the flow fluctuation caused by the boiling fluid in the experimental test section. Using the alternating current adjustable-frequency drivers made it possible to fine adjust flowrates through the experimental test section. The bladder-type accumulator was used in the experimental apparatus to give a stable control of the fluid pressure at the experimental test section within the specifications by adjusting the pressure in the accumulator. The flowmeter set, including a piston-type flowmeter with a readout meter (Max Machinery, Inc., Model 213-310/Model 120-200), a turbine-type flowmeter with a readout meter (Flowdata, Inc., Model ES02SS-6FM-DL-102-00/Model MR10-1A3A), and a rotameter (Omega Engineering, Inc., Model FL-3505ST-HRV), was arranged in a parallel-flow configuration in the experimental apparatus and was chosen to cover a large range of volumetric flowrates (Q). A thermocouple probe (T_{FM}) (Omega Engineering, Inc.) just upstream from the flowmeter set provided a means to determine the density of the fluid and subsequently the mass

flowrate of the fluid. Exiting the flowmeter set, the fluid flowed through the preheater, in which the fluid temperature was raised to the desired subcooled level for a given test. The preheater, consisting of an AISI type 304 stainless steel tube with a 4.572-mm inside diameter, a 6.096-mm outside diameter, and a 500-mm resistance-heated length, was heated by passing current through its wall to generate resistance heat. A direct current power supply (Sorensen Company, Model DCR 16-625T) was used, the output power of which could be regulated from 0 to 10 kW with the maximum voltage drop and the maximum current being 16 V and 625 A, respectively. As a safety precaution for protecting the preheater from overheating, the preheater was provided with a temperature interlock. At the middle of the preheater, the wall temperature (T_s) was measured and then fed to a high-temperature limit switch (Omega Engineering, Inc., Model CN76030) that would terminate power to the preheater when a preset upper-temperature limit was reached. After passing through the preheater, the fluid entered either the horizontal or the vertical experimental test section. The experimental test section was heated, by passing current through its wall to generate resistance heat, with a direct current power supply (Electronic Measurements, Inc., Model EMHP 40-450-D-11111-0933). The output power could be regulated from 0 to 18 kW with the maximum voltage drop and the maximum current being 40 V and 450 A, respectively. The voltage drop across the experimental test section (E) was measured directly, and the current through the experimental test section (I) was determined from a measurement of the voltage drop across a shunt resistor with known resistance of 0.0001 Ω . The heat input to the experimental test section was calculated as the product of the voltage drop and the current. Electrical isolation for eliminating ground loops was provided for the preheater and the experimental test section by short high-pressure hoses, designated ISO in Figure 1. Immediately beyond the experimental test section, a flow sight glass window provided a view of the flow pattern. The two-phase fluid out from the experimental test section was condensed into the single-phase fluid in the countercurrent condenser that used laboratory water as a heat rejection fluid, and the condensate left the condenser and returned to the pumps to close the two-phase loop.

2.2. Experimental Test Section

The details of the horizontal experimental test section (the setup for the vertical experimental test section being same) are shown schematically in Figure 1 and discussed below.

The experimental test section was fabricated from a 2.9845-mm-inside-diameter (d_i) and 4.7625-mm-outside-diameter (d_o) AISI type 316 stainless steel tube with a 0.9144-m heated length (L) between the voltage taps. The in-stream bulk fluid temperatures were measured at the inlet (T_{in}) and the outlet (T_{out}) of the experimental test section with type K thermocouple probes (Omega Engineering, Inc.). A type K KMTSS-062U-6 thermocouple probe, whose very small outside diameter of 1.5748 mm allowed the test fluid passing through without significantly affecting the flow, was selected to measure the inlet bulk fluid temperature. Figure 1 also illustrates the method used to measure wall temperatures. The wall temperatures (T_a, T_b, \dots, T_j) were measured at 10 axial locations over the heated length of the experimental test section with type K thermocouple junctions (Omega Engineering, Inc.). To electrically isolate these thermocouple junctions from the experimental test section tube, a thin coat of high-temperature ceramic epoxy (Omega Engineering, Inc., Omega bond 200) was applied around the

circumference of the tube at the measurement locations. After oven curing, the thermocouple junctions coated with the same high-temperature ceramic epoxy were bonded to the thin coating on the tube. This technique allowed the thermocouple junctions to be electrically insulated from the tube with current passing through it. The outlet fluid pressure (p_{out}) and the overall pressure drop across the test section (Δp) were measured in all tests with a piezoelectric pressure transducer (Endevco Corporation, Model 8510B-500) and a differential pressure transducer with variable reluctance (Validyne Engineering Corporation, Model DP15-36 1536N1S4A), respectively. These measurements were incorporated in the data reduction to calculate the stream temperature distribution along the boiling segment of the experimental test section. As a safety precaution for protecting the experimental test section from overheating, the experimental test section was provided with four temperature interlocks. At the locations of 0.2286 m, 0.5334 m, 0.7620 m from the inlet, and near the outlet of the experimental test section, the wall temperatures () were measured and then fed to a high-temperature limit switch (Omega Engineering, Inc., Model CN76030) that would terminate power to the experimental test section when a preset upper-temperature limit was reached.

2.3. Instrumentation Calibration

All the sensors for the measurements of the flowmeter temperature, the in-stream bulk fluid temperature, the wall temperature, the fluid pressure at outlet of the experimental test section, the overall pressure drop across the experimental test section, and the volumetric flowrate through the flowmeter set were calibrated before installation.

The flowmeter thermocouple probe, the in-stream temperature probes, and the wall thermocouple junctions were calibrated over the operation range with a type K reference probe (Omega Engineering Inc., No. 703998035), which was calibrated with the NIST-traceable standard. The thermocouple calibration was accomplished using a high-temperature heat transfer fluid (MultiTherm Corporation, MultiTherm IG-2) in which the thermocouple probes and thermocouple junctions, together with the reference probe, were inserted. A system calibration, including the isolation blocks (as applicable), the multiplexor, and the computer, was performed. The estimated uncertainty in the measurements of temperatures was ± 0.2 °C. The pressure transducers were calibrated over the operation range using a precise pressure gauge (Ashcroft, Inc., Model Hiese CM-21615), which was calibrated with the NIST-traceable standard. As with the thermocouples, the pressure transducers were calibrated through the multiplexor and the computer. The estimated uncertainty in the measurements of pressures was $\pm 3\%$. The flowmeters were calibrated over the operation range using a weighing-with-stop-watch technique. The estimated uncertainty in the measurements of flowrates was $\pm 3\%$. The correction equations developed based on the calibration data were incorporated into the data acquisition program.

2.4. Data Acquisition

A data acquisition system consisting of a personal computer and a multiplexor (Hewlett-Packard Company, Model 3421A) was assembled to record outputs from all sensors. The multiplexor channels assigned to the various measured variables are identified in Table 1. A data acquisition program, including all calibration equations and engineering-unit conversions, was

written. The data acquisition system functioned in two modes. During experimental test setup, the data acquisition system provided an on-screen display of analog signals from all sensors and graphs of representative temperature and flowrate measurements as a function of time to facilitate determination of steady-state conditions. When the system reached a steady state condition at desired parameters, the data acquisition system read all sensor-output voltages of in-stream temperatures, wall temperatures, outlet pressure, pressure drop, volumetric flowrate, voltage drop, and current 30 times and averaged them in three sets of 10-data scans each. As a check on the steady state condition, the three data sets were compared for consistency before all of the scans were averaged together for future processing. The final result was a set of measurements, each an average of 30 readings, plus a confirmation of steady-state system operation during the collection of data.

Table 1. Data acquisition matrix

Variable	Card No.	MUX channel No.	Patch panel No.	Description	Type	Unit	Location z (m)
T_a	"0"-1	1	1	Test section wall temperature	K	°C	0.0254
T_b	"0"-2	2	2	Test section wall temperature	K	°C	0.1778
T_c	"0"-3	3	3	Test section wall temperature	K	°C	0.3302
T_d	"0"-4	4	4	Test section wall temperature	K	°C	0.4826
T_e	"0"-5	5	5	Test section wall temperature	K	°C	0.5588
T_f	"0"-6	6	6	Test section wall temperature	K	°C	0.6350
T_g	"0"-7	7	7	Test section wall temperature	K	°C	0.7112
T_h	"0"-8	8	8	Test section wall temperature	K	°C	0.7874
T_i	"0"-9	9	9	Test section wall temperature	K	°C	0.8636
		10	10				
T_j	"1"-1	11	11	Test section wall temperature	K	°C	0.8890
	"1"-2	12	12		K	°C	
	"1"-3	13	13		K	°C	
P_{out}	"1"-4	14	14	Test section outlet pressure		kPa	
Δp	"1"-5	15	15	Test section pressure drop		kPa	
E	"1"-6	16	16	Voltage drop across test section		V	
I	"1"-7	17	17	Current through test section		A	
Q	"1"-8	18	18	Volumetric flowrate		cc/min	
$T_{ambient}$	"1"-9	19	19	Ambient temperature	K	°C	
		20	20				
T'_{in}	"2"-1	21	21	Preheater outlet temperature	K	°C	
T_{in}	"2"-2	22	22	Test section inlet temperature	T	°C	0.0254
	"2"-3	23	23		T	°C	
	"2"-4	24	24		T	°C	
T_{out}	"2"-5	25	25	Test section outlet temperature	K	°C	0.9144
	"2"-6	26	26		K	°C	
	"2"-7	27	27		K	°C	
T_{FM}	"2"-8	28	28	Flowmeter temperature	K	°C	
	"2"-9	29	29		K	°C	

To switch for data collection between the horizontal flow and the vertical flow, an interfacial connector was fabricated. As shown in Figure 2, this switcher device established a connection between the sensor instruments and the data acquisition computer system, and allowed for easily switching between horizontal flow tests and vertical flow tests.



Figure 2. Interfacial connector

2.5. Heat Loss Calibration

Although the experimental test section was well insulated thermally from the atmosphere to minimize heat loss to the environment, the heat loss was not negligible during flow boiling heat transfer tests because of the small experimental test section, the low fluid flowrates, and the relatively high driving temperatures. Therefore, heat loss tests were performed for the experimental test section wall temperatures up to the boiling heat transfer conditions, and the heat loss was subsequently incorporated into the data reduction procedure for boiling heat transfer data. The heat loss was characterized through a special series of experiments with no fluid in the experimental test section. Power was applied to the experimental test section to bring its wall temperature to a selected level. The input power required for maintaining the wall temperature at the selected value is the heat loss rate \dot{q}_{loss}

$$\dot{q}_{loss} = EI \quad (1)$$

which is related to the difference between the experimental test section wall temperature T_w and the ambient temperature T_{amb} . By assuming a linear dependence on the driving temperature,

which was confirmed by the experimental results of the heat loss tests, the heat loss rate can be expressed approximately as

$$\dot{q}_{loss} = c(T_w - T_{amb}) \quad (2)$$

where the proportional constant c , which depends on the heat transfer coefficient and the heat transfer surface area between the experimental test section and ambient for this particular experimental apparatus, was determined from the heat loss tests. Figure 3 shows the heat loss rate per length as a function of the driving temperature for both the horizontal and the vertical experimental test sections. The test section heat loss was <5% of the applied input power to the experimental test section in all subsequent heat transfer tests.

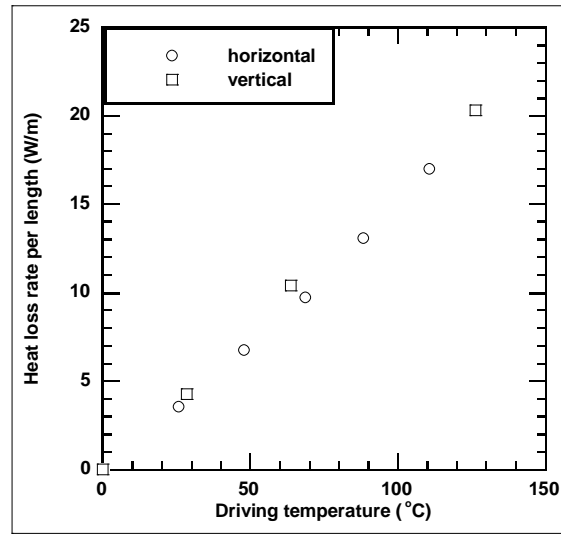


Figure 3. Heat loss calibration

2.6. Single-Phase Heat Transfer Verification

To validate the test apparatus, a series of single-phase heat transfer experiments was carried out before two-phase flow boiling experiments. The single-phase heat transfer experiments were performed at a system pressure of 120–200 kPa, sufficient to keep the test fluids in the liquid phase during heating. During the single-phase heat transfer experiments, the experimental parameters of the test fluids such as temperatures and flowrates were chosen to maintain turbulent flow conditions with their Reynolds numbers >2000. The results of the single-phase Nusselt numbers Nu for the Reynolds numbers in the range of $Re = 2250 - 13000$ and the Prandtl numbers in the range of $Pr = 2 - 18$ were compared with the well-known Gnielinski equation [15]

$$Nu = \frac{(f/8)(Re - 1000)Pr}{1 + 12.7(f/8)^{1/2}(Pr^{2/3} - 1)} \quad (3)$$

where the predicted friction factor f is defined as

$$f = (1.82 \log Re - 1.64)^{-2} \quad (4)$$

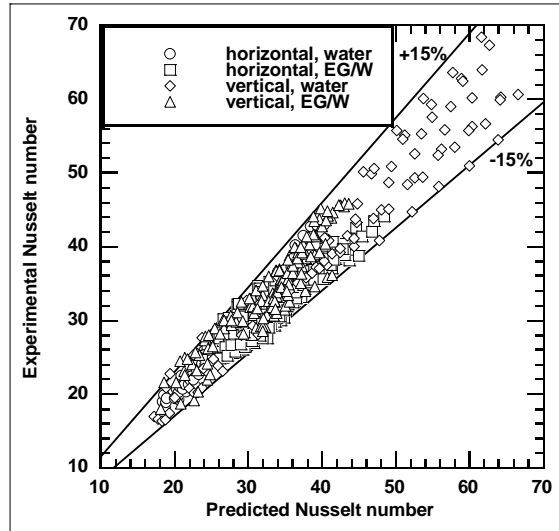


Figure 4. Nusselt number comparison

As shown in Figure 4 where the local Nusselt numbers are plotted, the experimental data are in good agreement with the predicted values from the Gnielinski equation with a mean deviation of <7%. Almost all experimental data are within $\pm 15\%$ of the predictions. The Fanning friction factors calculated from the experimental pressure drop data were compared with the standard Blasius equation [16]

$$f_{\text{Blasius}} = 0.0791 Re^{-0.25} \quad (5)$$

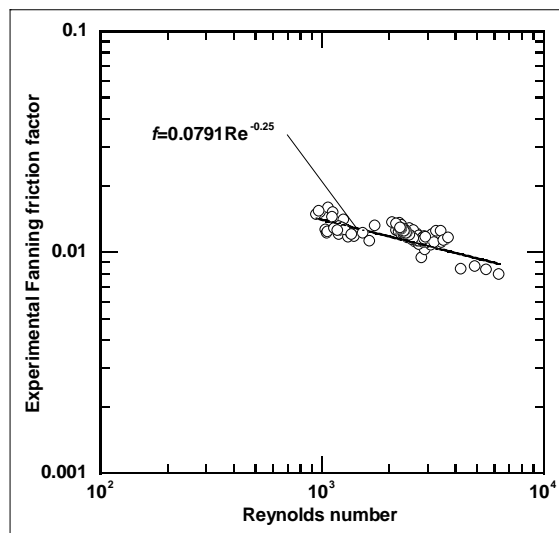


Figure 5. Fanning friction factor comparison

As shown in Figure 5, the experimental data are in good agreement with the predicted values from the Blasius equation with a mean deviation of <9%. These single-phase heat transfer coefficient and pressure-drop results serve as validation of the accuracy of the instrumentation, measurements, data acquisition, and data reduction procedures. They are an “end-to-end” final validation of the experimental apparatus.

3. Boiling Data Reduction

3.1. Ideal Mixture Assumption

EG/W mixtures are nonazeotropic mixtures. Figure 6 illustrates an example of their composition-temperature phase diagrams at a constant pressure $p = 100 \text{ kPa}$ [17]. The bubble-point line and the dew-point line divide the phase diagram into three regions: subcooled liquid, two-phase fluid, and superheated vapor. For a given EG/W mixture with water molar concentration Y_W , the boiling starts at the bubble-point temperature T_{bubble} with the water liquid molar concentration and the water vapor molar concentration $Y_{Wbubble}$ ($Y_{Wbubble} = Y_W$) and $Y_{Wvbubble}$, respectively. The mixture liquid phase becomes richer in the less-volatile-component ethylene glycol, while the mixture vapor phase becomes richer in the more-volatile-component water. As the boiling process continues, the mixture vapor mass quality gradually increases from 0 to 1, the mixture temperature increases from the bubble point T_{bubble} to the dew point T_{dew} , and the water liquid molar concentration and the water vapor molar concentration of the mixture change into Y_{Wldew} and Y_{Wvdew} ($Y_{Wvdew} = Y_W$), respectively. As evident from the phase diagram, unlike pure fluids, the mixture boiling process at a constant pressure does not occur at a constant temperature but rather over a range of temperatures from the bubble point T_{bubble} through the dew point T_{dew} , depending on the mixture vapor mass quality. This significant feature means that further information, in addition to the system pressure, is needed to calculate the boiling temperature and subsequently the heat transfer coefficient.

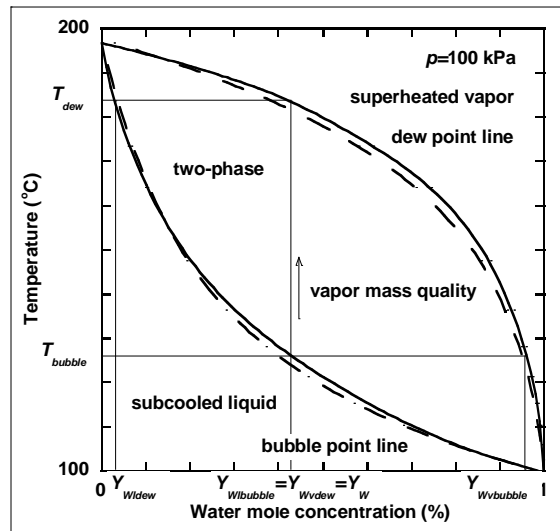


Figure 6. Ethylene glycol/water mixture phase diagram

In this study, forced convective boiling experiments were performed in a small circular tube, and boiling heat transfer data were obtained in the mixture vapor mass quality range away from the occurrence of the CHF. Consequently, the two-phase regions of bubble, slug, and annular flows were present along the experimental test section in various experiments, in which the liquid was adjacent to the heated experimental test section wall at all times. These two-phase

flow regions are relatively well mixed with small thermal gradients compared to the post-CHF mist flow region where vapor is adjacent to the wall. Therefore, for the purpose of data reduction in this study, the assumption was made that, in the thermodynamic sense, the mixture behaves ideally and is at equilibrium. In support of this assumption, Raoult's Law for ideal mixtures was used to generate a phase diagram for EG/W mixtures at a constant pressure $p = 100$ kPa. The results, plotted as dashed lines in Figure 6, show that the calculated values are very close to the data as solid lines from Chu, et al. [17] with a mean deviation of $<4.7\%$.

3.2. Ethylene Glycol Molar Concentration and Mass Concentration

By assuming an ideal mixture, the following equation applies

$$Y_v = p_v / p \quad (6)$$

where Y is the molar concentration, p is the pressure, and the subscript v indicates vapor. Raoult's law for an ideal mixture is

$$Y_l = p_v / p_{sat} \quad (7)$$

where the subscript l indicates liquid and the subscript sat indicates saturation. Further, Dalton's law of partial pressures for an ideal EG/W gas mixture may be written as

$$p = p_{EGv} + p_{Wv} \quad (8)$$

where the subscripts EG and W indicate ethylene glycol and water, respectively. By solving the above three equations, the ethylene glycol vapor molar concentration can be expressed as

$$Y_{EGv} = \frac{p_{EGsat}}{p} Y_{EGl} = \frac{p_{EGsat}}{p} \frac{p - p_{Wsat}}{p_{EGsat} - p_{Wsat}} \quad (9)$$

which can be expressed in terms of the ethylene glycol vapor mass concentration as

$$F_{EGv} = \frac{31(p_{EGsat}/p)F_{EGl}}{31 - 22(1 - p_{EGsat}/p)F_{EGl}} = \frac{31(p_{EGsat}/p)(p - p_{Wsat})}{9(p_{EGsat} - p_{Wsat}) + 22(p_{EGsat}/p)(p - p_{Wsat})} \quad (10)$$

where the ethylene glycol mass concentration F_{EG} is the ratio of the mass of the ethylene glycol to the total mass of the mixture and is a constant for a given EG/W mixture, the ethylene glycol liquid mass concentration F_{EGl} is the ratio of the mass of the ethylene glycol liquid to the mass of the liquid in the mixture, and the ethylene glycol vapor mass concentration F_{EGv} is the ratio of the mass of the ethylene glycol vapor to the mass of the vapor in the mixture. In arriving at the above equation, the following conversion was used

$$F_{EG} = \frac{Y_{EG}}{M_W/M_{EG} + (1 - M_W/M_{EG})Y_{EG}} \quad (11)$$

where M is the molecular mass.

3.3. Vapor Mass Quality

For an EG/W mixture, the species conservation of the ethylene glycol mass to the mixture gives

$$F_{EG} = (1 - x)F_{EGl} + xF_{EGv} \quad (12)$$

where the vapor mass quality x is the ratio of the mass of the vapor to the total mass in the mixture. The vapor mass quality can be obtained directly from the species conservation equation

$$x = \frac{F_{EGl} - F_{EG}}{F_{EGl} - F_{EGv}} = 1 - \frac{F_{EG} - F_{EGv}}{F_{EGl} - F_{EGv}} = 1 - \frac{[31 + 22(p/p_{EGsat} - 1)F_{EGv}](F_{EG} - F_{EGv})}{(p/p_{EGsat} - 1)(31 - 22F_{EGv})F_{EGv}} \quad (13)$$

3.4. Local Fluid Boiling Temperature

Researchers have used various approaches in determining the fluid boiling temperature along the experimental test section. Perhaps the simplest approach is to assume that the fluid boiling temperature is constant along the experimental test section and equals to the mean of the temperature at the zero vapor mass quality location and the temperature at the experimental test section outlet. Such an approach was taken by Murata and Hashizume [18] in the analysis of nonazeotropic refrigerant mixtures. However, this approach is not conducive to the determination of the local boiling heat transfer coefficients along the length of the experimental test section, as in this study. Accuracy can be increased by assuming a linear fluid temperature distribution along the experimental test section as done by Wenzel, et al. [19] for ternary mixtures. Still another approach is to utilize a fluid equation of state such as the hard sphere equation developed by Morrison and McLinden [20] and used by Ross, et al. [21] for refrigerant mixtures. However, none of these approaches is necessary because the ideal mixture assumption and the equilibrium assumption are sufficient to calculate the fluid boiling temperatures along the experimental test section and subsequently the local boiling heat transfer coefficients. This approach was adopted in this study.

As shown in Figure 7, the energy conservation to the EG/W mixture over a segment of the experimental test section length gives

$$\Delta q = \dot{m} \left\{ [1 - F_{EGout}](1 - x_{out})i_{Wout} + F_{EGout}(1 - x_{out})i_{EGout} + (1 - F_{EGvout})x_{out}i_{Wvout} + F_{EGvout}x_{out}i_{EGvout} \right. \\ \left. - [(1 - F_{EGin})(1 - x_{in})i_{Wlin} + F_{EGin}(1 - x_{in})i_{EGin} + (1 - F_{EGvin})x_{in}i_{Wvin} + F_{EGvin}x_{in}i_{EGvin}] \right\} \quad (14)$$

where Δq is the heat input to the segment, \dot{m} is the mass flowrate, i is the enthalpy, and subscripts *in* and *out* indicate inlet and outlet to the segment, respectively. By solving the

above equation together with the species conservation equation, the fluid temperature at the inlet of the segment can be expressed as

$$T_{fin} = T_{fout} - \frac{\Delta q / \dot{m} + [(1 - F_{EGvin})i_{fgWvin} + F_{EGvin}i_{fgEGin}]x_{in} - [(1 - F_{EGvout})i_{fgWout} + F_{EGvout}i_{fgEGout}]x_{out}}{[(1 - F_{EG})C_{pWl} + F_{EG}C_{pEGl}]} \quad (15)$$

where T is the temperature, i_{fg} is the latent heat of vaporization, C_p is the specific heat, and the subscript f indicates fluid. In arriving at the above equation, the terms $(i_{Wlout} - i_{Wlin})$ and $(i_{EGlout} - i_{EGlin})$ were approximated over a small incremental length by the terms $C_{pWl}(T_{out} - T_{in})$ and $C_{pEGl}(T_{out} - T_{in})$, respectively.

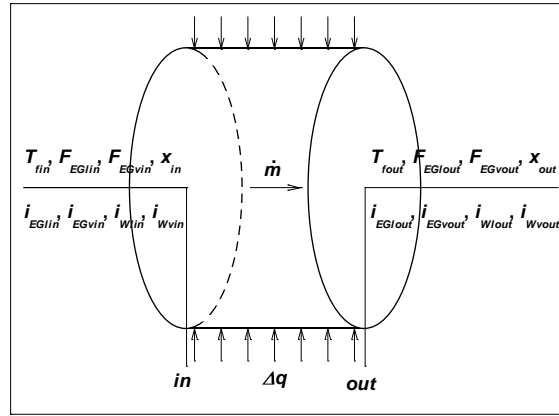


Figure 7. A segment of the experimental test section

3.5. Local Boiling Heat Transfer Coefficient

The local boiling heat transfer coefficient $h(z)$ at position z along the length of the experimental test section is defined as

$$h(z) = \frac{\dot{q}''(z)}{T_w(z) - T_f(z)} \quad (16)$$

where the local heat flux $\dot{q}''(z)$ was calculated from the overall input heating power by using the electrical resistivity of the AISI type 316 stainless steel as a function of the temperature, the local fluid temperature $T_f(z)$ was calculated at the location of the wall-temperature measurement with the method presented above, and the inner wall surface temperature $T_w(z)$ was determined from a radial heat conduction calculation by using the measured outer surface temperature $T'_w(z)$ and the local heat transfer rate $\dot{q}(z)$ in the wall with the known thermal conductivity $k_w(z)$ of the AISI type 316 stainless steel as a function of the temperature

$$T_w(z) = T'_w(z) + \frac{\dot{q}(z)}{4\pi k_w(z)L} \frac{1 + \ln(d_i/d_o)^2 - (d_i/d_o)^2}{1 - (d_i/d_o)^2} \quad (17)$$

3.6. Iteration Calculation Procedure

The data reduction was facilitated by dividing the experimental test section into ten segments corresponding to the locations of the wall thermocouples, and the data reduction proceeded starting from the exit of the experimental test section. With the measured fluid temperature and the measured system pressure at the exit of the experimental test section, the ethylene glycol vapor mass concentration and the vapor mass quality were calculated from the F_{EGv} equation (10) and the x equation (13), respectively. By using these values as the outlet parameters of the segment, the ethylene glycol vapor mass concentration, the vapor mass quality, and the fluid temperature upstream at the location of the nearest wall thermocouple were calculated as the inlet parameters of the segment. As the ethylene glycol vapor mass concentration, the vapor mass quality, and the fluid temperature were nonlinearly coupled together, iteration was used in arriving at the final results. As shown in Figure 8, this iteration calculation procedure continued over the incremental segments until the furthest upstream wall thermocouple was reached. In the above calculation, the system pressures at the locations of the wall thermocouples were calculated by assuming a linear pressure distribution with little error because two-phase pressure drops in the experimental test section were small in all experiments (<50 kPa). Finally, the local heat transfer coefficients were found from the h equation (16). Based on the uncertainties in each of the independent variables used to calculate the heat transfer coefficients, the uncertainties in heat transfer coefficients, estimated by using the method of sequential perturbation as outlined by Moffat [22] for single-sample data, were determined <5%. In this way, the heat transfer coefficients together with the other parameters were obtained at multiple local conditions along the experimental test section for every test.

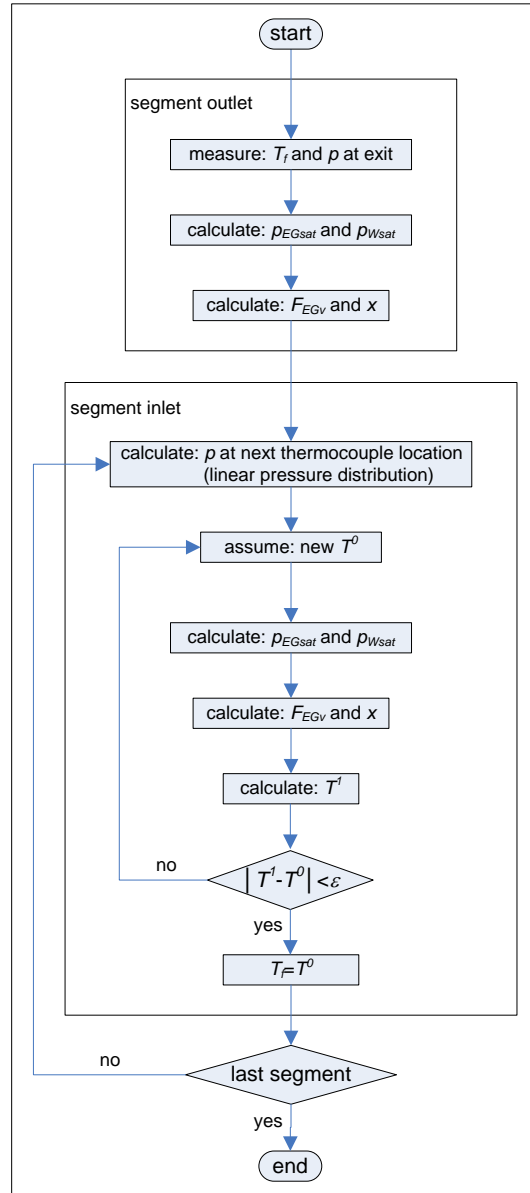


Figure 8. Iteration calculation procedure

3.7. Fluid Thermophysical Properties

The liquid thermal properties and the vapor thermal properties of the test fluid required for its boiling data reduction and for its boiling data correlation are listed in Table 2 as functions of its ethylene glycol mass concentration.

Table 2. Fluid thermophysical properties

Thermophysical properties	Ethylene glycol	Water	Ethylene glycol/water mixture
Liquid density	ρ_{EGl} [23]	ρ_{Wl} [24]	$\frac{1}{\rho_l} = \frac{F_{EGl}}{\rho_{EGl}} + \frac{1-F_{EGl}}{\rho_{Wl}}$

Vapor density	$\rho_{EGv} = \frac{p}{ZR_{EG}T_f}$ [25]	ρ_{Wv} [24]	$\frac{1}{\rho_v} = \frac{F_{EGv}}{\rho_{EGv}} + \frac{1-F_{EGv}}{\rho_{Wv}}$
Liquid specific heat	C_{pEGl} [26]	C_{pWl} [24]	$C_{pl} = F_{EGl}C_{pEGl} + (1-F_{EGl})C_{pWl}$
Vapor specific heat	C_{pEGv} [26]	C_{pWv} [24]	$C_{pv} = F_{EGv}C_{pEGv} + (1-F_{EGv})C_{pWv}$
Liquid viscosity	μ_{EGl} [26]	μ_{Wl} [24]	$\mu_l = \frac{9F_{EGl}}{31-22F_{EGl}}\mu_{EGl} + \left(1 - \frac{9F_{EGl}}{31-22F_{EGl}}\right)\mu_{Wl}$
Vapor viscosity	μ_{EGv} [26]	μ_{Wv} [24]	$\mu_v = \frac{9F_{EGv}}{31-22F_{EGv}}\mu_{EGv} + \left(1 - \frac{9F_{EGv}}{31-22F_{EGv}}\right)\mu_{Wv}$
Liquid thermal conductivity	k_{EGl} [26]	k_{Wl} [24]	$k_l = F_{EGl}k_{EGl} + (1-F_{EGl})k_{Wl}$
Vapor thermal conductivity	k_{EGv} [26]	k_{Wv} [24]	$k_v = F_{EGv}k_{EGv} + (1-F_{EGv})k_{Wv}$
Surface tension	σ_{EG} [23]	σ_W [24]	$\sigma = F_{EGl}\sigma_{EG} + (1-F_{EGl})\sigma_W$
Latent heat of vaporization	i_{fgEG} [23]	i_{fgW} [24]	$i_{fg} = F_{EGv}i_{fgEG} + (1-F_{EGv})i_{fgW}$
Saturation pressure	p_{EGsat} [23]	p_{Wsat} [24]	$p_{sat} = \frac{9F_{EGv}}{31-22F_{EGv}}p_{EGsat} + \left(1 - \frac{9F_{EGv}}{31-22F_{EGv}}\right)p_{Wsat}$

4. Boiling Experimental Results – Boiling Curve

4.1. Ranges of Experimental Parameters

A series of experiments was carried out to investigate the characteristics of the two-phase pressure drop, forced convective boiling heat transfer, and boiling limitation under conditions of small channels and low mass fluxes for distilled water and EG/W mixtures with volume concentration ratios of 40/60, 50/50, and 60/40 in both the horizontal flow and the vertical flow. In these experiments, the preheater power supply was adjusted to keep the test fluid inlet temperature at the experimental test section at a desired subcooled point. The experimental test section power supply was increased progressively until the CHF or the preset upper-temperature limit was reached. During each test section power supply increase, the measurements of in-stream temperatures, wall temperatures, outlet pressure, pressure drop, volumetric flowrate, voltage drop, and current were recorded for further data reduction. The detailed experimental parameters are listed in Table 3.

Table 3. Ranges of experimental parameters

Parameter	Range
Flow channel	Circular channel
Inside channel diameter (mm)	2.9845
Flow direction	Horizontal flow or vertical flow
Heated length (m)	0.9144
Test fluid	1. Distilled water 2. 40/60 ethylene glycol/water 3. 50/50 ethylene glycol/water 4. 60/40 ethylene glycol/water
Outlet pressure (kPa)	~150 and ~200
Inlet temperature (°C)	20–80
Mass flux (kg/m ² s)	30–200
Heat flux (kW/m ²)	5–300
Vapor mass quality	0–1
Liquid Reynolds number	<1700
Vapor Reynolds number	>2000
Liquid Prandtl number	1.4–8.3

4.2. Effect of System Pressure on Boiling Curve

Two-phase flow boiling was conducted under two test section outlet pressures of ~150 kPa and ~200 kPa. To compare the effect of the system pressure on flow boiling, the exit boiling curves of the heat flux versus the wall superheat are shown in Figure 9 for experiments with 50/50 EG/W mixture boiling inside the horizontal test section at one mass flux of ~100 kg/m²s, two test section outlet pressures of ~150 kPa and ~200 kPa, and four test section inlet temperatures of ~25 °C, ~40 °C, ~60 °C, and ~80 °C. At any given inlet temperature, the symbols in Figure 9 correspond to the steps in the test procedure where the heat flux was increased incrementally. It can be seen from Figure 9 that, for the fixed mass flux and the fixed test section inlet temperature, the system pressure is of very slight effect on the exit boiling curves for the two test section outlet pressures of ~150 kPa and ~200 kPa, which might result from the fact that the difference between the two test pressures is not large enough. Therefore, for the practical application purpose, the results from the experiments under the two test section outlet pressures of ~150 kPa and ~200 kPa in this study can be considered essentially equivalent.

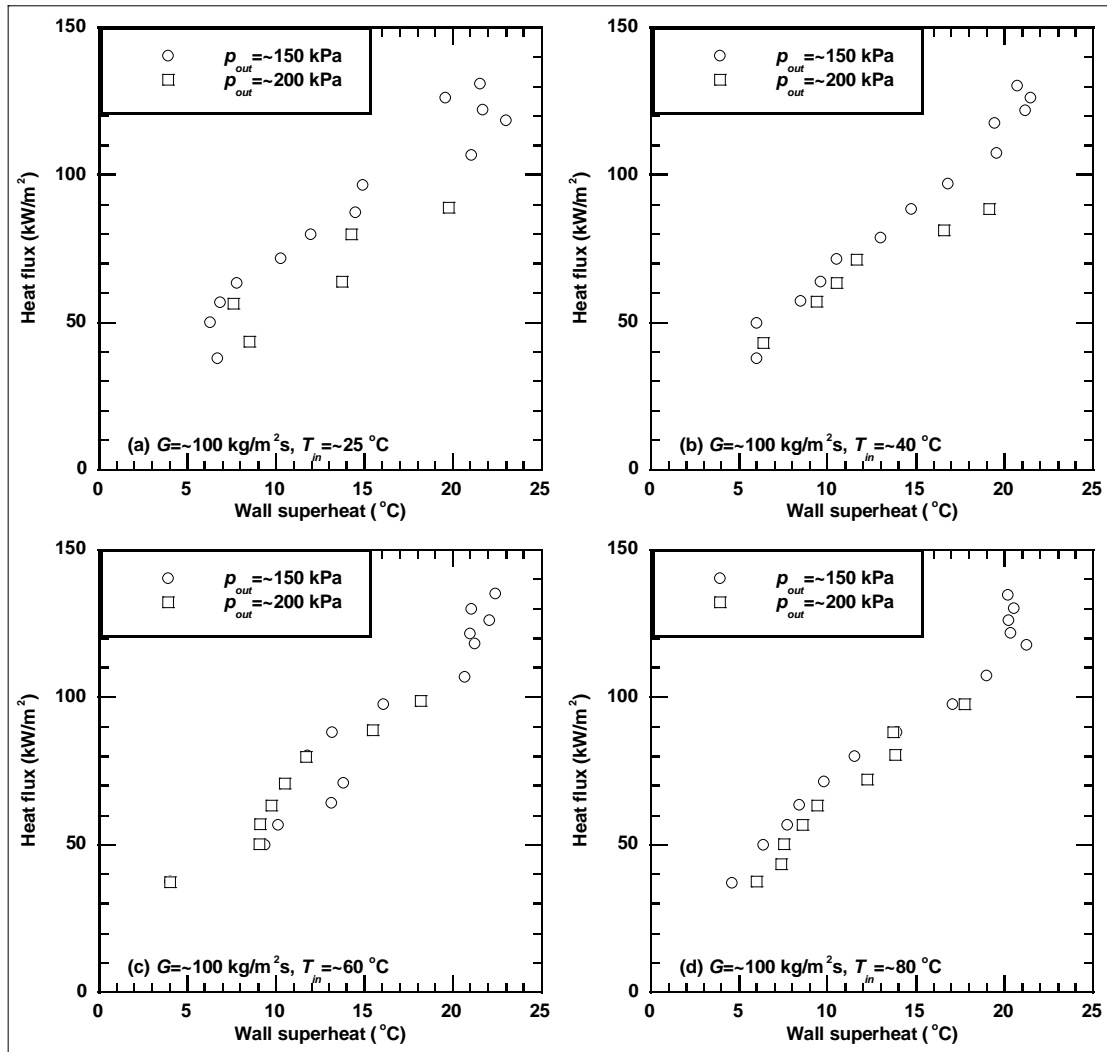


Figure 9. Heat flux as a function of wall superheat for horizontal flow boiling of 50/50 EG/W mixture

4.3. Effect of Test Section Inlet Temperature on Boiling Curve

As mentioned above, two-phase flow boiling was conducted for four test section inlet temperatures of ~ 25 °C, ~ 40 °C, ~ 60 °C, and ~ 80 °C. To compare the effect of the test section inlet temperature on flow boiling, the exit boiling curves of the heat flux versus the wall superheat are shown in Figure 10 for experiments with water flow boiling and 50/50 EG/W mixture flow boiling inside the horizontal test section and the vertical test section at a mass flux of ~ 100 kg/m²s. It can be seen from Figure 10 that, under the current test conditions, the exit boiling curves for water and EG/W mixtures are insensitive to the test section inlet temperature for both the horizontal flow and the vertical flow. However, changing the inlet temperature would cause a change in the boiling length as calculated from a heat balance.

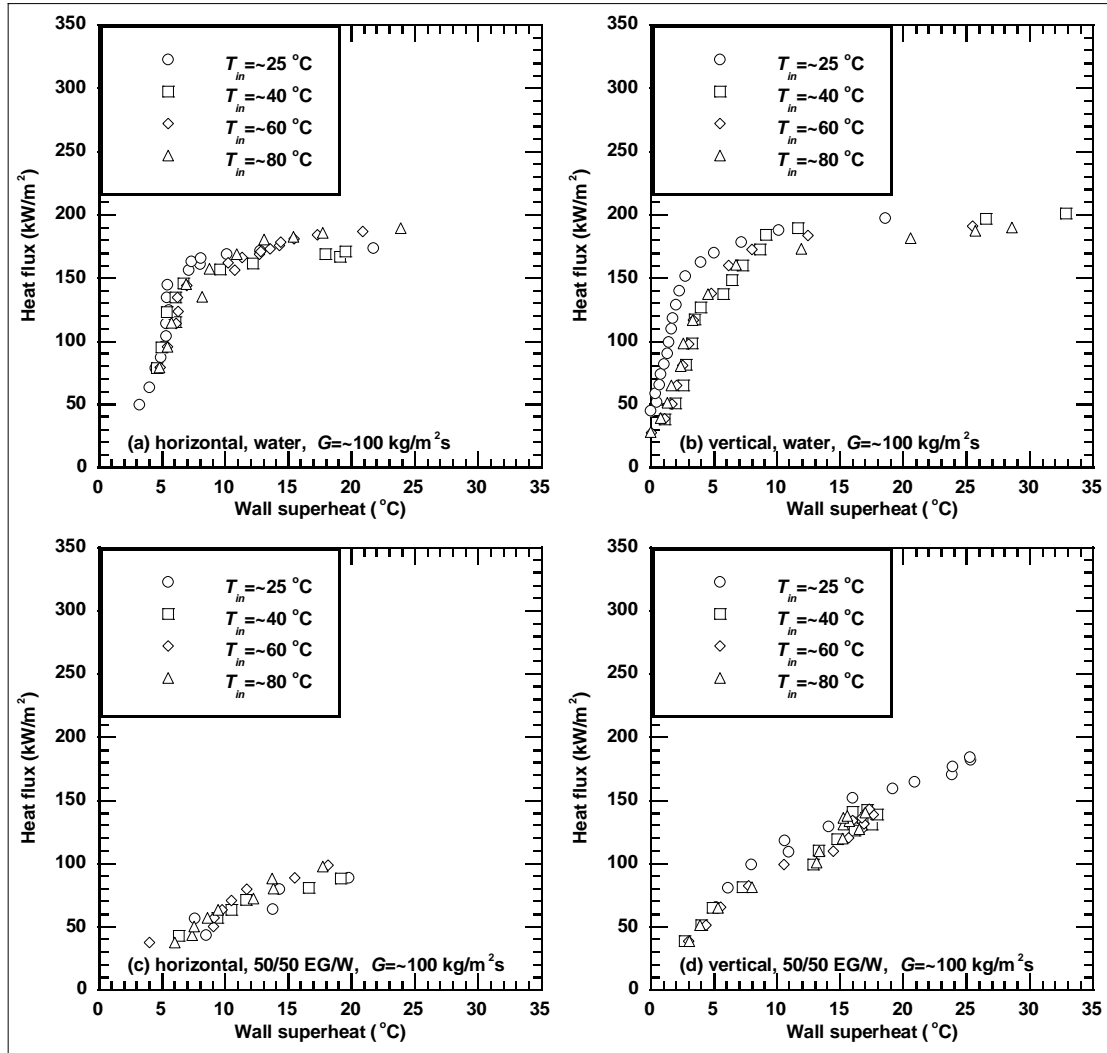


Figure 10. Heat flux as a function of wall superheat for flow boiling of water and 50/50 EG/W mixture

4.4. Effect of Ethylene Glycol Volume Concentration on Boiling Curve

Even though the 50/50 EG/W mixture is used in practical vehicle cooling systems, it is almost impossible to keep the ethylene glycol volume concentration of an EG/W mixture exactly at 50%. Therefore, in addition to the 50/50 EG/W mixture, it is also important to study the boiling characteristics of EG/W mixtures with volume concentrations other than 50%. In this study, boiling experiments with EG/W mixtures of three ethylene glycol volume concentrations of 40%, 50%, and 60% were conducted; and the effect of the ethylene glycol volume concentration on the exit boiling curve is shown in Figure 11 for flow boiling inside the horizontal test section and the vertical test section at a mass flux of $\sim 100\text{ kg/m}^2\text{s}$. It can be seen from Figure 11 that while there is an obvious difference between the water flow boiling and the EG/W mixture flow boiling, the difference between the exit boiling curves of the EG/W mixtures with various ethylene glycol volume concentrations of 40%, 50%, and 60% is much less, the reason for which probably is due to the small ethylene glycol volume concentration deviation of

10% from the 50/50 EG/W mixture. Generally, the EG/W mixture of the higher ethylene glycol volume concentration boils at a higher wall superheat for the same heat flux or at a lower heat flux for the same wall superheat. These results should be taken into consideration in analyzing the pressure drop, heat transfer, and flow stability of EG/W mixture flow boiling.

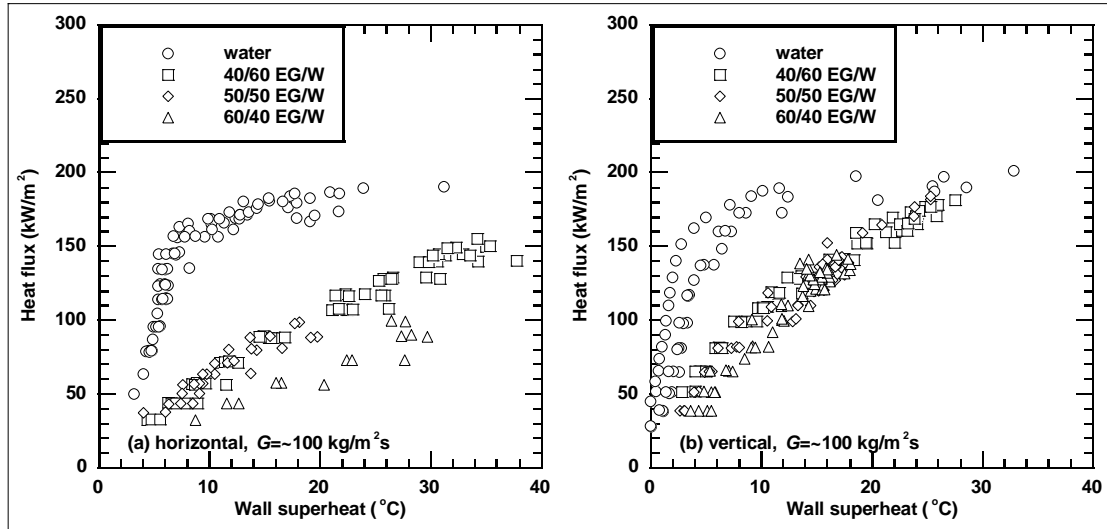


Figure 11. Heat flux as a function of wall superheat for flow boiling of water and EG/W mixtures

4.5. Effect of Flow Direction on Boiling Curve

In the application of practical vehicle cooling systems, both the horizontal flow and the vertical flow exist. Therefore, it is necessary to investigate the impact of the vertical flow versus the horizontal flow on two-phase flow boiling. Figure 12 shows the exit boiling curves of the heat flux versus the wall superheat for experiments with water flow boiling and EG/W mixture flow boiling inside the horizontal test section and the vertical test section at a mass flux of $\sim 100 \text{ kg/m}^2\text{s}$. It can be seen from Figure 12 that the exit boiling curve for the vertical flow follows the same trend as that for the horizontal flow. However, to reach the same wall superheat, the heat fluxes and, in turn, the CHF's for vertical flow boiling are higher than those for horizontal flow boiling. These results are expected because the vapor distribution for vertical flow boiling is more uniform than that for horizontal flow boiling due to the influence of gravity in horizontal flow boiling. These phenomena are important for the design of nucleate boiling vehicle cooling systems. Because a practical vehicle cooling system usually contains both horizontal channels and vertical channels, the design of a nucleate boiling vehicle cooling system will be too conservative if based only on the horizontal flow boiling data and too optimistic if based only on the vertical flow boiling data.

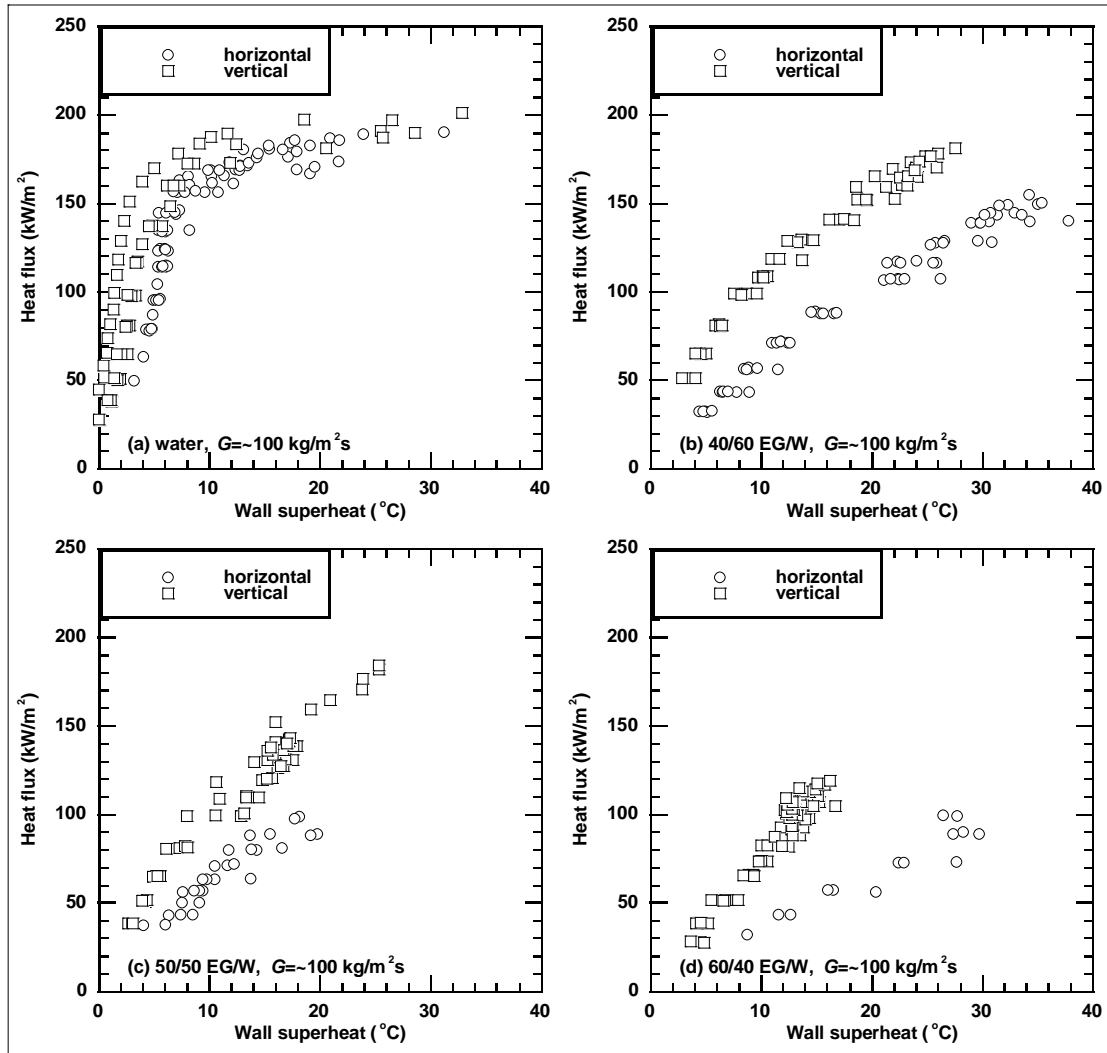


Figure 12. Heat flux as a function of wall superheat for flow boiling of water and EG/W mixtures

4.6. Effect of Mass Flux on Boiling Curve

4.6.1. Water Boiling – Three Flow-Boiling Regions

The effect of the mass flux on water flow boiling is shown in Figure 13 with five mass fluxes of $\sim 50 \text{ kg/m}^2\text{s}$, $\sim 75 \text{ kg/m}^2\text{s}$, $\sim 100 \text{ kg/m}^2\text{s}$, $\sim 130 \text{ kg/m}^2\text{s}$, and $\sim 150 \text{ kg/m}^2\text{s}$ for the horizontal flow and five mass fluxes of $\sim 50 \text{ kg/m}^2\text{s}$, $\sim 75 \text{ kg/m}^2\text{s}$, $\sim 100 \text{ kg/m}^2\text{s}$, $\sim 125 \text{ kg/m}^2\text{s}$, and $\sim 145 \text{ kg/m}^2\text{s}$ for the vertical flow. It can be seen from the Figure 13 that, for forced convective boiling in small channels as in this study, there exist three flow-boiling regions: convection-dominant boiling, nucleation-dominant boiling, and transition boiling [27-28]. At low wall superheats, usually less than a few degrees Celsius, the heat fluxes are relatively independent of the wall superheat, and the situation is characterized as the convection-dominant-boiling region. At high wall superheats, the system moves into the transition-boiling region, in which the wall temperatures show oscillations, the heat fluxes separate as a function of the mass flux, and the flow boiling is susceptible to flow instabilities and, at high enough wall superheats, to the CHF condition. The

highest wall-superheat data obtained in Figure 13 were limited by reaching the CHF condition, which is clearly a function of the mass flux. Between these two boiling regions, there is an extensive nucleation-dominant-boiling region, which is the focus of this study.

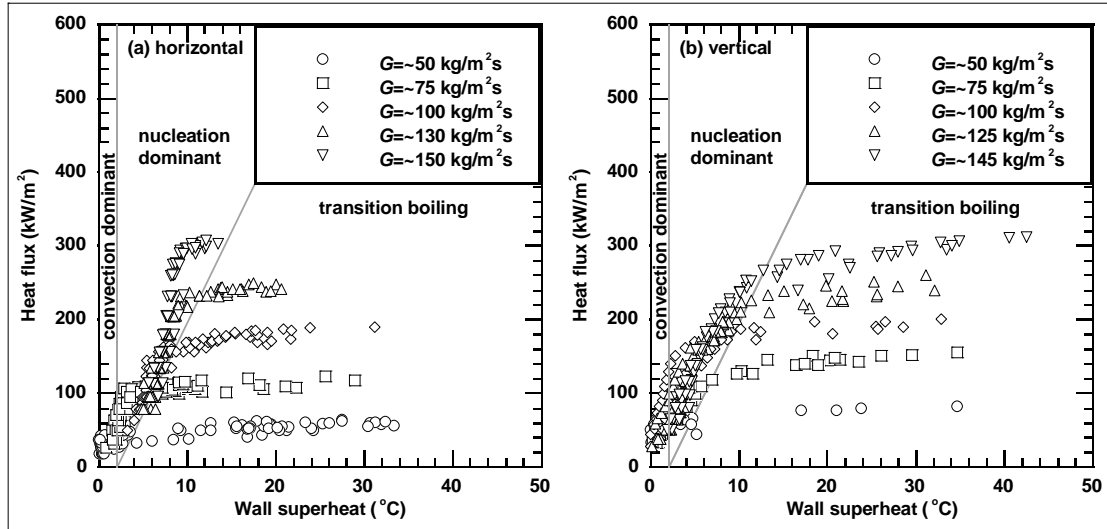


Figure 13. Heat flux as a function of wall superheat for flow boiling of water

The nucleation-dominant-boiling region shown in Figure 13 is typical in small-channel flow boiling and is considerably more extensive than that found in larger-channel flow boiling. In the nucleation-dominant-boiling region, the heat fluxes follow a strong power-law trend of the wall superheat nearly independent of the mass flux, which, coupled with the inlet temperature effect discussed above, implies that the nucleate-boiling heat transfer coefficients up to the transition-boiling region are a function of the heat flux only but not a function of the mass flux or the inlet subcooling. This phenomenon, which is the same as findings for refrigerant flow boiling in small channels [29], is attributed to the large slug-flow regime found in small-channel two-phase flows [30], which gives rise to the domination of the nucleation heat transfer mechanism and the minimization of the convective heat transfer mechanism over a large mass flux range and a large inlet-subcooling range. Small channel flow boiling is usually confined to relatively low mass fluxes due to pressure-drop restrictions, which also contributes to the minimization of the convection contribution to flow boiling heat transfer. This fact would be incorporated into the correlation of the boiling heat transfer data. The nucleation-dominant-boiling region is the generally-desired operating region for flow boiling in small channels due to its relatively high heat transfer rates and flow stability.

4.6.2. Ethylene Glycol/Water Mixture Boiling

The exit boiling curves of the heat flux versus the wall superheat are shown in Figure 14 for experiments with 40/60 EG/W, 50/50 EG/W, and 60/40 EG/W mixture flow boiling inside the horizontal test section and the vertical test section at various mass fluxes. Some interesting features can be seen from the exit boiling curves in Figure 14.

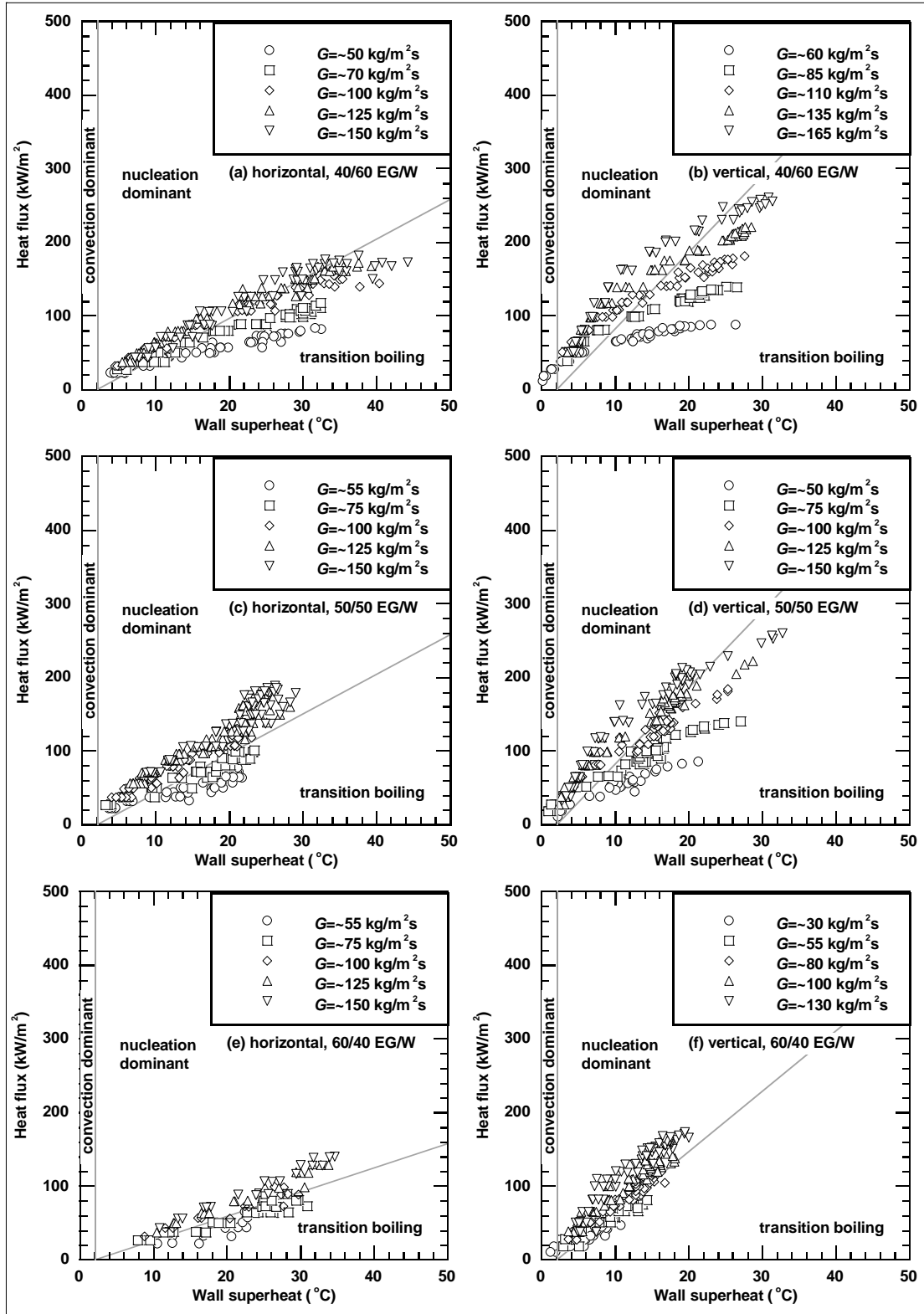


Figure 14. Heat flux as a function of wall superheat for flow boiling of EG/W mixtures

The exit boiling curve trends of EG/W mixture flow boiling are seen to be similar to those of single-component pure water flow boiling with differences in magnitudes. Three boiling regions still exist for EG/W mixture flow boiling: the convection-dominant boiling occurs below certain wall superheats of a few degrees Celsius; the nucleation-dominant-boiling region is clearly present in Figure 14; and the transition-boiling region occurs at higher wall superheats even though the transition-boiling region for EG/W mixture flow boiling is less extensive than for water flow boiling, especially for 60/40 EG/W mixture flow boiling.

In the nucleation-dominant-boiling region, the magnitude of the heat fluxes and therefore the heat transfer rates for 40/60 EG/W, 50/50 EG/W, and 60/40 EG/W mixture flow boiling fall below those for water flow boiling at the same wall superheats, as shown in Figure 11. The heat fluxes of 40/60 EG/W, 50/50 EG/W, and 60/40 EG/W mixture flow boiling follow a similar power-law trend nearly independent of the mass flux as those of water flow boiling but, of course, at a different magnitude. Therefore, the conclusion for water flow boiling that the nucleate-boiling heat transfer coefficients up to the transition-boiling region are a function of the heat flux only but not a function of the mass flux or the inlet subcooling is also true for 40/60 EG/W, 50/50 EG/W, and 60/40 EG/W mixture flow boiling.

In this study, the highest wall-superheat data obtained in Figure 14 for 40/60 EG/W, 50/50 EG/W, and 60/40 EG/W mixture flow boiling, which was less stable than for water flow boiling under the similar experimental conditions, were generally limited by excessively large-amplitude flow oscillations. The CHF for 40/60 EG/W, 50/50 EG/W, and 60/40 EG/W mixture flow boiling was almost never attainable in the experimental apparatus.

4.6.3. Criteria for Nucleation-dominant Boiling

Generally, the nucleation-dominant boiling region may be defined in terms of the wall superheat ΔT_{sat} being between the lower wall-superheat limit $(\Delta T_{sat})_{lower}$ and the upper wall-superheat limit $(\Delta T_{sat})_{upper}$

$$(\Delta T_{sat})_{lower} \leq \Delta T_{sat} \leq (\Delta T_{sat})_{upper} \quad (18)$$

where the lower wall-superheat limit has been found to approximately be a constant and was taken as ~ 2 °C for all the test fluids and the test conditions in this study, while the upper wall-superheat limit is usually a function of the mass flux and should be determined based on the test fluids. This upper wall-superheat limit is shown in Figure 13 and Figure 14 as a solid line dividing the nucleation-dominant-boiling region and the transition-boiling region.

5. Boiling Experimental Results – Pressure Drop

5.1. Predictive Models for Two-Phase Pressure Drop in the Literature

5.1.1. Two-Phase Parameters

To analyze the two-phase pressure drop, the following four two-phase flow parameters are commonly utilized: the cross-sectional void fraction α defined by the ratio of the cross-sectional vapor area A_v over the cross-sectional total area A

$$\alpha = \frac{A_v}{A} = \frac{A_v}{A_l + A_v} = \frac{1}{1 + [(1-x)/x](\rho_v/\rho_l)S} \quad (19)$$

the vapor mass quality x defined by the ratio of the vapor mass m_v over the total mass m

$$x = \frac{m_v}{m} = \frac{m_v}{m_l + m_v} = \frac{1}{1 + [(1-\alpha)/\alpha](\rho_l/\rho_v)(1/S)} \quad (20)$$

the slip ratio S defined by the ratio of the vapor velocity v_v over the liquid velocity v_l

$$S = \frac{v_v}{v_l} = \frac{1-\alpha}{\alpha} \frac{x}{1-x} \frac{\rho_l}{\rho_v} \quad (21)$$

and the effective density ρ defined based on the presumption of the homogeneous liquid and vapor phases

$$\rho = (1-\alpha)\rho_l + \alpha\rho_v = \frac{1 + x[(1/S) - 1]}{1 + x[(\rho_l/\rho_v)(1/S) - 1]} \rho_l \quad (22)$$

or on the presumption of the completely-separated liquid and vapor phases

$$\begin{aligned} \rho &= \frac{1}{[(1-x)^2/(1-\alpha)](1/\rho_l) + (x^2/\alpha)(1/\rho_v)} \\ &= \frac{\{1 + \alpha[(\rho_v/\rho_l)S - 1]\}^2}{1 + \alpha[(\rho_v/\rho_l)S^2 - 1]} \rho_l = \frac{1}{[1 + x(S-1)][1 + x[(\rho_l/\rho_v)(1/S) - 1]]} \rho_l \end{aligned} \quad (23)$$

5.1.2. Two-Phase Pressure Drops

The total pressure drop Δp for a two-phase flow with a single-phase length of L_{SP} and a boiling two-phase length of L_{TP} can be obtained as the sum of the single-phase pressure drop

Δp_{ST} and the two-phase pressure drop Δp_{TP} each of which has three additive contribution sources: gravity, acceleration, and friction

$$\Delta p = \Delta p_{ST} + \Delta p_{TP} = (\Delta p_g + \Delta p_a + \Delta p_f)_{SP} + (\Delta p_g + \Delta p_a + \Delta p_f)_{TP} \quad (24)$$

In the above equation, the gravitation pressure drop Δp_g is defined from the density ρ and gravitational acceleration g as

$$\Delta p_g = \int_0^L \rho g \sin \theta dL \quad (25)$$

where $\theta = 0$ for the horizontal flow and $\theta = 2/\pi$ for the vertical flow. For single-phase flow, the gravitation pressure drop $(\Delta p_g)_{SP}$ can be calculated from the average liquid density ρ_l as

$$(\Delta p_g)_{SP} = \rho_l g L_{SP} \sin \theta \quad (26)$$

For two-phase flow, the gravitation pressure drop $(\Delta p_g)_{TP}$ can be calculated from the average liquid density ρ_l , the average vapor density ρ_v , the outlet vapor mass quality x_{out} , and the slip ratio S as

$$(\Delta p_g)_{TP} = \rho_l g L_{TP} \left\{ \frac{S-1}{S - (\rho_l/\rho_v)} + \frac{[(\rho_l/\rho_v) - 1]S \ln \{1 + x_{out} [(\rho_l/\rho_v)(1/S) - 1]\}}{[(\rho_l/\rho_v) - S]^2 x_{out}} \right\} \sin \theta \quad (27)$$

which is obtained from the homogeneous effective density and is based on the following presumptions [31]: (a) uniform heating with $dL/L_{TP} = dx/x_{out}$, (b) a constant slip ratio in the two-phase flow range, and (c) a constant liquid density and a constant vapor density in the two-phase flow range. Based on the same presumptions but using the completely-separated effective density instead of the homogeneous effective density, the authors have derived the two-phase gravitation pressure drop $(\Delta p_g)_{TP}$ as

$$(\Delta p_g)_{TP} = \rho_l g L_{TP} \left\{ \frac{1}{S - (\rho_l/\rho_v)(1/S)} \frac{\ln \frac{1 + x_{out}(S-1)}{1 + x_{out} [(\rho_l/\rho_v)(1/S) - 1]}}{x_{out}} \right\} \sin \theta \quad (28)$$

Generally, the completely-separated model gives a smaller but more accurate two-phase gravitation pressure drop than the homogeneous model. It should be noted that the constant ρ_l and ρ_v presumption is reasonable for pure-component flow boiling but is only approximate for mixture flow boiling. The acceleration pressure drop Δp_a is defined from the mass flowrate \dot{m} and the flow velocity v as

$$\Delta p_a = \int_0^L (1/A) [d(\dot{m}v)/dL] dL \quad (29)$$

which, using the effective density for two-phase flow, can be calculated from the mass flux G as

$$\begin{cases} (\Delta p_a)_{SP} = G^2 (1/\rho_l) \Big|_{in}^{out} \\ (\Delta p_a)_{TP} = G^2 [1 + x(S-1)] \{1 + x[(\rho_l/\rho_v)(1/S) - 1]\} (1/\rho_l) \Big|_{in}^{out} \end{cases} \quad (30)$$

The friction pressure drop Δp_f is defined from the density ρ and the Fanning friction factor f as

$$\Delta p_f = \int_0^L [2G^2/(\rho d_i)] dL \quad (31)$$

where the Fanning friction factor for laminar flow is calculated from the classic equation as

$$f_{\text{classic}} = 16 \text{Re}_l^{-1} \quad (32)$$

and the Fanning friction factor for turbulent flow is calculated from the classic equation as

$$f_{\text{classic}} = 0.046 \text{Re}_l^{-0.2} \quad (33)$$

or from the Blasius equation [16] as

$$f_{\text{Blasius}} = 0.079 \text{Re}_l^{-0.25} \quad (34)$$

For single-phase flow, the friction pressure drop $(\Delta p_f)_{SP}$ can be calculated from the average liquid density ρ_l as

$$(\Delta p_f)_{SP} = \frac{2L_{SP} G^2}{\rho_l d_i} f \quad (35)$$

For two-phase flow, the friction pressure drop $(\Delta p_f)_{TP}$ can be calculated based on the frequently-used concept of the two-phase multipliers proposed by Lockhart and Martinelli [32] from the liquid friction pressure drop $(\Delta p_f)_l$ as

$$(\Delta p_f)_{TP} = \phi_l^2 (\Delta p_f)_l \quad (36)$$

where the liquid friction pressure drop $(\Delta p_f)_l$ is defined as

$$(\Delta p_f)_l = \frac{2L_{TP}[G(1-x)]^2}{\rho_l d_i} f_l \quad (37)$$

and the two-phase friction multiplier ϕ_l can be correlated as a function of the Lockhart-Martinelli parameter X [33-34]

$$\phi_l = \left(1 + \frac{C}{X} + \frac{1}{X^2}\right)^{1/2} \quad (38)$$

with $C = 5$ for laminar-liquid/laminar-vapor flow, $C = 10$ for turbulent-liquid/laminar-vapor flow, $C = 12$ for laminar-liquid/turbulent-vapor flow, and $C = 20$ for turbulent-liquid/turbulent-vapor flow. In the above equation, the Lockhart-Martinelli parameter X is defined as

$$X = \sqrt{\frac{(dp/dL)_l}{(dp/dL)_v}} = \sqrt{\frac{2[G(1-x)]^2 f_l}{\rho_l d_i} \frac{\rho_v d_i}{2(Gx)^2 f_v}} = \left(\frac{\rho_v}{\rho_l}\right)^{0.5} \frac{1-x}{x} \left(\frac{f_l}{f_v}\right)^{0.5} \quad (39)$$

which can be calculated based on the flow region as

$$\left\{ \begin{array}{ll} X_{ll} = \left(\frac{\rho_v}{\rho_l}\right)^{0.5} \left(\frac{\mu_l}{\mu_v}\right)^{0.5} \left(\frac{1-x}{x}\right)^{0.5} & \text{laminar-liquid/laminar-vapor} \\ X_{tl} = \frac{1}{18.65} \left(\frac{\rho_v}{\rho_l}\right)^{0.5} \frac{1-x}{x} \frac{(Gx d_i / \mu_v)^{0.5}}{[G(1-x) d_i / \mu_l]^{0.1}} & \text{turbulent-liquid/laminar-vapor} \\ X_{lv} = 18.65 \left(\frac{\rho_v}{\rho_l}\right)^{0.5} \frac{1-x}{x} \frac{(Gx d_i / \mu_v)^{0.1}}{[G(1-x) d_i / \mu_l]^{0.5}} & \text{laminar-liquid/turbulent-vapor} \\ X_{tv} = \left(\frac{\rho_v}{\rho_l}\right)^{0.5} \left(\frac{\mu_l}{\mu_v}\right)^{0.1} \left(\frac{1-x}{x}\right)^{0.9} & \text{turbulent-liquid/turbulent-vapor} \end{array} \right. \quad (40)$$

if the classic friction factor equation is used for the turbulent flow or

$$\left\{ \begin{array}{ll} X_{ll} = \left(\frac{\rho_v}{\rho_l}\right)^{0.5} \left(\frac{\mu_l}{\mu_v}\right)^{0.5} \left(\frac{1-x}{x}\right)^{0.5} & \text{laminar-liquid/laminar-vapor} \\ X_{tl} = \frac{1}{14.23} \left(\frac{\rho_v}{\rho_l}\right)^{0.5} \frac{1-x}{x} \frac{(Gx d_i / \mu_v)^{0.5}}{[G(1-x) d_i / \mu_l]^{0.125}} & \text{turbulent-liquid/laminar-vapor} \\ X_{lv} = 14.23 \left(\frac{\rho_v}{\rho_l}\right)^{0.5} \frac{1-x}{x} \frac{(Gx d_i / \mu_v)^{0.125}}{[G(1-x) d_i / \mu_l]^{0.5}} & \text{laminar-liquid/turbulent-vapor} \\ X_{tv} = \left(\frac{\rho_v}{\rho_l}\right)^{0.5} \left(\frac{\mu_l}{\mu_v}\right)^{0.125} \left(\frac{1-x}{x}\right)^{0.875} & \text{turbulent-liquid/turbulent-vapor} \end{array} \right. \quad (41)$$

if the Blasius friction factor equation is used for the turbulent flow.

5.1.3. Slip Ratio Models

One of the critical unknown parameters involved in predicting the two-phase pressure drop for a boiling flow is the slip ratio or equivalent the void fraction. Many theoretical and empirical models for predicting the slip ratio and the void fraction have been developed over the last several decades. Woldesemayat and Ghajar [35] gave a comprehensive comparison of the performance of 68 void fraction correlations based on unbiased data set covering wide range of parameters. Several commonly-used models are listed in Table 4 for the purpose of analyzing the two-phase friction pressure drop in this study.

Table 4. Equations for slip ratios

Homogeneous model		
	$S = 1$	(42)
Zivi 1964 [36]		
	$S = (\rho_l / \rho_v)^{1/3}$	(43)
Smith 1969 [37]		
	$S = K + (1 - K) \left\{ \frac{(\rho_l / \rho_v) + K[(1 - x)/x]}{1 + K[(1 - x)/x]} \right\}^{1/2}$, where $K = 0.4$.	(44)
Wallis 1969 [38]; Domanski and Didion 1983 [39]		
	$S = \frac{1 - (1 + X_u^{0.8})^{-0.378}}{(1 + X_u^{0.8})^{-0.378}} \frac{x}{1 - x} \frac{\rho_l}{\rho_v}$	(45)
Premoli, et al. 1971 [40]		
	$S = 1 + 1.578(Gd_l / \mu_l)^{-0.19} (\rho_l / \rho_v)^{0.22} \left\{ \frac{\frac{x}{1 - x} \frac{\rho_l}{\rho_v}}{1 + 0.0273 \frac{x}{1 - x} \text{We}_l \left(\frac{Gd_l}{\mu_l} \right)^{-0.51} \left(\frac{\rho_l}{\rho_v} \right)^{0.92}} - 0.0273 \frac{x}{1 - x} \text{We}_l \left(\frac{Gd_l}{\mu_l} \right)^{-0.51} \left(\frac{\rho_l}{\rho_v} \right)^{0.92} \right\}^{0.5}$	(46)
Chisholm 1973 [34]		
	$S = \sqrt{1 - x[1 - (\rho_l / \rho_v)]}$	(47)
Rigot 1973 [41]		
	$S = 2$	(48)

5.2. Effect of Slip Ratio on Experimental Two-Phase Friction Multiplier

Based on the total measured experimental pressure drop Δp_{exp} , the experimental two-phase friction multiplier $(\phi_l)_{exp}$ is defined as

$$(\phi_l)_{exp} = \left[\frac{\Delta p_{exp} - (\Delta p_g + \Delta p_a + \Delta p_f)_{SP} - (\Delta p_g + \Delta p_a)_{TP}}{(\Delta p_f)_l} \right]^{1/2} \quad (49)$$

It can be seen from the above equation that the experimental two-phase friction multiplier is a function of the slip ratio because both the two-phase gravitation pressure drop and the two-phase acceleration pressure drop are dependent on the slip ratio. Therefore, an appropriate slip ratio model has to be chosen before the experimental two-phase friction multiplier can be calculated.

The influence of the slip ratio on the experimental two-phase friction multiplier for experiments with water boiling and EG/W boiling in both the horizontal flow and the vertical flow are shown in Figure 15 as a function of the Lockhart-Martinelli parameter for various slip ratios predicted from the equations listed in Table 4. While all the boiling experiments of this study are under the condition of the laminar-liquid/turbulent-vapor flow, the Lockhart-Martinelli parameter $X_{tt} = (\rho_v/\rho_l)^{0.5}(\mu_l/\mu_v)^{0.1}[(1-x)/x]^{0.9}$ calculated based on the classic Fanning friction factor for the turbulent-liquid/turbulent-vapor flow is used in Figure 15 because, as shown below, it represents the experimental two-phase friction multipliers best. It can be seen from Figure 15 that (a) the average experimental two-phase friction multiplier for vertical flow boiling is smaller than that for horizontal flow boiling; (b) the variation in the experimental two-phase friction multiplier for water flow boiling is smaller than for EG/W mixture flow boiling, probably due to the approximate assumptions of a constant slip ratio, a constant liquid density, and a constant vapor density introduced in the calculation of the two-phase gravitation pressure drop; and (c) the experimental two-phase friction multiplier is insensitive to the slip ratio when the completely-separated liquid and vapor model is used with the slip ratio being greater than two, which is not true for the homogeneous liquid and vapor model with the slip ratio being unity. Since all the slip ratio models other than the homogeneous model predict the slip ratio greater than two, the Zivi equation $S = (\rho_l/\rho_v)^{1/3}$ is applied in the following calculations and analyses for simplicity.

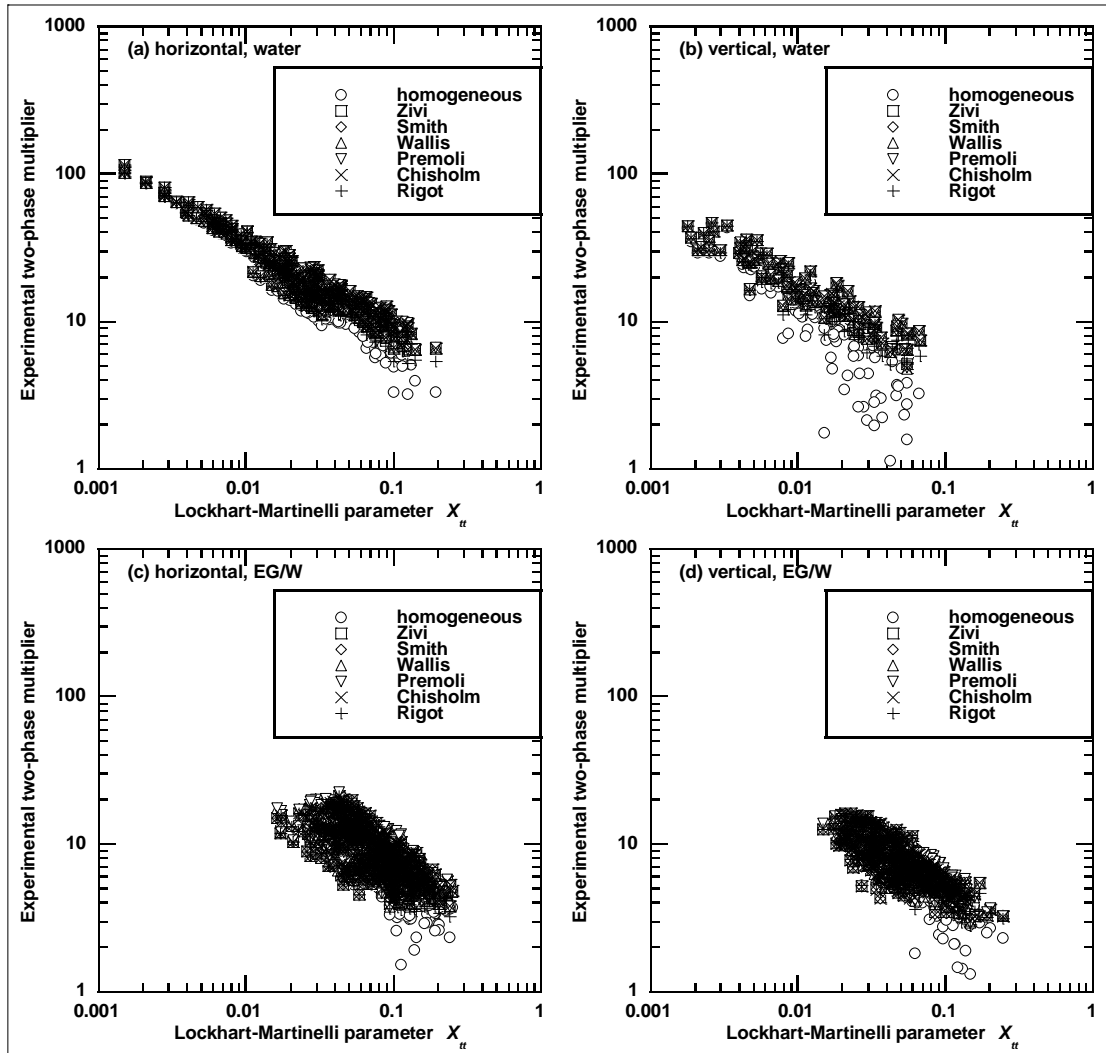


Figure 15. Effect of slip ratio on experimental two-phase multiplier

5.3. Effect of Vapor Mass Quality on Experimental Two-Phase Friction Multiplier

The experimental two-phase friction multiplier is plotted in Figure 16 as a function of the exit vapor mass quality for experiments with water boiling and EG/W mixture boiling in both the horizontal flow and the vertical flow. The effect of the exit vapor mass quality is to increase the experimental two-phase friction multiplier, as clearly displayed in Figure 16. The trend, which the variation in the experimental two-phase friction multiplier for water flow boiling is smaller than that for EG/W mixture flow boiling shown in Figure 15 when plotted against the Lockhart-Martinelli parameter, is also shown in Figure 16 when plotted against the exit vapor mass quality, probably for the same reason explained above.

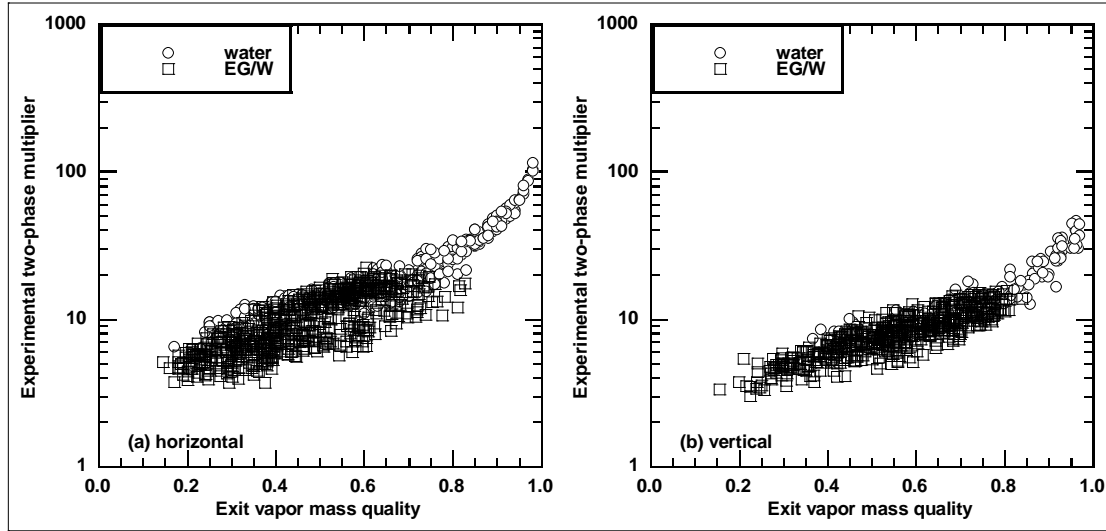


Figure 16. Experimental two-phase multiplier as a function of vapor mass quality

5.4. Correlation of Experimental Two-Phase Friction Multiplier

Because all the boiling experiments of this study are under the condition of the laminar-liquid/turbulent-vapor flow, the Chisholm equation for the two-phase friction multiplier is [33-34]

$$\phi_l = \left(1 + \frac{12}{X_{lt}} + \frac{1}{X_{lt}^2} \right)^{1/2} \quad (50)$$

where the Lockhart-Martinelli parameter calculated based on the classic Fanning friction factor for the laminar-liquid/turbulent-vapor flow is

$$X_{lt} = 18.65 \left(\frac{\rho_v}{\rho_l} \right)^{0.5} \frac{1-x}{x} \frac{(Gx d_i / \mu_v)^{0.1}}{[G(1-x) d_i / \mu_l]^{0.5}} \quad (51)$$

The predicted two-phase friction multiplier values from the Chisholm equation are compared with the experimental two-phase friction multiplier data in Figure 17 as a function of the Lockhart-Martinelli parameter, where it is seen that the Chisholm equation consistently over predicts the experimental two-phase friction multiplier data of water flow boiling. This phenomenon may be caused by the occurrence of the slug flow over a large quality range in small channels that reduces the pressure gradients from the annular flow condition found in large tubes upon which the Chisholm equation is substantially based. It is also seen from Figure 17 that the Lockhart-Martinelli parameter X_{lt} for the laminar-liquid/turbulent-vapor flow is not the best parameter for correlating the experimental data of this study because, for both the horizontal flow and the vertical flow, the experimental two-phase friction multiplier data of EG/W mixture flow boiling follow a different decrease trend from those of the water flow boiling.

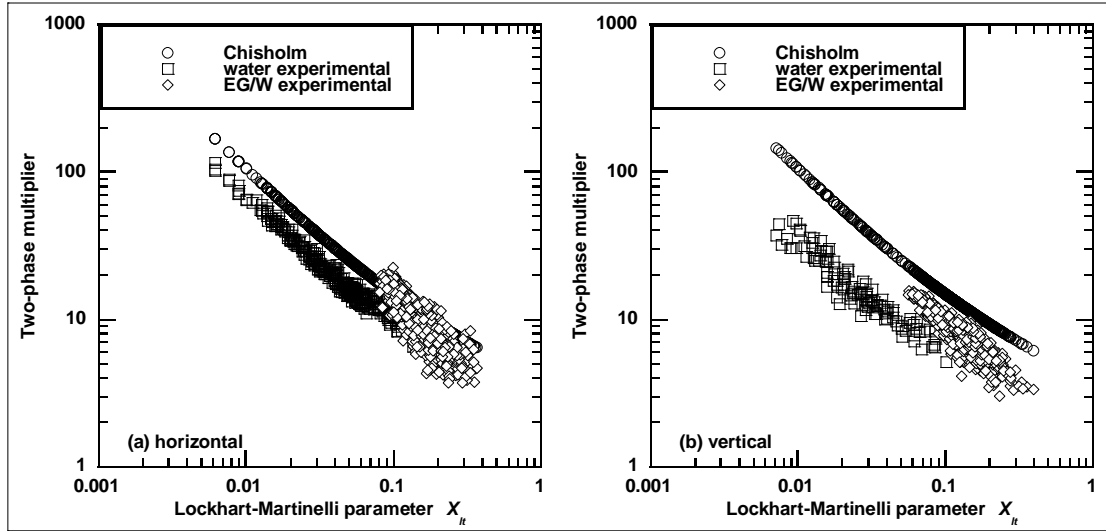


Figure 17. Two-phase multiplier comparison

A further close examination shows the following facts about the experimental two-phase friction multiplier data of this study: (a) among the four different expressions, the Lockhart-Martinelli parameter X_{tt} for the turbulent-liquid/turbulent-vapor flow is the best one for representing the experimental two-phase friction multiplier data; (b) the Lockhart-Martinelli parameter X_{tt} for the turbulent-liquid/turbulent-vapor flow calculated by using either the classic Fanning friction factor or the Blasius Fanning friction factor gives very similar results for the experimental two-phase friction multiplier data; and (c) the experimental two-phase friction multiplier data for the horizontal flow and the vertical flow follow different trends. Therefore, the experimental two-phase friction multiplier data of this study were separately correlated as functions of the Lockhart-Martinelli parameter X_{tt}

$$\phi_l = 1 + 1.3340 X_{tt}^{-0.6926} = 1 + 1.3340 \left[\left(\frac{\rho_v}{\rho_l} \right)^{0.5} \left(\frac{\mu_l}{\mu_v} \right)^{0.1} \left(\frac{1-x}{x} \right)^{0.9} \right]^{-0.6926} \quad (52)$$

for the horizontal flow and

$$\phi_l = 1 + 1.1592 X_{tt}^{-0.5878} = 1 + 1.1592 \left[\left(\frac{\rho_v}{\rho_l} \right)^{0.5} \left(\frac{\mu_l}{\mu_v} \right)^{0.1} \left(\frac{1-x}{x} \right)^{0.9} \right]^{-0.5878} \quad (53)$$

for the vertical flow, as shown in Figure 18, both of which reduce to unity for the mass vapor quality $x = 0$. These equations predict the experimental two-phase friction multiplier data of this study reasonably well with mean deviations of 17% for water boiling of the horizontal flow, 32% for EG/W mixture boiling of the horizontal flow, 27% for overall horizontal flow boiling, 20% for water boiling of the vertical flow, 19% for EG/W mixture boiling of the vertical flow, and 19% for overall vertical flow boiling. As shown in Figure 19, the majority of the experimental

two-phase friction multiplier data are within $\pm 30\%$ of the predictions. The higher mean deviation for EG/W mixture boiling of the horizontal flow may be explained by the fact that its experimental two-phase friction multiplier data include the results for test section outlet pressures of both ~ 150 kPa and ~ 200 kPa.

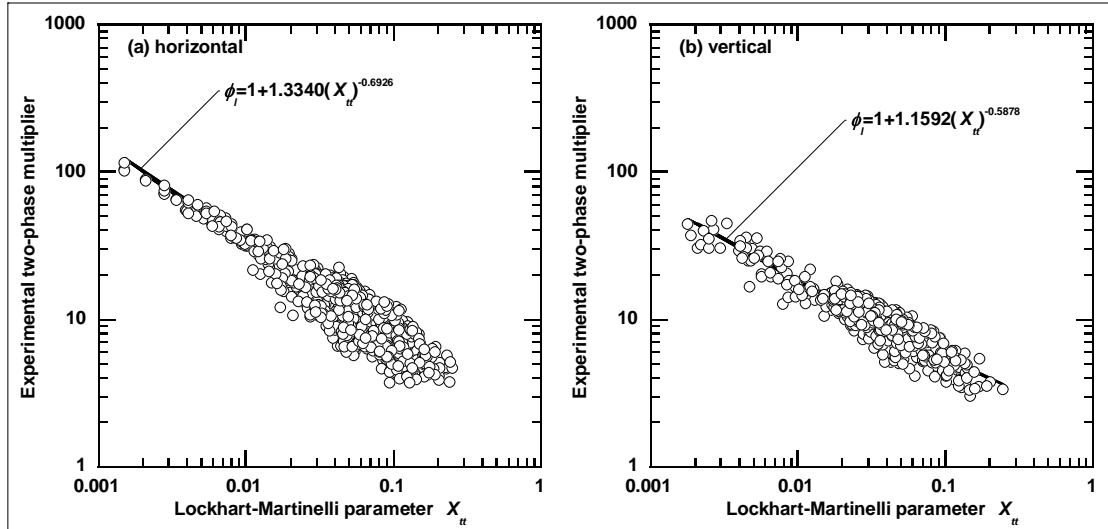


Figure 18. Experimental two-phase multiplier correlation

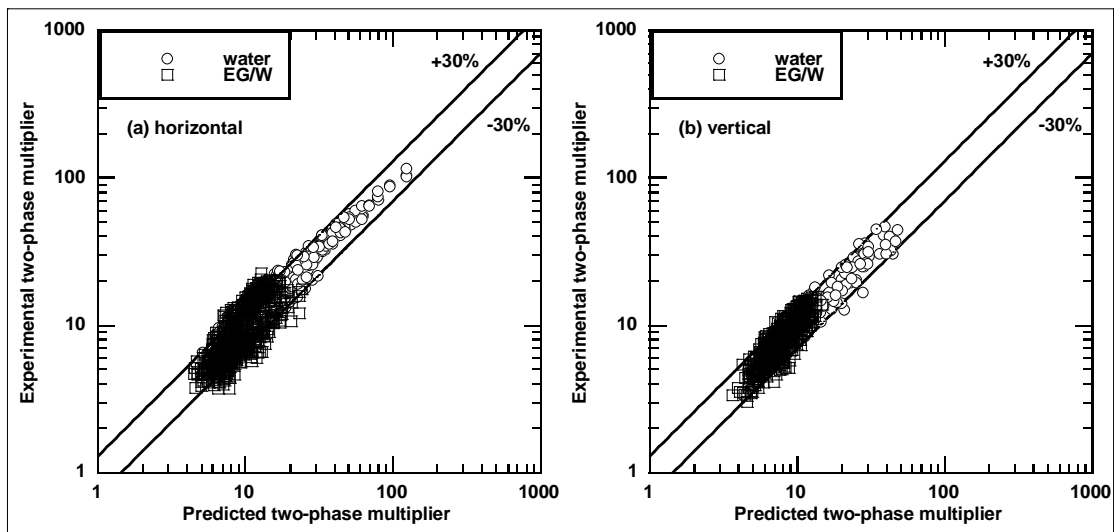


Figure 19. Two-phase multiplier comparison

6. Boiling Experimental Results – Heat Transfer Coefficient

6.1. Predictive Models for Boiling Heat Transfer Coefficient in the Literature

Many equations for heat transfer coefficients of internal forced convective boiling with pure component fluids and mixtures have been developed and appear in the engineering literature [42-47]. These equations usually pertain to a range of working fluids, flow channel geometries, heat fluxes, mass fluxes, and system pressures. As can be seen in Table 5 in which some of them are summarized, these equations can generally be divided into three types. The first type is the enhancement model that treats two-phase phenomena as a kind of perturbation to single-phase heat transfer and, as a result, such equations utilize a form of single-phase convective heat transfer equations, modified to include boiling impact. The second type is the superposition model or the asymptotic model that uses the superposition or the power-type superposition of convective heat transfer and nucleation-boiling heat transfer to account for two-phase heat transfer. The third type is the nucleation-domination model that contains only a nucleation term or exhibits a heat flux but no mass flux dependence.

Table 5. Equations for boiling heat transfer coefficients

Chen 1966 [48] (pure component, superposition model)	
$h = h_{mac} + h_{mic} = h_l F + h_{pool} S \quad (54)$	
where the liquid heat transfer coefficient h_l is determined as (Dittus and Boelter 1930 [49])	
$h_l = 0.023 \text{Re}_l^{0.8} \text{Pr}_l^{0.4} (k_l / d_i) \quad (55)$	
the pool boiling heat transfer coefficient h_{pool} is determined as (Forster and Zuber 1955 [50])	
$h_{pool} = 0.00122 \frac{\rho_l^{0.49} C_{pl}^{0.45} k_l^{0.79}}{\rho_v^{0.24} \mu_l^{0.29} \nu_{fg}^{0.24} \sigma^{0.5}} \Delta T_{sat}^{0.24} \Delta p_{sat}^{0.75} \quad (56)$	
the effective two-phase Reynolds number factor F is determined as (Edelstein, et al. 1984 [51])	
$F = (1 + X_u^{-0.5})^{1.78} \quad (57)$	
and the bubble-growth suppression factor S is determined as (Edelstein, et al. 1984 [51])	
$S = 0.9622 - 0.5822 \tan^{-1} \left(\frac{F^{1.25} \text{Re}_l}{6.18 \times 10^4} \right) \quad (58)$	
Shah 1976 [52] and Shah 1982 [53] (pure component, enhancement model)	
$h = h_l \max \left[1.8N^{-0.8}, \begin{cases} F \text{Bo}^{0.5} e^{2.47N^{-0.15}} & N < 0.1 \\ F \text{Bo}^{0.5} e^{2.47N^{-0.10}} & 0.1 \leq N < 1.0 \\ \begin{cases} 1 + 46 \text{Bo}^{0.5} & \text{Bo} < 3 \times 10^{-5} \\ 230 \text{Bo}^{0.5} & 3 \times 10^{-5} \leq \text{Bo} \end{cases} & 1.0 \leq N \end{cases} \right] \quad (59)$	
where the liquid heat transfer coefficient h_l is determined as (Dittus and Boelter 1930 [49])	

$$h_i = 0.023 \text{Re}_l^{0.8} \text{Pr}_l^{0.4} (k_l/d_i) \quad (60)$$

the parameter N is determined as

$$N = \begin{cases} 0.38 \text{Co} \text{Fr}_l^{-0.3} & \text{horizontal flow with } \text{Fr}_l < 0.04 \\ \text{Co} & \text{other} \end{cases} \quad (61)$$

and the constant parameter F is determined as

$$F = \begin{cases} 15.43 & \text{Bo} < 1.1 \times 10^{-3} \\ 14.70 & 1.1 \times 10^{-3} \leq \text{Bo} \end{cases} \quad (62)$$

Bennett and Chen 1980 [54] (ethylene glycol/water mixture, superposition model)

$$h = h_{mac} + h_{mic} = h_l F_{\text{Binary}} + h_{pool} S_{\text{Binary}} \quad (63)$$

where the liquid heat transfer coefficient h_l is determined as (Dittus and Boelter 1930 [49])

$$h_l = 0.023 \text{Re}_l^{0.8} \text{Pr}_l^{0.4} (k_l/d_i) \quad (64)$$

the pool boiling heat transfer coefficient h_{pool} is determined as (Forster and Zuber 1955 [50])

$$h_{pool} = 0.00122 \frac{\rho_l^{0.49} C_{pl}^{0.45} k_l^{0.79}}{\rho_v^{0.24} \mu_l^{0.29} i_{fg}^{0.24} \sigma^{0.5}} \Delta T_{sat}^{0.24} \Delta p_{sat}^{0.75} \quad (65)$$

the effective two-phase Reynolds number factor F_{Binary} is determined from the same F as defined in the Chen equation (Chen 1966 [48])

$$F_{\text{Binary}} = \left\{ 1 - \frac{(1 - F_v) \dot{q}''}{[0.023 \text{Re}_l^{0.8} \text{Sc}_l^{0.4} (D_l/d_i) \rho_l i_{fg} \Delta T_{sat}] \text{Pr}_l^{0.296} F} \frac{\partial T_{sat}}{\partial F_l} \right\} \text{Pr}_l^{0.296} F \quad (66)$$

and the suppression factor S_{Binary} is determined from the same S as defined in the Chen equation (Scriven 1959 [55]; Chen 1966 [48])

$$S_{\text{Binary}} = \frac{1}{1 - (F_v - F_l) [C_{pl} (\partial T_{sat} / \partial F_l) / i_{fg}] (\kappa_l / D_l)^{0.5}} S \quad (67)$$

Mishra, et al.1981 [56] (R12/R22 mixture, enhancement model)

$$h = A X_a^{-m} \text{Bo}^n (1 - x)^{-0.8} h_l \quad (68)$$

where the liquid heat transfer coefficient h_l is determined as (Dittus and Boelter 1930 [49])

$$h_l = 0.023 \text{Re}_l^{0.8} \text{Pr}_l^{0.4} (k_l/d_i) \quad (69)$$

and A , m , and n are mixture-mass-concentration-ratio-dependent parameters.

Bjorge, et al.1981 [57] (pure component, superposition model)

$$h = \{ \dot{q}_{FC}'' + \dot{q}_B'' [1 - (\Delta T_{sat,ib} / \Delta T_{sat})^3] \} / \Delta T_{sat} \quad (70)$$

where the forced convection heat flux \dot{q}_{FC}'' is determined as (Traviss, et al. 1972 [58])

$$\dot{q}_{FC}'' = \frac{\text{Re}_l^{0.9} \text{Pr}_l (k_l/d_l) [0.15(X_u^{-1} + 2.0X_u^{-0.32})]}{F_2} \Delta T_{sat} \quad (71)$$

with the parameter F_2 being determined as

$$F_2 = \begin{cases} 0.0707 \text{Pr}_l \text{Re}_l^{0.5} & \text{Re}_l < 50 \\ 5 \text{Pr}_l + 5 \ln[1 + \text{Pr}_l (0.0964 \text{Re}_l^{0.585} - 1)] & 50 \leq \text{Re}_l < 1125 \\ 5 \text{Pr}_l + 5 \ln(1 + 5 \text{Pr}_l) + 2.5 \ln(0.0031 \text{Re}_l^{0.812}) & 1125 \leq \text{Re}_l \end{cases} \quad (72)$$

the boiling heat flux \dot{q}_b'' is determined as (Mikic and Rohsenow 1969 [59])

$$\dot{q}_b'' = B_M \frac{\rho_l^{1.7/8} \rho_v^{1/8} C_{pl}^{1.9/8} k_l^{1/2} i_{fg}^{1/8}}{(\rho_l - \rho_v)^{9/8} \sigma^{5/8} T_{sat}^{1/8} \sqrt{\sigma/[g(\rho_l - \rho_v)]}} \Delta T_{sat}^3 \quad (73)$$

with the fluid-dependent parameter $B_M = 1.89 \times 10^{-14}$ for water boiling, and the wall superheat value at the incipient boiling point is determined from the forced convection heat transfer coefficient h_{FC} as (Bergles and Rohsenow 1964 [60])

$$\Delta T_{sat,b} = \frac{8(1/\rho_v - 1/\rho_l) \sigma T_{sat} h_{FC}}{k_l i_{fg}} \quad (74)$$

Lazarek and Black 1982 [61] (pure component, nucleation-domination model)

$$h = 30(Gd_i/\mu_l)^{0.857} \text{Bo}^{0.714} (k_l/d_i) \quad (75)$$

Gungor and Winterton 1986 [62] (pure component, superposition model)

$$h = h_l E + h_{pool} S \quad (76)$$

where the liquid heat transfer coefficient h_l is determined as (Dittus and Boelter 1930 [49])

$$h_l = 0.023 \text{Re}_l^{0.8} \text{Pr}_l^{0.4} (k_l/d_i) \quad (77)$$

the pool boiling heat transfer coefficient h_{pool} is determined as (Cooper 1984 [63])

$$h_{pool} = 55 p_r^{0.12} (-\log_{10} p_r)^{-0.55} M^{-0.5} \dot{q}''^{2/3} \quad (78)$$

the enhancement factor E is determined as

$$E = \begin{cases} (1 + 24000 \text{Bo}^{1.16} + 1.37 X_u^{-0.86}) \text{Fr}_l^{0.1-2\text{Fr}_l} & \text{horizontal flow with } \text{Fr}_l < 0.05 \\ 1 + 24000 \text{Bo}^{1.16} + 1.37 X_u^{-0.86} & \text{other} \end{cases} \quad (79)$$

and the suppression factor S is determined as

$$S = \begin{cases} (1 + 1.15 \times 10^{-6} E^2 \text{Re}_l^{1.17})^{-1} \text{Fr}_l^{0.5} & \text{horizontal flow with } \text{Fr}_l < 0.05 \\ (1 + 1.15 \times 10^{-6} E^2 \text{Re}_l^{1.17})^{-1} & \text{other} \end{cases} \quad (80)$$

Klimenko 1988 [64] and Klimenko 1990 [65] (pure component, nucleation-domination model)

$$h = C \dot{q}_b'' \sqrt{\sigma/[g(\rho_l - \rho_v)]} / (\rho_v k_l i_{fg})^{0.3} \sqrt{\sigma/[g(\rho_l - \rho_v)]} / \sigma^{0.34} \text{Pr}_l^{-0.33} (k_w/k_l)^{0.12} k_l \sqrt{\sigma/[g(\rho_l - \rho_v)]} \quad (81)$$

where the fluid-dependent parameter C has a value between 4.9×10^{-3} for water boiling and 7.6×10^{-3} for freon boiling.

Jung, et al. 1989 [66] (R22/R114 and R12/R152a mixtures, superposition model)

$$h = h_l F + h_{pool} N \quad (82)$$

where the liquid heat transfer coefficient h_l is determined as (Dittus and Boelter 1930 [49])

$$h_l = 0.023 \text{Re}_l^{0.8} \text{Pr}_l^{0.4} (k_l/d_l) \quad (83)$$

the pool boiling heat transfer coefficient h_{pool} is determined from the component pool boiling heat transfer coefficients h_{pool1} and h_{pool2} calculated by the Stephan-Abdelsalam equations for various fluids (Stephan and Abdelsalam 1980 [67])

$$h_{pool} = \left(\frac{Y_{l1}}{h_{pool1}} + \frac{Y_{l2}}{h_{pool2}} \right)^{-1} \quad (84)$$

the enhancement factor F is determined as

$$F = \begin{cases} 2.37(0.29 + X_u^{-1})^{0.85} & \text{for pure component} \\ 2.37(0.29 + X_u^{-1})^{0.85} (1 - 0.35|Y_v - Y_l|^{1.56}) & \text{for mixture} \end{cases} \quad (85)$$

and the suppression factor N is determined from the reduced pressure p_r of the more volatile component

$$N = \begin{cases} 4048 X_u^{1.22} \text{Bo}^{1.13} & \text{for pure component} \\ \frac{4048 X_u^{1.22} \text{Bo}^{1.13}}{[1 + b(1 + 152 p_r^{3.9})]^2 (1 + 0.92|Y_v - Y_l|^{0.001} p_r^{0.66})^2} & \text{for mixture} \end{cases} \quad (86)$$

with the parameter b being determined from the molar concentration Y of the more volatile component (Ünal 1986 [68])

$$b = \begin{cases} (1 - Y_l) \ln[(1.01 - Y_l)/(1.01 - Y_v)] + Y_l \ln(Y_l/Y_v) + |Y_v - Y_l|^{1.5} + (Y_v/Y_l)^{0.1} - 1 & Y_l < 0.01 \\ (1 - Y_l) \ln[(1.01 - Y_l)/(1.01 - Y_v)] + Y_l \ln(Y_l/Y_v) + |Y_v - Y_l|^{1.5} & 0.01 \leq Y_l \end{cases} \quad (87)$$

Kandlikar 1990 [69] (pure component, enhancement model)

$$h = h_l \max[.1360 \text{Co}^{-0.9} f(\text{Fr}_l) + 667.2 \text{Bo}^{0.7} F_\beta, 0.6683 \text{Co}^{-0.2} f(\text{Fr}_l) + 1058.0 \text{Bo}^{0.7} F_\beta] \quad (88)$$

where the liquid heat transfer coefficient h_l is determined as (Dittus and Boelter 1930 [49])

$$h_l = 0.023 \text{Re}_l^{0.8} \text{Pr}_l^{0.4} (k_l/d_l) \quad (89)$$

the Froude number multiplier function $f(\text{Fr}_l)$ is determined as

$$f(\text{Fr}_l) = \begin{cases} (25 \text{Fr}_l)^{0.3} & \text{horizontal flow with } \text{Fr}_l < 0.04 \\ 1 & \text{other} \end{cases} \quad (90)$$

and the fluid-dependent parameter F_β has a value between 1.00 for water boiling and 4.70 for nitrogen boiling.

Murata and Hashizume 1990 [70] (R11/R114 mixture, superposition model)

$$h = h_l F + h_{pool} S \quad (91)$$

where the liquid heat transfer coefficient h_l is determined as (Dittus and Boelter 1930 [49])

$$h_l = 0.023 \text{Re}_l^{0.8} \text{Pr}_l^{0.4} (k_l/d_l) \quad (92)$$

the pool boiling heat transfer coefficient h_{pool} is determined as (Stephan and Körner 1969 [71])

$$h_{pool} = \frac{Y_{l1}h_{pool1} + Y_{l2}h_{pool2}}{1 + 1.65|Y_v - Y_l|} \quad (93)$$

the enhancement factor F is determined as

$$F = 2.44X_u^{-0.863} \quad (94)$$

and the suppression factor S is determined as (Bennett, et al. 1980 [72])

$$S = \frac{1 - e^{-4.49 \times 10^{-3} \text{Re}_l^{0.8} \text{Pr}_l^{0.4} X_u^{-0.863} \{\sqrt{\sigma/[g(\rho_l - \rho_v)]}/d_i\}}}{4.49 \times 10^{-3} \text{Re}_l^{0.8} \text{Pr}_l^{0.4} X_u^{-0.863} \{\sqrt{\sigma/[g(\rho_l - \rho_v)]}/d_i\}} \quad (95)$$

Takamatsu, et al. 1990 [73] (R22/R114 mixture, enhancement model)

$$h = h_l(C_1 \text{Bo} \times 10^4 + C_2 X_u^{-C_3}) \quad (96)$$

where the liquid heat transfer coefficient h_l is determined as (Dittus and Boelter 1930 [49])

$$h_l = 0.023 \text{Re}_l^{0.8} \text{Pr}_l^{0.4} (k_l/d_i) \quad (97)$$

the coefficient C_1 is determined as

$$C_1 = 1.60 - 8.08Y_{R114} + 22.0Y_{R114}^2 - 28.4Y_{R114}^3 + 14.2Y_{R114}^4 \quad (98)$$

the coefficient C_2 is determined as

$$C_2 = 6.71 - 13.0Y_{R114} + 28.2Y_{R114}^2 - 37.5Y_{R114}^3 + 20.0Y_{R114}^4 \quad (99)$$

and the exponent C_3 is determined as

$$C_3 = 0.95 - 1.91Y_{R114} + 5.92Y_{R114}^2 - 6.67Y_{R114}^3 + 2.66Y_{R114}^4 \quad (100)$$

Liu and Winterton 1991 [74] (pure component, asymptotic model)

$$h = [(h_l F)^2 + (h_{pool} S)^2]^{1/2} \quad (101)$$

where the liquid heat transfer coefficient h_l is determined as (Dittus and Boelter 1930 [49])

$$h_l = 0.023 (Gd_i/\mu_l)^{0.8} \text{Pr}_l^{0.4} (k_l/d_i) \quad (102)$$

the pool boiling heat transfer coefficient h_{pool} is determined as (Cooper 1984 [63])

$$h_{pool} = 55 p_r^{0.12} (-\log_{10} P_r)^{-0.55} M^{-0.5} \dot{q}^{2/3} \quad (103)$$

the forced convective heat transfer enhancement factor F is determined as

$$F = \begin{cases} [1 + x \text{Pr}_l(\rho_l/\rho_v - 1)]^{0.35} \text{Fr}_l^{0.1-2\text{Fr}_l} & \text{horizontal flow with } \text{Fr}_l < 0.05 \\ [1 + x \text{Pr}_l(\rho_l/\rho_v - 1)]^{0.35} & \text{other} \end{cases} \quad (104)$$

and the suppression factor S is determined as

$$S = \begin{cases} [1 + 0.055 F^{0.1} (Gd_i/\mu_l)^{0.16}]^{-1} \text{Fr}_l^{0.5} & \text{horizontal flow with } \text{Fr}_l < 0.05 \\ [1 + 0.055 F^{0.1} (Gd_i/\mu_l)^{0.16}]^{-1} & \text{other} \end{cases} \quad (105)$$

Steiner and Taborek 1992 [75] (pure component, asymptotic model)

$$h = [(h_l F)^3 + (h_{p_{oo0}} S)^3]^{1/3} \quad (106)$$

where the liquid heat transfer coefficient h_l is determined as (Gnielinski 1975 [15])

$$h_l = \frac{\{8[1.82 \log(Gd_i/\mu_l) - 1.64]^2\}^{-1} [(Gd_i/\mu_l) - 1000] Pr_l}{1 + 12.7\{8[1.82 \log(Gd_i/\mu_l) - 1.64]^2\}^{-1/2} (Pr_l^{2/3} - 1)} (k_l/d_i) \quad (107)$$

the nucleate pool boiling heat transfer coefficient $h_{p_{oo0}}$ at the normalized conditions of $p_{r0} = 0.1$, $\dot{q}''_{a0} = 20000$ W/m², $d_{i0} = 0.01$ m, and $R_{a0} = 1$ μm is determined as (Gorenflo 1988 [76])

$$h_{p_{oo0}} = h_{p_{oo0}} [1/F_{01}(p_r)] (\dot{q}''_0/\dot{q}''_0)^{F_{02}(p_r)} (R_{a0}/R_a)^{0.133} \quad (108)$$

with the reduced pressure-related parameter $F_{01}(p_r)$ being determined as

$$F_{01}(p_r) = \begin{cases} 1.73 p_r^{0.27} + [6.1 + 0.68/(1 - p_r)] p_r^2 & \text{water} \\ 1.2 p_r^{0.27} + [2.5 + 1/(1 - p_r)] p_r & \text{other} \end{cases} \quad (109)$$

the reduced pressure-related parameter $F_{02}(p_r)$ being determined as

$$F_{02}(p_r) = \begin{cases} 0.9 - 0.3 p_r^{0.15} & \text{water} \\ 0.9 - 0.3 p_r^{0.3} & \text{other} \end{cases} \quad (110)$$

and the nucleate pool boiling heat transfer coefficient $h_{p_{ool}}$ at other than the normalized conditions being calculated from prediction equations or data, the two-phase flow convective factor F is determined from the total flow liquid and vapor heat transfer coefficients h_l and h_v as

$$F = \begin{cases} [(1-x)^{1.5} + 1.9x^{0.6}(\rho_l/\rho_v)^{0.35}]^{1.1} & x < 0.6 \\ [(1-x)^{1.5} + 1.9x^{0.6}(1-x)^{0.01}(\rho_l/\rho_v)^{0.35}]^{-2.2} + \{(h_v/h_l)x^{0.01}[1 + 8(1-x)^{0.7}(\rho_l/\rho_v)^{0.67}]\}^{-2} & 0.6 \leq x \end{cases} \quad (111)$$

and the nucleate flow boiling correction factor S is determined as (Steiner 1988 [77])

$$S = \{2.816 p_r^{0.45} + [3.4 + 1.7/(1 - p_r^7)] p_r^{3.7}\} (\dot{q}''/\dot{q}''_0)^{F(p_r)} (d_i/d_{i0})^{-0.4} (R_a/R_{a0})^{0.133} F(M) \quad (112)$$

with the reduced pressure-related parameter $F(p_r)$ being determined as

$$F(p_r) = \begin{cases} 0.7 - 0.13 e^{1.105 p_r} & \text{cryogenics} \\ 0.8 - 0.1 e^{1.75 p_r} & \text{other} \end{cases} \quad (113)$$

and the molecular mass-related parameter $F(M)$ being determined as

$$F(M) = \begin{cases} 0.377 + 0.199 \ln M + 2.8427 \times 10^{-5} M^2 & 10 \leq M, F(M) \leq 2.5 \\ 0.36 M^{0.27} & \text{other} \end{cases} \quad (114)$$

Tran, et al. 1996 [29] (pure component, nucleation-domination model)

$$h = 8.4 \times 10^5 (\text{Bo}^2 \text{We}_l)^{0.3} (\rho_v/\rho_l)^{0.4} \quad (115)$$

Yu, et al. 2002 [27] (pure component, nucleation-domination model)

$$h = 6.4 \times 10^6 (\text{Bo}^2 \text{We}_l)^{0.27} (\rho_v/\rho_l)^{0.2} \quad (116)$$

Yu, et al. 2005 [28] (ethylene glycol/water mixture, nucleation-domination model)

$$h = 1.35 \times 10^5 (\text{Bo}^2 \text{We}_t)^{0.25} [(\rho_v / \rho_l)^{0.5} (\mu_l / \mu_v)^{0.7}]^{-1.5} \quad (117)$$

6.2. Boiling Heat Transfer Coefficient Comparison

6.2.1. Water Boiling

Eight equations from the engineering literature are chosen to analyze the experimental heat transfer coefficients of water and EG/W mixture flow boiling of this study [48, 52-53, 57, 62, 64-65, 69, 74, 28]. In Figures 20–27, the experimental heat transfer coefficients of water flow boiling of this study are compared to the predictions from these equations. It can be seen from Figures 20–27 that (a) all equations correctly predict the trend of the experimental heat transfer coefficients of water flow boiling of this study, which is expected because the heat transfer coefficient databases for water flow boiling are always used in developing these equations; (b) generally, the predictions for vertical water flow boiling are better than those for horizontal water flow boiling, which may be explained by the fact that vertical flow boiling is more stable than horizontal flow boiling due to the symmetrical boiling condition without gravitational effects; and (c) for vertical water flow boiling, almost all equations predict the experimental heat transfer coefficients reasonably well, while for horizontal water flow boiling, the Gungor-Winterton equation [62] gives the best prediction for the experimental heat transfer coefficients of this study.

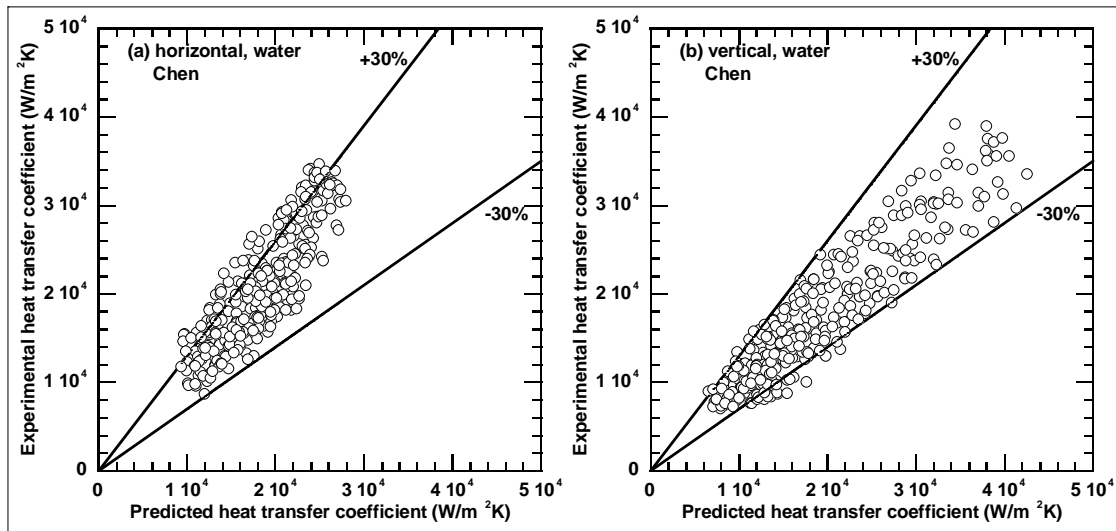


Figure 20. Heat transfer coefficient comparison

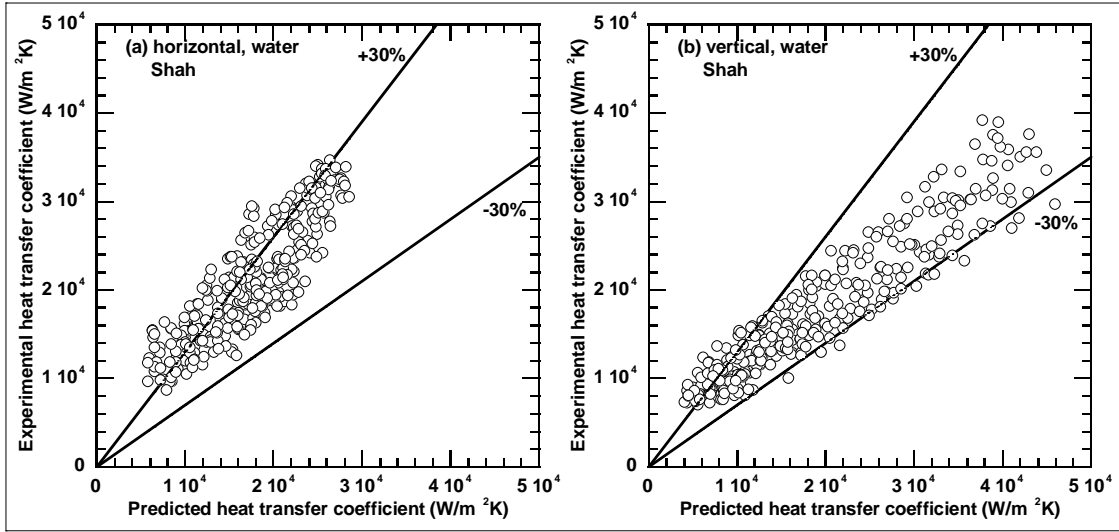


Figure 21. Heat transfer coefficient comparison

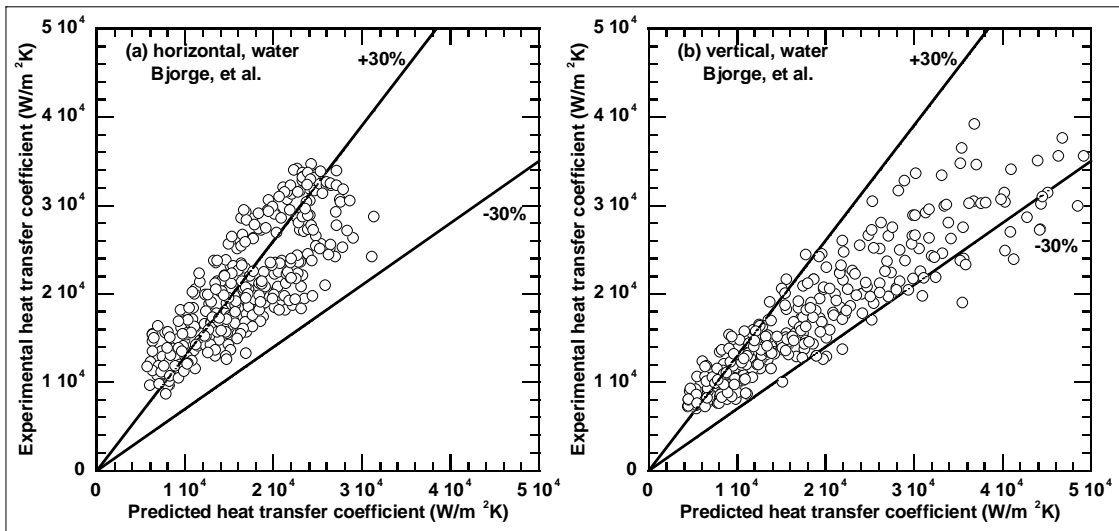


Figure 22. Heat transfer coefficient comparison

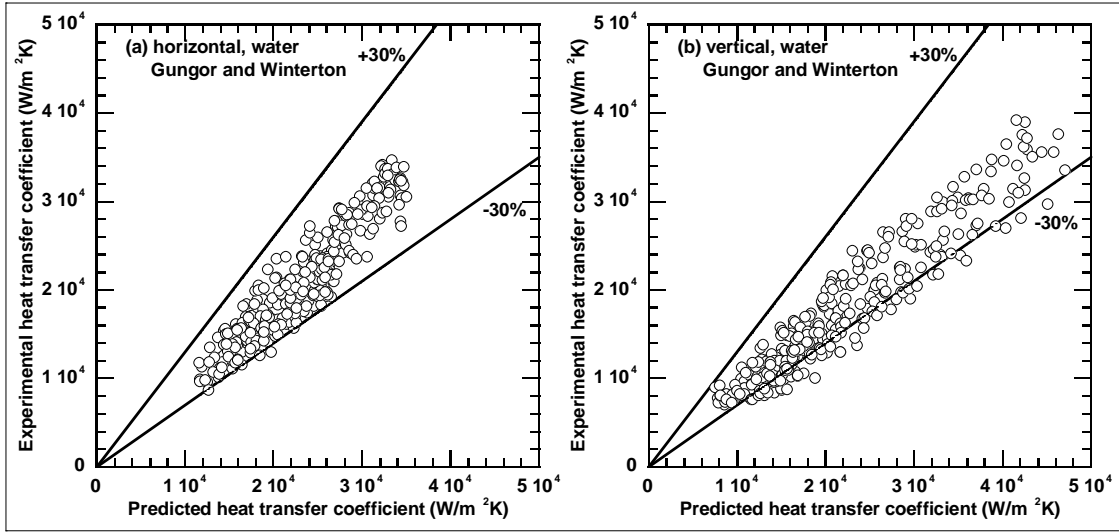


Figure 23. Heat transfer coefficient comparison

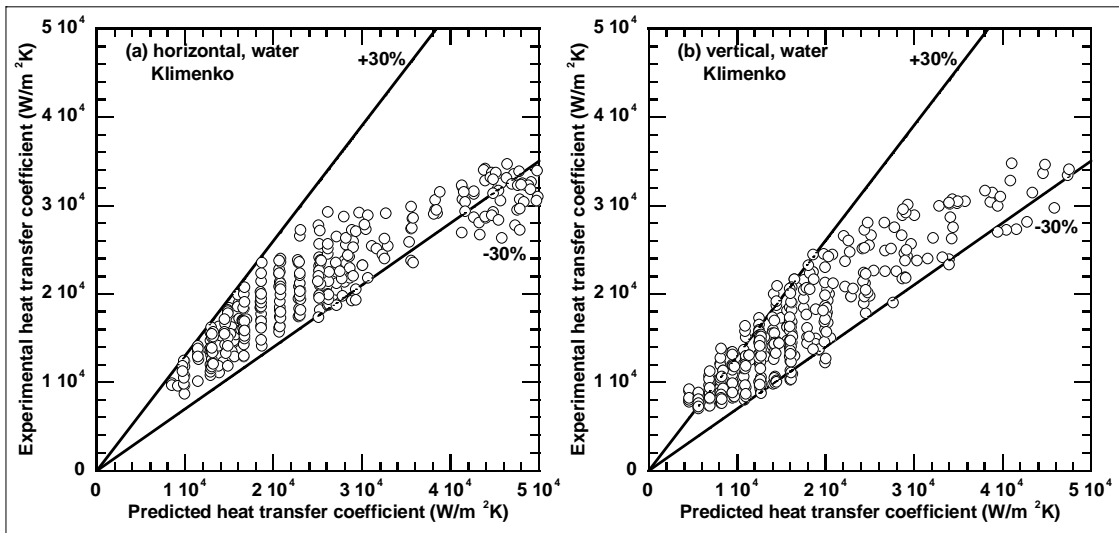


Figure 24. Heat transfer coefficient comparison

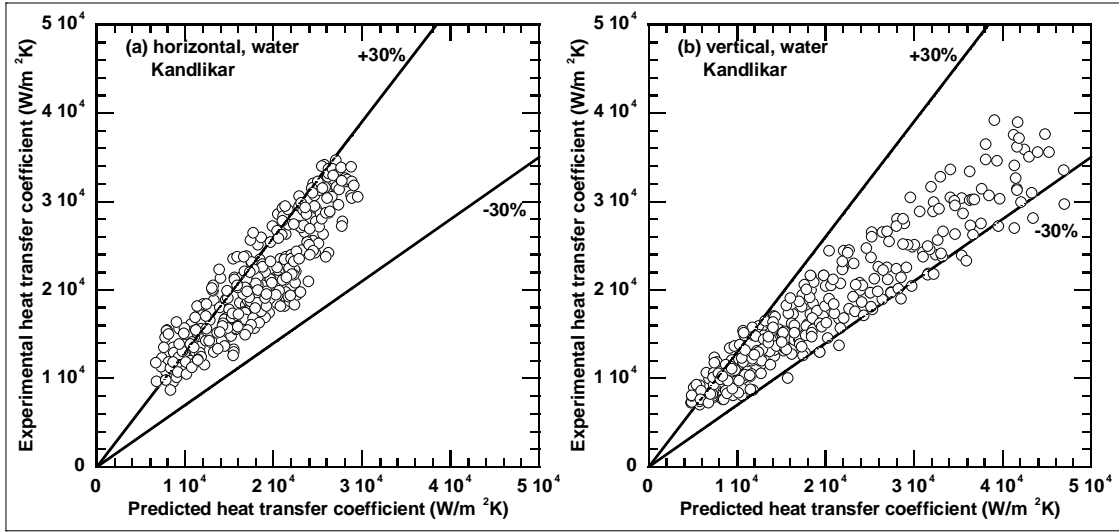


Figure 25. Heat transfer coefficient comparison

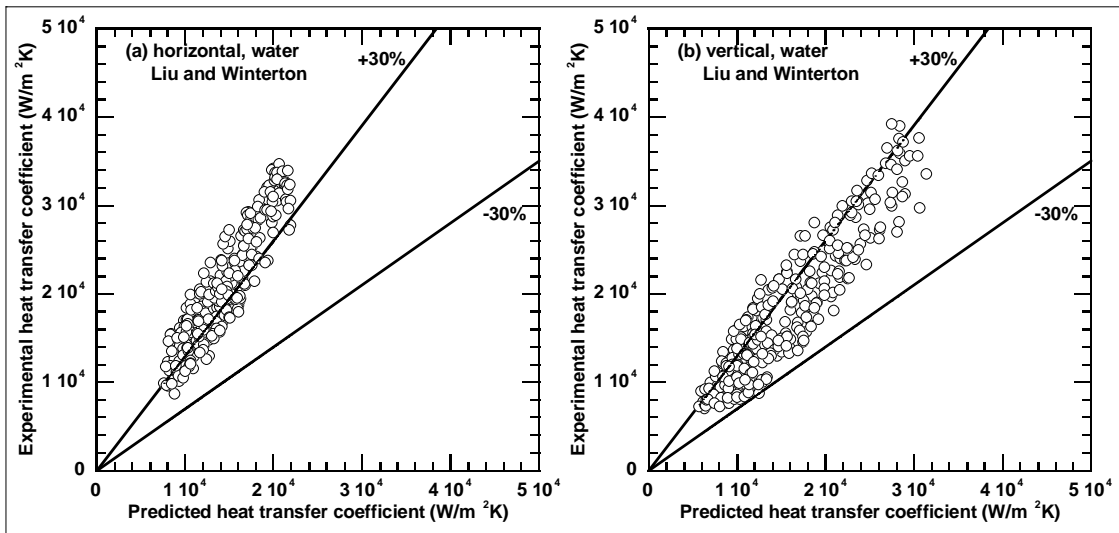


Figure 26. Heat transfer coefficient comparison

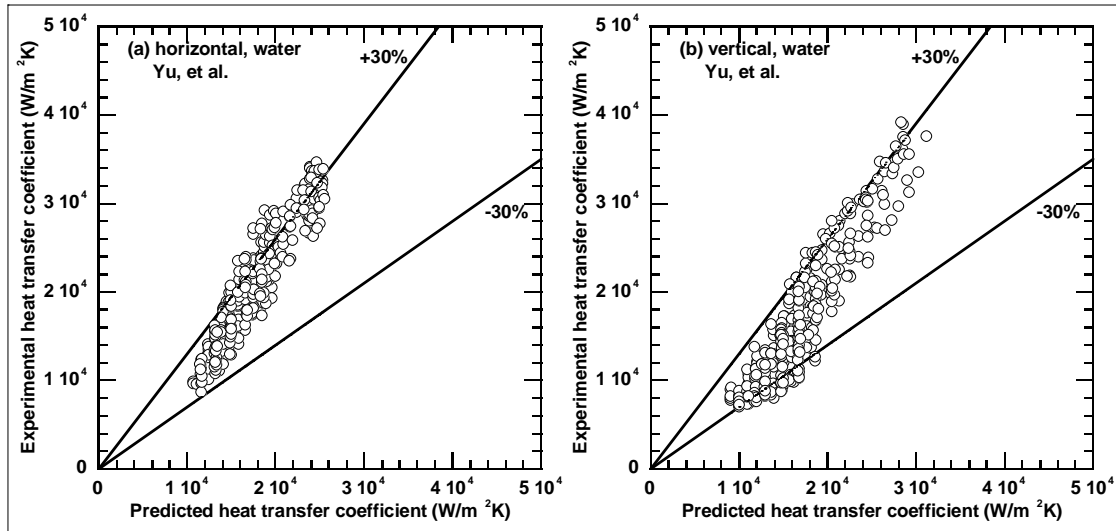


Figure 27. Heat transfer coefficient comparison

6.2.2. Ethylene Glycol/Water Mixture Boiling

The experimental heat transfer coefficients of EG/W mixture flow boiling of this study are also compared with the predictions from the same eight equations. The empirical parameters for the Klimenko equation [64-65] and the Kandlikar equation [69] are chosen to be the same as water flow boiling. It can be seen from Figures 28–35 that the predictions for the experimental heat transfer coefficients of EG/W mixture flow boiling of this study generally are not satisfied, which may be due to the fact that the complicated boiling conditions of two- or multi-component fluids such as EG/W mixtures are not taken into account in developing most of these equations. The best predictions for the experimental heat transfer coefficients of EG/W mixture flow boiling of this study are given by the equation developed based on the horizontal water and 50/50 EG/W mixture flow boiling data by Yu, et al. [28], but the discrepancy between the experimental data and the predicted values are still rather large. Therefore, further data analyses and correlation developments are necessary.

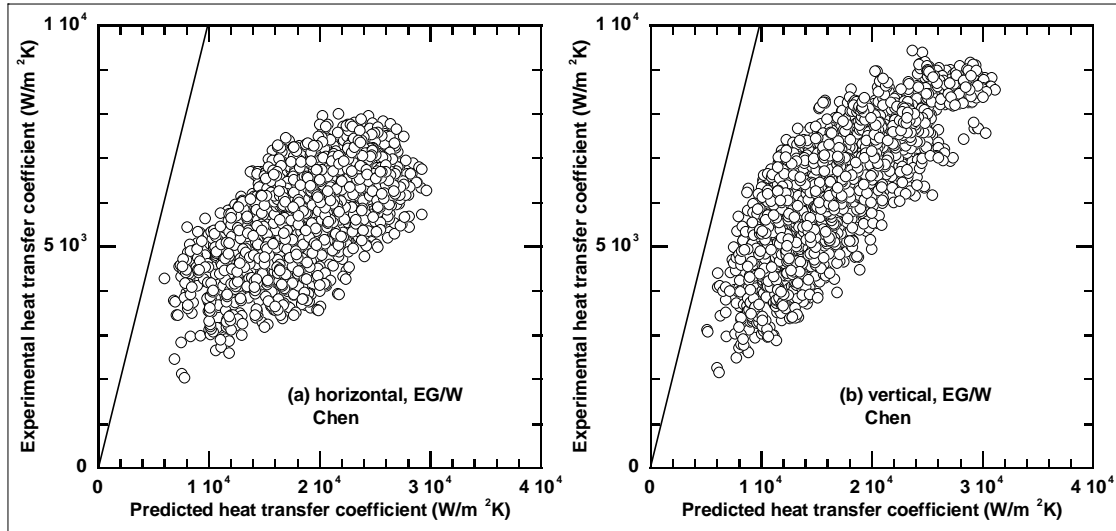


Figure 28. Heat transfer coefficient comparison

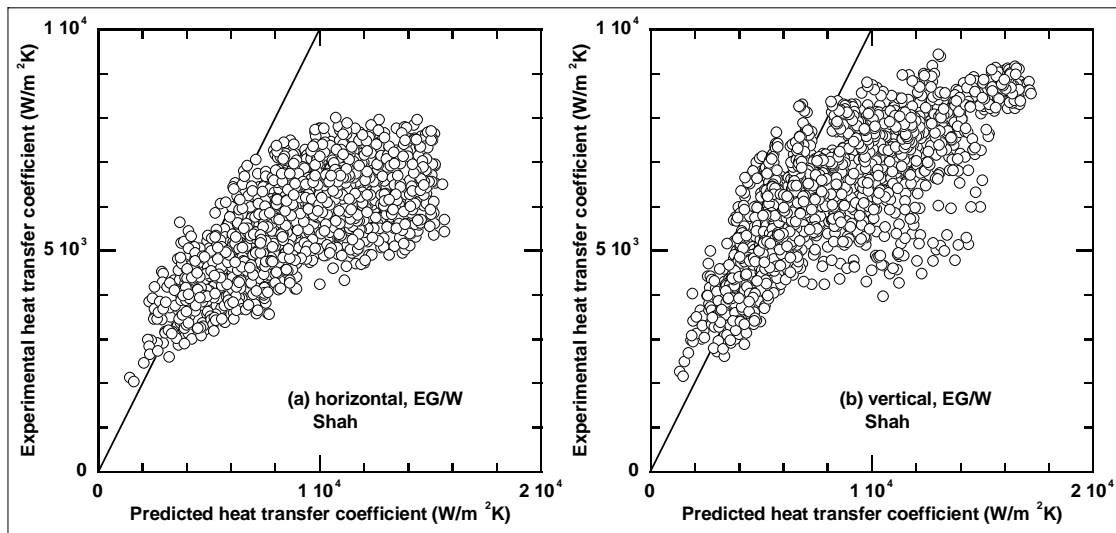


Figure 29. Heat transfer coefficient comparison

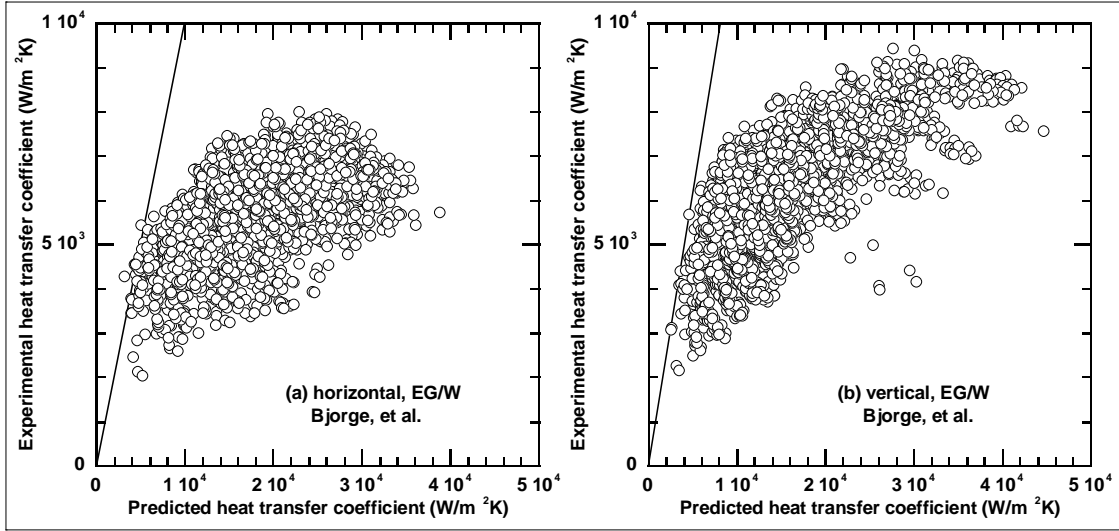


Figure 30. Heat transfer coefficient comparison

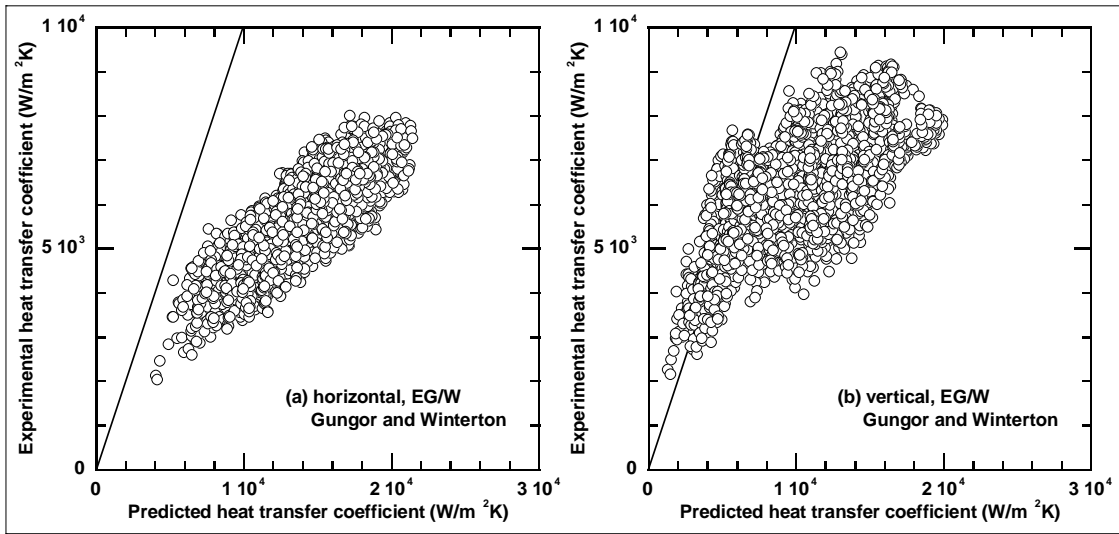


Figure 31. Heat transfer coefficient comparison

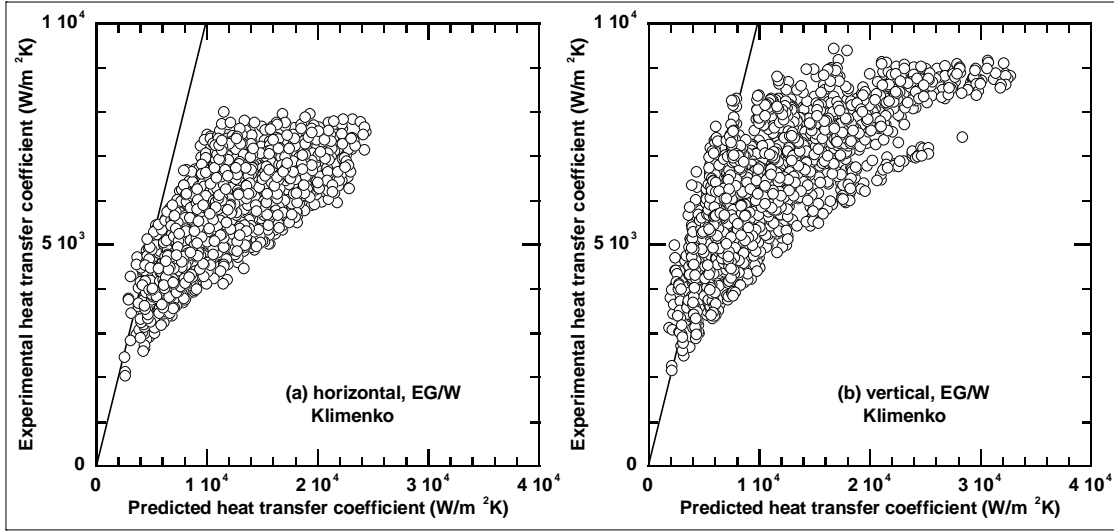


Figure 32. Heat transfer coefficient comparison

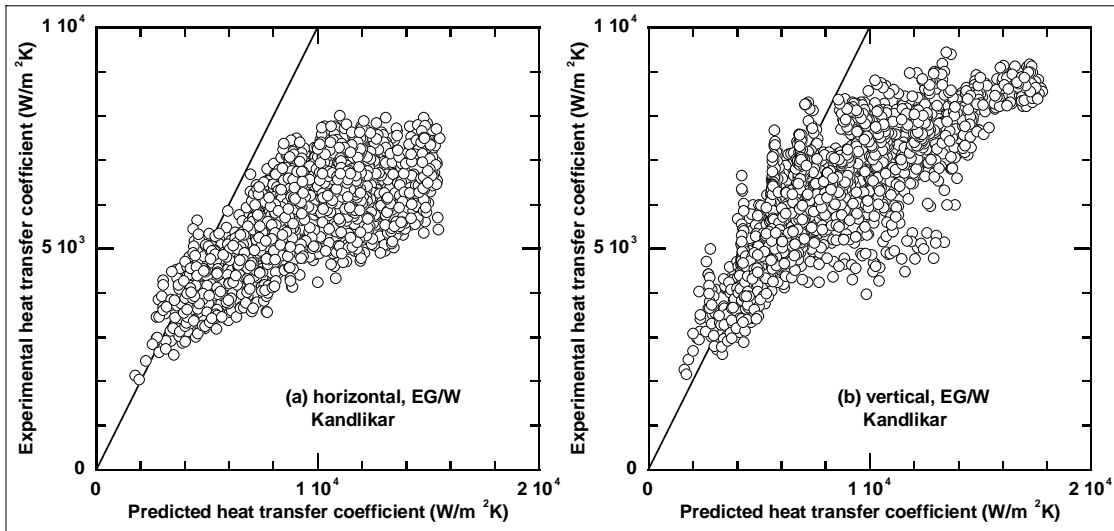


Figure 33. Heat transfer coefficient comparison

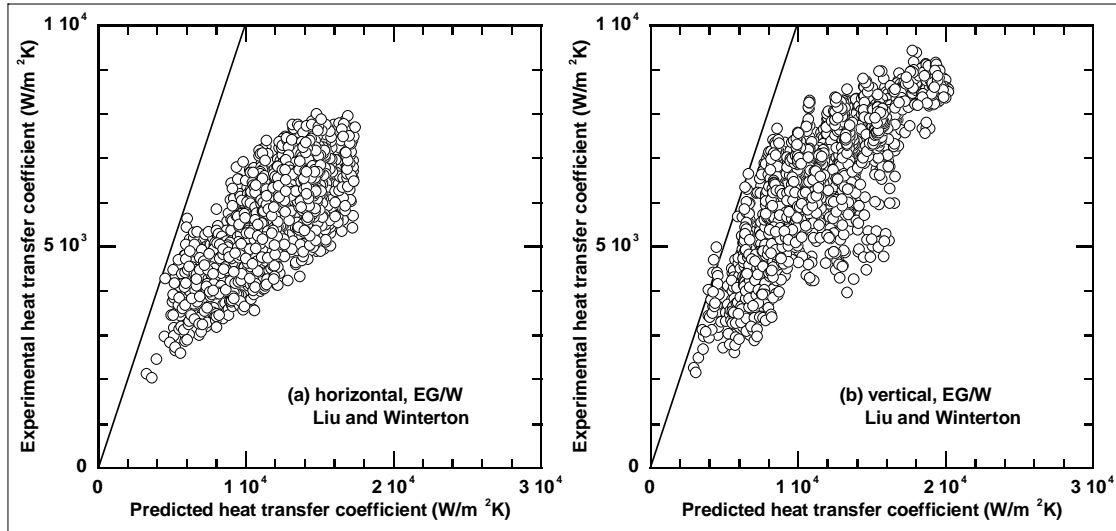


Figure 34. Heat transfer coefficient comparison

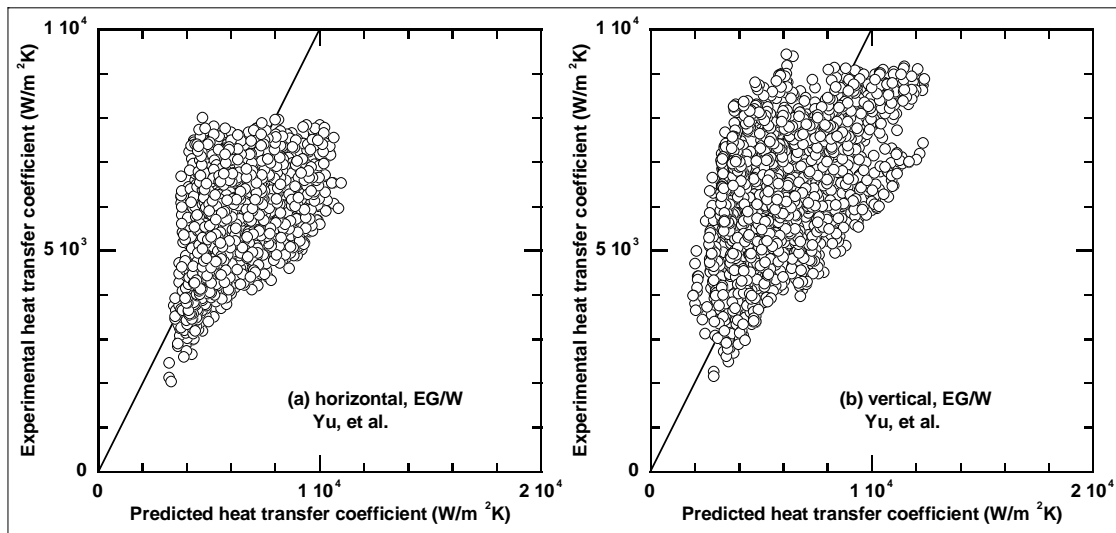


Figure 35. Heat transfer coefficient comparison

6.3. Correlation of Experimental Boiling Heat Transfer Coefficient

6.3.1. General Considerations

In correlating the experimental boiling heat transfer coefficients of this study, the following facts are taken into account: (a) the goal is to develop simple and practically useful equations to predict the experimental heat transfer coefficients for water and EG/W mixture flow boiling of this study; (b) while both the convective heat transfer and the nucleate boiling heat transfer exist, the dominant heat transfer mechanism for the experimental data of this study is nucleate boiling, which means that the convective heat transfer, much lower than the nucleate boiling heat transfer

in magnitude, can be neglected; (c) as shown previously, the boiling heat transfer is dependent on the heat flux but almost independent of the mass flux, which means that, for a certain fluid in this study, the boiling heat transfer coefficient can be expressed as a function of the heat flux; and (d) the heat transfer coefficients have different dependence on the heat flux for different fluids and therefore it is necessary to include the fluid thermal properties or the ethylene glycol volume concentration or both to get a general equation for predicting all boiling heat transfer coefficients of this study.

6.3.2. Equation for All Experimental Data

A prediction equation for the boiling heat transfer coefficient was developed based on the experimental heat transfer coefficients of water and EG/W mixture flow boiling of this study through the following steps.

(a) Based on the characteristics of the experimental boiling heat transfer coefficients of this study, a dimensionless combination form ($BoWe_l^{0.5}$) of Boiling number Bo and liquid Weber number We_l was chosen to be the primary correlating parameter [27-29]. It can be seen from Figure 36, where the experimental boiling heat transfer coefficients for both the horizontal flow and the vertical flow are plotted as a function of $BoWe_l^{0.5}$, that the heat transfer coefficients of water and EG/W flow boiling of this study follow certain but different trends quite well.

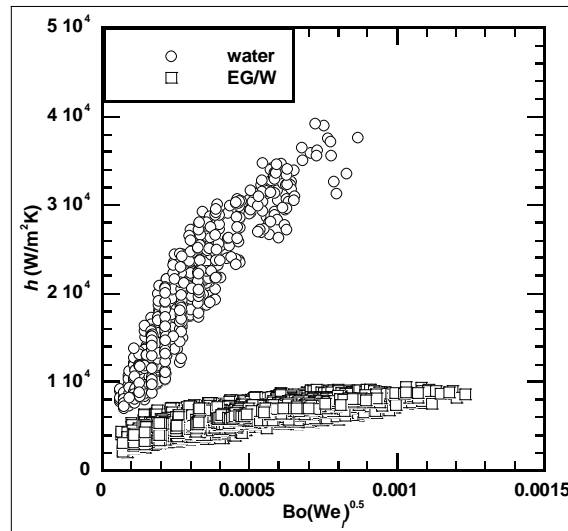


Figure 36. h as a function of $Bo(We_l)^{0.5}$

(b) The experimental boiling heat transfer coefficients were nondimensionalized by dividing them by the combination form (k_l/d_i) of the liquid thermal conductivity k_l of the experimental fluids and the inside diameter d_i of the experimental test section. As it can be seen from Figure 37, where $h/(k_l/d_i)$ is plotted as a function of $BoWe_l^{0.5}$, that this process not only narrowed the distribution range of the experimental boiling heat transfer coefficients but also reduced the

experimental boiling heat transfer coefficient gap between water flow boiling and EG/W mixture flow boiling.

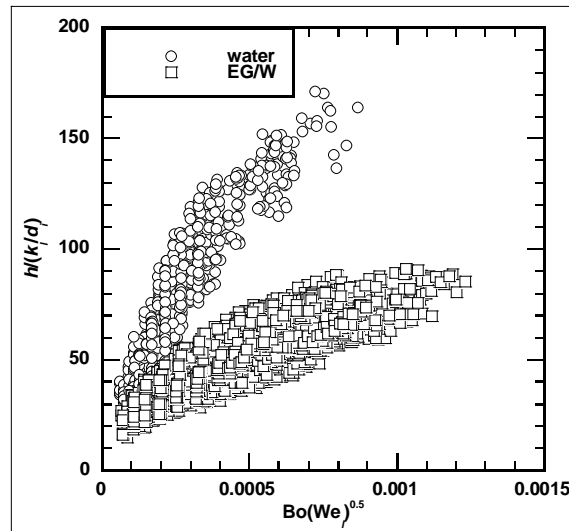


Figure 37. $h/(k_l/d_l)$ as a function of $Bo(We)^{0.5}$

(c) Various combinations of the thermal properties and the ethylene glycol volume concentration of the experimental fluids were tested in an attempt to merge the experimental heat transfer coefficients of water flow boiling and EG/W mixture flow boiling of this study, and it was found that a simple exponential factor ($e^{1.25V_{EG}}$) of the ethylene glycol volume concentration V_{EG} works quite well as shown in Figure 38, where $he^{1.25V_{EG}}/(k_l/d_l)$ is plotted as a function of $BoWe^{0.5}$. This exponential factor reduces to unity for pure water with the ethylene glycol volume concentration of zero.

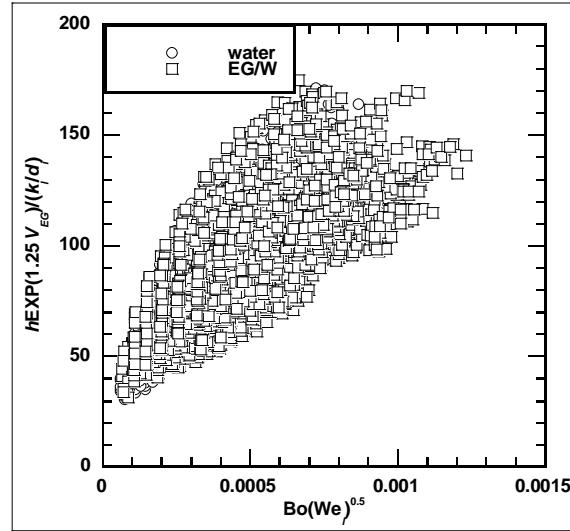


Figure 38. $h_{EXP}(1.25V_{EG})/(k_l/d_i)$ as a function of $Bo(We_p)^{0.5}$

(d) The final equation developed based on the experimental heat transfer coefficients of water and EG/W mixture boiling in both the horizontal flow and the vertical flow of this study is

$$h = 320Qe^{-1.25V_{EG}} (BoW\dot{\xi}^{0.5})^{0.45} (k_l/d_i) \quad (118)$$

As it can be seen from Figure 39, where the experimental boiling heat transfer coefficients are compared with the predictions of the above equation, this equation predicts the experimental boiling heat transfer coefficients of this study reasonably well with mean deviations of 22% for water flow boiling, 25% for EG/W mixture flow boiling, and 25% for overall water and EG/W mixture flow boiling, and the majority of the experimental boiling heat transfer coefficients are within $\pm 30\%$ of the predictions.

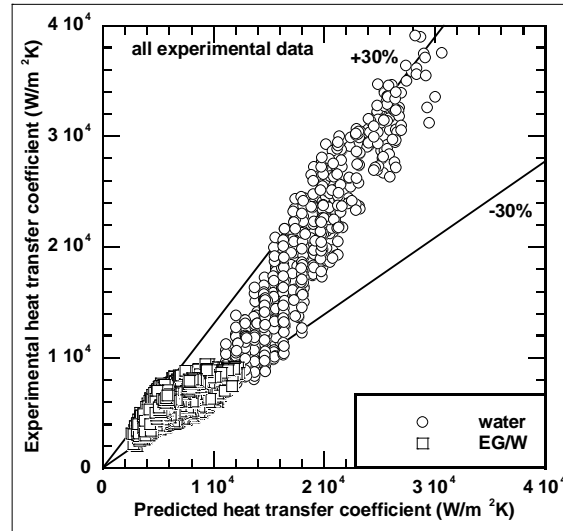


Figure 39. Heat transfer coefficient comparison

6.3.3. Equation for Water Boiling

The prediction accuracy can be improved if the experimental heat transfer coefficients of water flow boiling and EG/W mixture flow boiling of this study are separately correlated, which eliminates the need to merge them together. The final equation developed based on the experimental heat transfer coefficients of water boiling in both the horizontal flow and the vertical flow of this study is

$$h = 25770(\text{Bo} \text{We}_q^{0.5})^{0.7} (k_f/d_i) \quad (119)$$

As it can be seen from Figure 40, where the experimental boiling heat transfer coefficients are compared with the predictions of the above equation, this equation predicts the experimental boiling heat transfer coefficients of this study reasonably well with a mean deviation of 16% and the most of the experimental boiling heat transfer coefficients are within $\pm 30\%$ of the predictions.

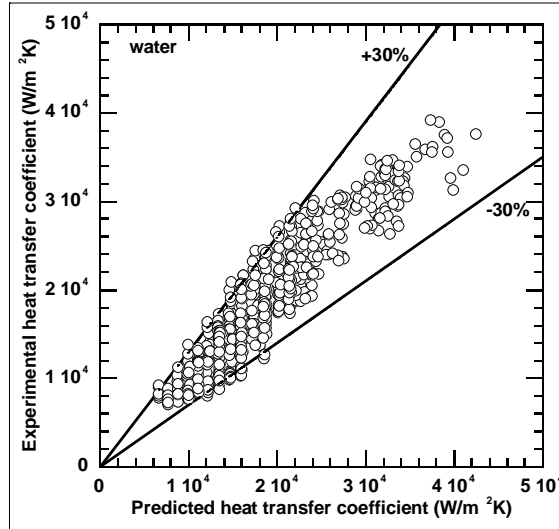


Figure 40. Heat transfer coefficient comparison

6.3.4. Equation for Ethylene Glycol/Water Mixture Boiling

The final equation developed based on the experimental heat transfer coefficients of EG/W mixture boiling in both the horizontal flow and the vertical flow of this study is

$$h = 1650(BoW\dot{q}^{0.5})^{0.45}(k_l/d_i) \quad (120)$$

As it can be seen from Figure 41, where the experimental boiling heat transfer coefficients are compared with the predictions of the above equation, this equation predicts the experimental boiling heat transfer coefficients of this study reasonably well with mean deviations of 16% for the horizontal flow, 13% for the vertical flow, and 14% for overall EG/W mixture flow boiling, and the majority of the experimental boiling heat transfer coefficients are within $\pm 30\%$ of the predictions.

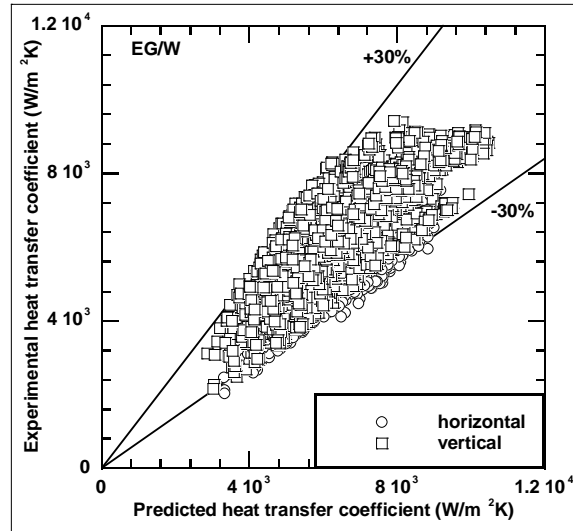


Figure 41. Heat transfer coefficient comparison

The prediction accuracy can be further improved if the experimental heat transfer coefficients of EG/W mixture boiling in the horizontal flow and the vertical of this study are separately correlated. The final equation developed based on the experimental heat transfer coefficients of EG/W mixture boiling in the horizontal flow of this study is

$$h = 1520(\text{Bo}W\dot{\epsilon}^{0.5})^{0.45} (k_l/d_i) \quad (121)$$

As it can be seen from Figure 42, where the experimental boiling heat transfer coefficients are compared with the predictions of the above equation, this equation predicts the experimental boiling heat transfer coefficients of this study reasonably well with a mean deviation of 11% and the most of the experimental boiling heat transfer coefficients are within $\pm 30\%$ of the predictions.

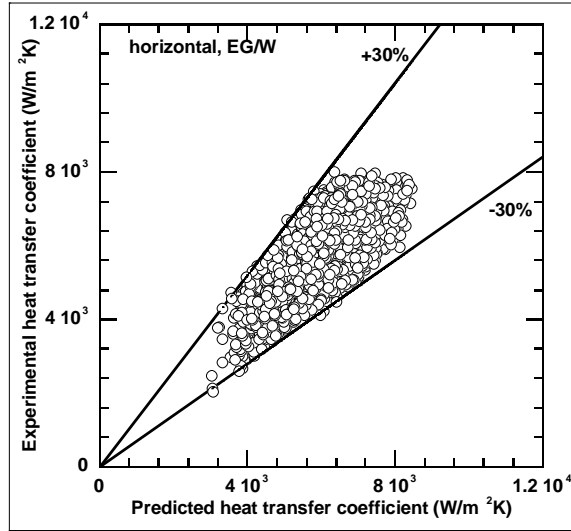


Figure 42. Heat transfer coefficient comparison

The final equation developed based on the experimental heat transfer coefficients of EG/W mixture boiling in the vertical flow of this study is

$$h = 235Q(BoWe_{\dot{q}}^{0.5})^{0.49} (k_i/d_i) \quad (122)$$

As it can be seen from Figure 43, where the experimental boiling heat transfer coefficients are compared with the predictions of the above equation, this equation predicts the experimental boiling heat transfer coefficients of this study reasonably well with a mean deviation of 12% and the most of the experimental boiling heat transfer coefficients are within $\pm 30\%$ of the predictions.

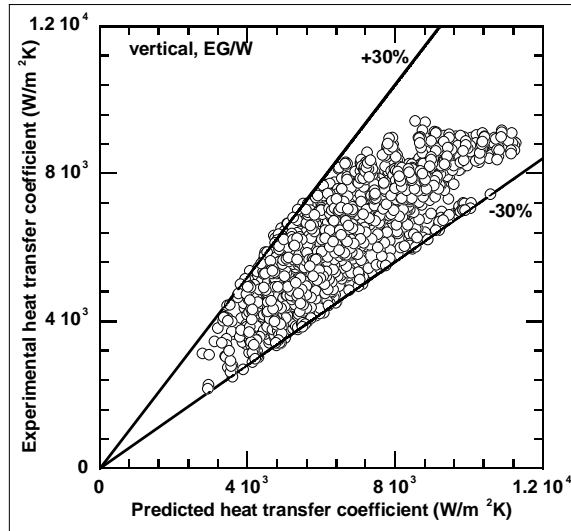


Figure 43. Heat transfer coefficient comparison

All of the correlations presented in this section for EG/W mixture boiling omitted the concentration term $e^{1.25V_{BG}}$. It was found that the small concentration range of the EG/W data did not significantly influence the heat transfer rates. However, as presented previously, when EG/W data are combined with pure water data in the same correlation the concentration parameter is significant because the concentration range of the combined data is large.

7. Boiling Experimental Results – Critical Heat Flux and Flow Stability

7.1. Predictive Models for Critical Heat Flux in the Literature

Over the years, hundreds of equations have been developed for the prediction of CHF in vertical flow boiling. However, no pure theoretically-based predictive procedure is available [78] and most of the ad hoc equations are for the conditions of high pressure and high mass flux [79]. As an attempt of developing a predictive method for wide ranges of various parameters, Groeneveld, et al. [80], based on a data bank of more than 15000 tube CHF data points, proposed a CHF lookup table for a vertical upward water flow in an 8-mm-diameter tube covering the parameter ranges of pressure 100–20000 kPa, mass flux 0–7500 kg/m²s, and vapor mass quality -50%–100%. Further extension of the lookup table can be achieved with multiplying the table CHF value by appropriate correction factors including subchannel or tube cross section factor K_1 , bundle factor K_2 , grid spacer factor K_3 , heated length factor K_4 , axial flux distribution factor K_5 , and flow factor K_6 [80-81]. With proper modifications, the lookup table can also be used for the prediction of CHFs of non-aqueous fluids [80, 82].

In contrast to vertical flow boiling, CHF prediction models for horizontal flow boiling are scarce and inaccurate, especially for horizontal flow boiling at low mass fluxes as in this study [78, 83]. One way to avoid this difficulty is to obtain the CHF prediction of horizontal flow boiling $(\dot{q}_{CHF}'')_{hor}$ based on correction of the CHF prediction for vertical flow boiling $(\dot{q}_{CHF}'')_{ver}$ [80]

$$(\dot{q}_{CHF}'')_{hor} = K_{hor} (\dot{q}_{CHF}'')_{ver} \quad (123)$$

where, for a mass flux-related correction, the horizontal flow factor K_{hor} can be expressed as a linear function of the mass flux [80]

$$K_{hor} = \begin{cases} 0.0 & G \leq G_{min} \\ \frac{G - G_{min}}{G_{max} - G_{min}} & G_{min} < G < G_{max} \\ 1.0 & G_{max} \leq G \end{cases} \quad (124)$$

or as a nonlinear function of the mass flux [83]

$$K_{hor} = \begin{cases} 0.0 & G \leq G_{min} \\ \left(\frac{G - G_{min}}{G_{max} - G_{min}} \right)^{0.62} & G_{min} < G < G_{max} \\ 1.0 & G_{max} \leq G \end{cases} \quad (125)$$

with the minimum mass flux G_{min} and the maximum mass flux G_{max} being calculated, respectively, as [83-85]

$$\begin{cases} G_{\min} = \frac{[gd_i \rho_v (\rho_l - \rho_v)]^{0.5}}{x} \left(\frac{1}{0.65 + 1.11 X_{tt}^{0.6}} \right) \\ G_{\max} = \left[\frac{gd_i^{1.2} \rho_l (\rho_l - \rho_v)}{0.092(1-x)^{1.8} \mu_l^{0.2}} \left(-0.3470 + 0.2920 \ln X_{tt} - 0.0556 \ln^2 X_{tt} \right) \right]^{0.556} \end{cases} \quad (126)$$

Obviously, the horizontal flow factor from the nonlinear-mass-flux correction is larger than that from the linear-mass-flux correction.

Another equation for the horizontal flow factor suggested by Wong, et al. [83] is based on a force-balance analysis

$$K_{hor} = 1 - e^{-\left\{ \frac{1}{3} \left[0.046 \left(\frac{Gd_i}{\mu_l} \right)^{-0.2} \left(\frac{1-x}{1-\alpha} \right)^2 \frac{G^2}{gd_i \rho_l (\rho_l - \rho_v) \alpha^{0.5}} \right] \right\}^{0.5}} \quad (127)$$

where the cross-sectional void fraction α is estimated from the following slip ratio S [40]

$$\begin{aligned} S &= 1 + 1.578 (Gd_i / \mu_l)^{-0.19} (\rho_l / \rho_v)^{0.22} \\ &\times \left\{ \frac{\frac{x}{1-x} \frac{\rho_l}{\rho_v}}{1 + 0.0273 \frac{x}{1-x} \text{We}_l \left(\frac{Gd_i}{\mu_l} \right)^{-0.51} \left(\frac{\rho_l}{\rho_v} \right)^{0.92}} - 0.0273 \frac{x}{1-x} \text{We}_l \left(\frac{Gd_i}{\mu_l} \right)^{-0.51} \left(\frac{\rho_l}{\rho_v} \right)^{0.92} \right\}^{0.5} \end{aligned} \quad (128)$$

7.2. Critical Heat Flux of Water Boiling

7.2.1. Effect of Mass Flux on Critical Heat Flux

All water boiling tests inside the horizontal test section and the vertical test section were limited by the CHF, which was calculated from the power to the experimental test section just before it was terminated automatically because the wall temperature rose quickly beyond the preset upper-temperature limit. These experimental water CHF data for test conditions of various system pressures, test section inlet temperatures, and mass fluxes are plotted in Figure 44 as a function of the mass flux. It can be seen from Figure 44 that (a) the CHF is almost independent of the system pressure and the test section inlet temperature for the test parameter ranges of this study judged by the fact that the CHF data group closely for similar mass flux flows, (b) the CHF for vertical flow boiling is slightly higher than that for horizontal flow boiling under similar mass fluxes, and (c) the CHF depends strongly on the mass flux and increases almost linearly with the mass flux.

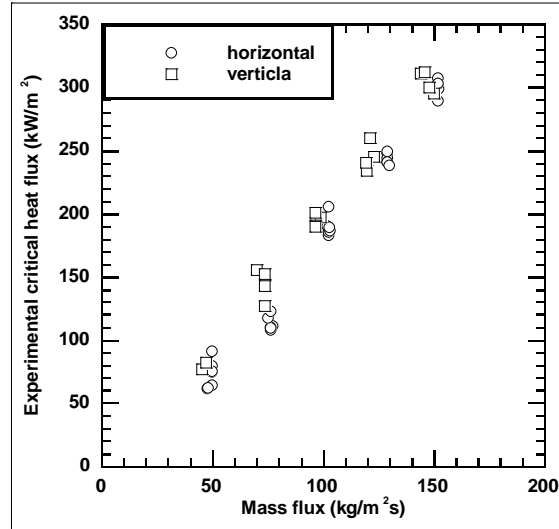


Figure 44. Mass flux effect on critical heat flux

7.2.2. Critical Heat Flux Comparison

The experimental CHF data for water boiling inside the horizontal test section and the vertical test section are compared in Figure 45 to the predictions from the procedures discussed above. It can be seen from Figure 45 that (a) the linear-mass-flux-correction procedure predicts the CHF data of horizontal flow boiling reasonably well except under predicting the data for the highest mass flux of $G \sim 150 \text{ kg/m}^2\text{s}$ (Figure 45 a); (b) the nonlinear-mass-flux-correction procedure largely over predicts most of the CHF data of horizontal flow boiling but under predicts the data for the highest mass flux of $G \sim 150 \text{ kg/m}^2\text{s}$ (Figure 45 b), which implies over correction of the nonlinear-mass-flux procedure; (c) the force-balance procedure slightly over predicts most of the CHF data of horizontal flow boiling but under predicts the data for the highest mass flux of $G \sim 150 \text{ kg/m}^2\text{s}$ (Figure 45 c); and (d) the predictions for the CHF data of vertical flow boiling are quite poor (Figure 45 d). These results contradict the fact that the predictions for horizontal flow boiling are based on corrections to the predictions for vertical flow boiling. This seeming contradiction can be well explained by the following facts obtained by closely examining the CHF lookup table and the experimental CHF data: (a) the experimental data show an increase trend of the CHF with regarding to the vapor mass quality, which is opposite to the trend given in the CHF lookup table; (b) the CHF vapor mass qualities of >0.5 in this study are relatively high when compared with large-diameter-tube data [79] and, in addition, unlike other experimental CHFs for horizontal flow boiling, almost all the experimental CHFs for horizontal flow boiling with the mass flux of $G \sim 150 \text{ kg/m}^2\text{s}$ and for vertical flow boiling occur at the vapor mass quality near 1.0 where the CHF data from the lookup table change significantly for the tested parameter ranges of this study; and (c) the CHF lookup table gives no data for the vapor mass quality of $x > 0.9$ and, in the result, the extrapolation, which is less accurate than the interpolation, had to be used to calculate the CHF predictions for the condition of the vapor mass quality of $x > 0.9$.

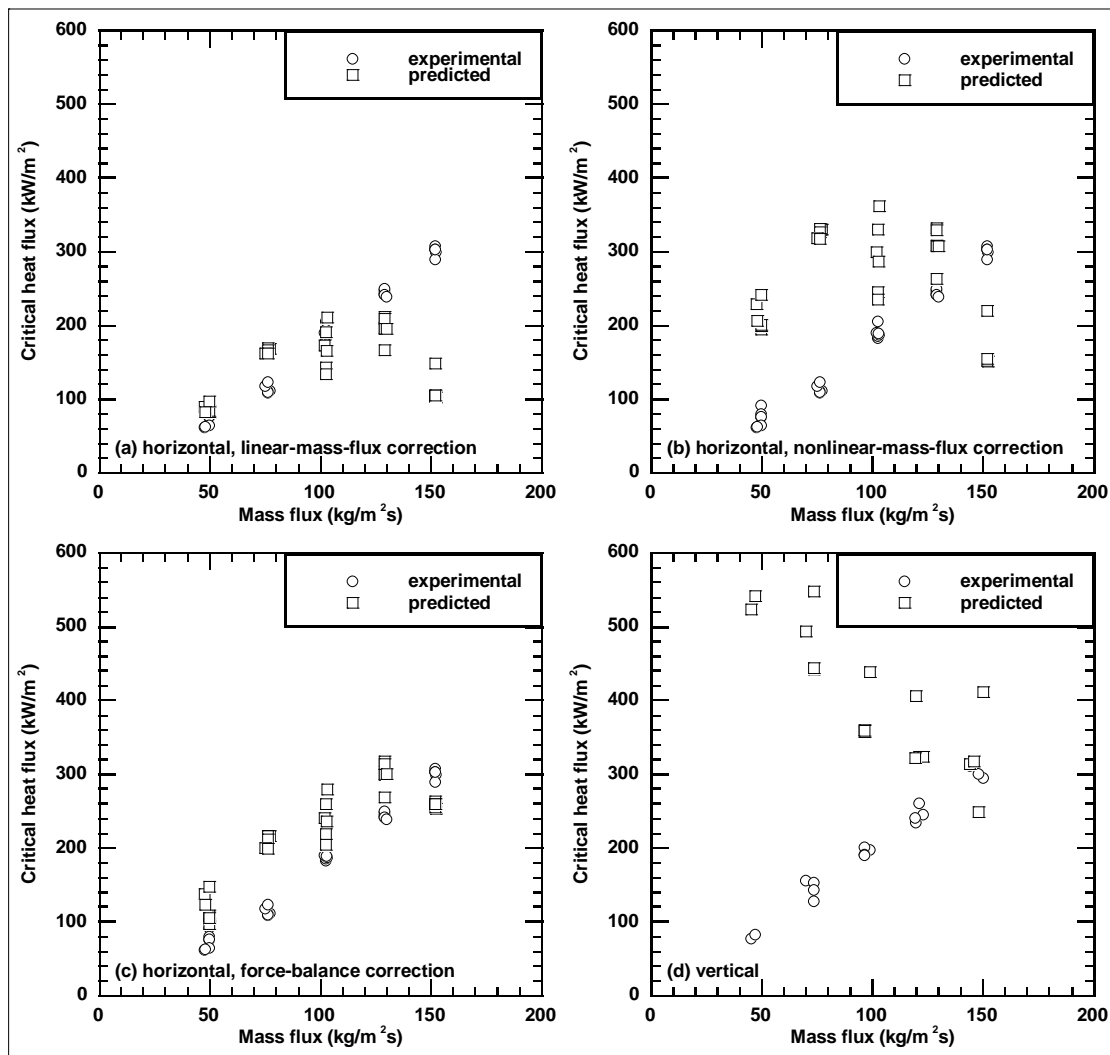


Figure 45. Critical heat flux comparison

No further attempt is made to better correlate the experimental CHF data because (a) while the experimental tests cover various parameter ranges, there are not enough data to develop a general predictive equation; (b) with the CHF for vertical flow boiling being higher than that for horizontal flow boiling, the limiting CHF occurs under horizontal flow boiling, which, when happens in practical applications, is unlikely to be at a quality near 1.0 and therefore can be predicted reasonably with the linear-mass-flux-correction procedure or with the force-balance-correction procedure; and (c) in engine cooling systems, a 50/50 EG/W mixture is the cooling medium, which, unlike water, is limited by the flow instability rather than the CHF.

7.3. Flow Stability of Ethylene Glycol/Water Mixture Boiling

As pointed out previously, rather than being CHF limited, EG/W mixture flow boiling is mainly limited by flow instability that can occur at a vapor mass quality much lower than that found near the CHF. Therefore, it is essential for practical applications to limit flow instability of EG/W mixture flow boiling within a certain range. Figure 46 shows a set of experiments

conducted over a 4.5-hour period for 50/50 EG/W mixture flow boiling inside the horizontal test section at a low vapor mass quality associated with a fixed mass flux and a fixed heat flux. It can be seen from Figure 46 that, after initial oscillation, the mass flux and the vapor mass quality were towards constant values. This result indicates that stable long-term flow boiling is possible for EG/W mixtures as long as the vapor mass quality is less than a certain critical value related to the mass flux. In general, it was found that, within the parameter ranges of this study, the system was always stable for exit qualities less than 20%.

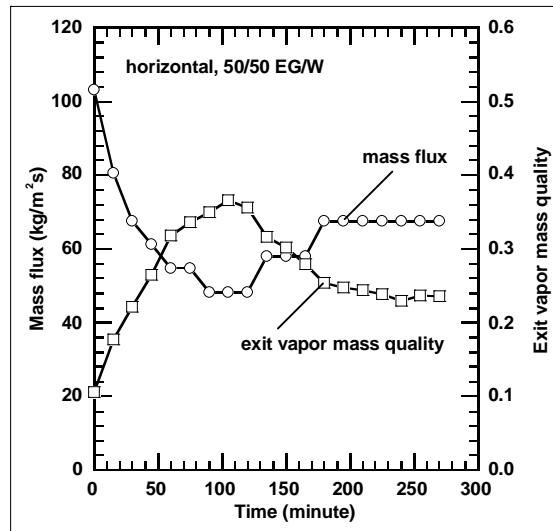


Figure 46. Flow stability

8. Summary

A series of experiments was carried out to investigate the characteristics of the two-phase pressure drop, forced convective boiling heat transfer, and boiling limitation under conditions of small channels and low mass fluxes for distilled water and EG/W mixtures with volume concentration ratios of 40/60, 50/50, and 60/40 in both the horizontal flow and the vertical flow. The following conclusions can be derived from the experimental data and theoretical analyses.

(i) A new boiling data reduction procedure has been developed that allows to analytically calculate the fluid boiling temperatures along the experimental test section and subsequently the local boiling heat transfer coefficients by applying the ideal mixture assumption and the equilibrium assumption along with Raoult's law. Due to its analytical nature, this procedure can easily be adapted for designing practical cooling systems with flow boiling.

(ii) The experimental data show that (a) the system pressure is of very slight effect on the exit boiling curves for the two test section outlet pressure of ~150 kPa and ~200 kPa and therefore, for the practical application purpose, the results from the experiments under these two test section outlet pressures in this study can be considered essentially equivalent; (b) under the current test conditions, the exit boiling curves are insensitive to the test section inlet temperature although changing the inlet temperature would cause a change in the boiling length as calculated from a heat balance; (c) the EG/W mixture of the higher ethylene glycol volume concentration generally boils at a higher wall superheat for the same heat flux or at a lower heat flux for the same wall superheat; and (d) to reach the same wall superheat, the heat fluxes for vertical flow boiling are higher than those for horizontal flow boiling, which is expected because the vapor distribution for vertical flow boiling is more uniform than that for horizontal flow boiling due to the influence of gravity in horizontal flow boiling.

(iii) The mass flux effect on the exit boiling curve is more predominant and more complicated and can be characterized according to boiling regions. In the convection-dominant-boiling region where the wall superheat is usually less than the lower wall-superheat limit of ~2 °C, the heat fluxes are relatively independent of the wall superheat and the flow acts more like a single-phase rather than two-phase. In the nucleation-dominant-boiling region, the heat flux is dependent on the wall superheat but almost independent of the mass flux. In the transition-boiling region where the wall superheat is usually larger than the upper wall-superheat limit that depends on the mass flux, the wall temperatures show oscillations, the heat fluxes separate as a function of the mass flux, and the flow boiling is susceptible to flow instabilities and, at high enough wall superheats, to the CHF condition that also depends on the mass flux.

(iv) While there exist three boiling regions, the large nucleation-dominant-boiling region, as the focus of this study, is the generally-desired operating region for flow boiling in small channels due to its relatively high heat transfer rates and flow stability. In the nucleation-dominant-boiling region, the heat fluxes follow a strong power-law trend of the wall superheat nearly independent of the mass flux, which, coupled with the negligible inlet temperature effect, implies that the nucleate-boiling heat transfer coefficients up to the transition-boiling region are a function of the heat flux only but not a function of the mass flux or the inlet subcooling. This phenomenon indicates the domination of the nucleation heat transfer mechanism and the

minimization of the convective heat transfer mechanism over a large mass flux range and a large inlet-subcooling range.

(v) An equation based on the completely-separated effective density instead of the homogeneous effective density for more accurately calculating the two-phase gravitation pressure drop has been developed.

(vi) The experimental two-phase friction multiplier defined as the square root of the ratio of the experimental two-phase friction pressure drop (the total experimental pressure drop minus the predictions of the single-phase gravitation pressure drop, the single-phase acceleration pressure drop, the single-phase friction pressure drop, the two-phase gravitation pressure drop, and the two-phase acceleration pressure drop) over the predicted liquid friction pressure drop has the following characteristics: (a) the experimental two-phase friction multiplier is insensitive to the slip ratio as far as the completely-separated liquid and vapor model is used with the slip ratio being greater than two; (b) the average experimental two-phase friction multiplier for vertical flow boiling is smaller than that for horizontal flow boiling; (c) the experimental two-phase friction multiplier increases with the increase of the exit vapor mass quality; and (d) when plotted against the Lockhart-Martinelli parameter or the exit vapor mass quality, the variation in the experimental two-phase friction multiplier for water flow boiling is smaller than for EG/W mixture flow boiling, probably due to the approximate assumptions of a constant slip ratio, a constant liquid density, and a constant vapor density introduced in the calculation of the two-phase gravitation pressure drop.

(vii) The Chisholm equation based on the laminar-liquid/turbulent-vapor flow of this study consistently over predicts the experimental two-phase friction multiplier data, probably due to the occurrence of the slug flow over a large quality range in small channels that reduces the pressure gradients from the annular flow condition found in large tubes upon which the Chisholm equation is substantially based. The proposed correlations of the experimental two-phase friction multiplier data, as power functions of the Lockhart-Martinelli parameter based on the turbulent-liquid/turbulent-vapor flow that best represents the experimental two-phase friction multiplier data, give reasonable predictions of the experimental data with mean deviation of 26% for horizontal flow boiling and 20% for vertical flow boiling.

(viii) For the vertical flow, most prediction equations from the literature predict the experimental heat transfer coefficients of water boiling of this study reasonably well, while for the horizontal flow, the Gungor-Winterton equation gives the best prediction for the experimental heat transfer of water boiling of this study. Generally, the predictions for vertical flow boiling of water are better than those for horizontal flow boiling of water, which may be explained by the fact that vertical flow boiling is more stable than horizontal flow boiling due to the symmetrical boiling condition without gravitational effects.

(ix) No prediction equations from the literature can predict the experimental heat transfer coefficients of EG/W mixture flow boiling of this study well, which may be due to the fact that the complicated boiling conditions of two- or multi-component fluids such as EG/W mixtures are not taken into account in developing these equations.

(x) Five prediction equations for the boiling heat transfer coefficient have been developed based on the experimental heat transfer coefficients of water and EG/W mixture flow boiling of this study including (a) a general equation for both water and EG/W mixture boiling in the horizontal flow and the vertical flow with a mean deviation of 25%, (b) an equation for water boiling in the horizontal flow and the vertical flow with a mean deviation of 16%, (c) an equation for EG/W mixture boiling in the horizontal flow and the vertical flow with a mean deviation of 14%, (d) an equation for EG/W mixture boiling in the horizontal flow with a mean deviation of 11%, and (e) an equation for EG/W mixture boiling in the vertical flow with a mean deviation of 12%.

(xi) The experimental data of water flow boiling show that (a) the CHF is almost independent of the system pressure and the test section inlet temperature for the test parameter ranges of this study; (b) the CHF for vertical flow boiling is slightly higher than that for horizontal flow boiling under similar mass fluxes; (c) the CHF increases with the vapor mass quality, which is opposite to the trend given in the CHF lookup table; (d) the CHF depends strongly on the mass flux and increases almost linearly with the mass flux; (e) all the CHFs occur at vapor mass qualities of >0.5 , which are relatively high when compared with large-diameter-tube data; and (f) almost all the experimental CHFs for horizontal flow boiling with the mass flux of $G \sim 150 \text{ kg/m}^2\text{s}$ and for vertical flow boiling occur at the vapor mass quality near 1.0.

(xii) While the comparison between the experimental CHFs for vertical water flow boiling (which occur at the vapor mass quality near 1.0) and the lookup table predictions is poor, the comparison between the experimental CHFs for horizontal water flow boiling and the lookup table predictions with the linear-mass-flux correction or with the force-balance correction is quite good except the CHFs for the highest mass flux, which occur at the vapor mass quality near 1.0. Therefore, for practical application purpose where the vapor mass quality is much less than 1.0, the lookup table values with appropriate correction procedures are expected to give reasonable predictions to CHFs of water flow boiling.

(xiii) Rather than the CHF that usually constitutes the limits for water flow boiling, EG/W mixture flow boiling is mainly limited by flow instability, which can occur at a vapor mass quality much lower than that found near the CHF. However, after initial oscillation, stable long-term flow boiling is possible for EG/W mixtures as long as the vapor mass quality is less than a certain critical value related to the mass flux.

References

- [1] I. C. Finlay, R. J. Boyle, J. P. Pirault, and T. Biddulph, Nucleate and Film Boiling of Engine Coolants Flowing in a Uniformly Heated Duct of Small Cross Section, SAE Technical Paper 870032, 1987.
- [2] I. C. Finlay, G. R. Gallacher, T. W. Biddulph, and R. A. Marshall, The Application of Precision Cooling to the Cylinder Head of a Small Automotive Petrol Engine, SAE Technical Paper 880263, 1988.
- [3] M. J. Clough, Precision Cooling of a Four Valve per Cylinder Engine, SAE Technical Paper 931123, 1993.
- [4] M. Pretscher and N. S. Ap, Nucleate Boiling Engine Cooling System – Vehicle Study, SAE Technical Paper 931132, 1993.
- [5] D. Gentile and S. Zidat, Influential Parameters in a Boiling Cooling System, Heat and Technology, vol. 11, pp. 28-51, 1993.
- [6] E. V. McAssey, Jr., C. Stinson, and M. Gollin, Evaluation of Engine Coolants under Flow Boiling Conditions, Proceedings of the ASME Heat Transfer Division, vol. 317-1, pp. 193-200, 1995.
- [7] N. A. F. Campbell, S. J. Charlton, and L. Wong, Designing towards Nucleate Boiling in Combustion Engines, IMechE Paper C496/092/95, 1995.
- [8] N. A. F. Campbell, D. G. Tilley, S. A. MacGregor, and L. Wong, Incorporating Nucleate Boiling in a Precision Cooling Strategy for Combustion Engines, SAE Technical Paper 971791, 1997.
- [9] G. Ambrogi, E. V. McAssey, Jr., G. Cozzone, and C. Hoover, The Effect of Off-Design Operation on the Thermal Performance of Propylene-Glycol and Ethylene-Glycol Engine Coolants, SAE Technical Paper 971827, 1997.
- [10] N. A. F. Campbell, J. G. Hawley, D. G. Tilley, L. Wong, and R. W. Horrocks, Nucleate Boiling Investigations Using Simulated Engine Cooling Passages, IMechE Paper C543/002/99, 1999.
- [11] N. S. Ap, A. Maire, P. Porot, P. Menegazzi, F. Souidi, C. Le. Devehat, D. Godeau, P. Olivier, J. B. Vinot, and G. Vincens, New Components Development for New Engine Cooling System, IMechE Paper C543/047/99, 1999.
- [12] M. W. Wambsganss, Thermal Management in Heavy Vehicles: A Review Identifying Issues and Research Requirements, IMechE Paper C543/086/99, 1999.

[13] N. A. F. Campbell, J. G. Hawley, M. J. Leathard, R. W. Horrocks, and L. Wong, Nucleate Boiling Investigations and the Effects of Surface Roughness, SAE Technical Paper 1999-01-0577, 1999.

[14] K. Robinson, N. A. F. Campbell, J. G. Hawley, and D. G. Tilley, A Review of Precision Engine Cooling, SAE Technical Paper 1999-01-0578, 1999.

M. W. Wambsganss, Thermal Management Concepts for Higher-Efficiency Heavy Vehicles, SAE Technical Paper 1999-01-2240, 1999.

[15] Von V. Gnielinski, Neue Gleichungen für den Wärme- und den Stoffübergang in turbulent durchströmten Rohren und Kanälen, *Forschung im Ingenieurwesen*, vol. 41, pp.8-16, 1975.

[16] H. Blasius, Das Ähnlichkeitsgesetz bei Reibungsvorgängen in Flüssigkeiten, *Mitteilungen über Forschungsarbeiten auf dem Gebiete des Ingenieurwesens insbesondere aus den Laboratorien der technischen Hochschule*, herausgegeben vom Verein deutscher Ingenieure, Heft 131, pp. 1-40, 1913.

[17] J. C. Chu, S. L. Wang, S. L., Levy, and R. Paul, Vapor-Liquid Equilibrium Data, J. W. Edwards Publisher, Inc., Michigan, USA, 1956.

[18] K. Murata and K. Hashizume, An Investigation on Forced Convection Boiling of Nonazeotropic Refrigerant Mixtures, *Heat Transfer Japanese Research*, vol. 19, pp. 95-109, 1990.

[19] U. Wenzel, B. Hartmuth, and H. Muller-Steinhagen, Heat Transfer to Mixtures of Acetone, Isopropanol and Water under Subcooled Flow Boiling Conditions—I. Experimental Results, *International Journal of Heat and Mass Transfer*, vol. 37, pp. 175-183, 1994.

[20] G. Morrison and M. O. McLinden, Application of a Hard Sphere Equation of State to Refrigerants and Refrigerant Mixtures, National Bureau of Standards Technical Note 1226, Gaithersburg, Maryland, USA, 1986.

[21] H. Ross, R. Radermacher, M. di Marzo, and D. Didion, Horizontal Flow Boiling of Pure and Mixed Refrigerants, *International Journal of Heat and Mass Transfer*, vol. 30, pp. 979-992, 1987.

[22] R. J. Moffat, Describing the Uncertainties in Experimental Results, *Experimental Thermal and Fluid Science*, vol. 1, pp. 3-17, 1988.

[23] R. W. Gallant, Physical Properties of Hydrocarbons, Gulf Publishing Company, Houston, Texas, USA, 1968.

[24] ASHRAE Handbook: Fundamentals, American Society of Heating, Refrigerating and Air-Conditioning Engineers, Inc., Atlanta, GA, USA, 1993.

- [25] D. L. Bennett, A Study of Internal Forced Convective Boiling Heat Transfer for Binary Mixtures, Ph.D. Dissertation, Lehigh University, 1975.
- [26] P. E. Liley, T. Makita, and Y. Tanaka, Properties of Inorganic and Organic Fluids (CINDAS Data Series on Material Properties, Volume V-1, Edited by C. Y. Ho), Hemisphere Publishing Corporation (A Member of the Taylor & Francis Group), 1988.
- [27] W. Yu, D. M. France, M. W. Wambsganss, and J. R. Hull, Two-Phase Pressure Drop, Boiling Heat Transfer, and Critical Heat Flux to Water in a Small-Diameter Horizontal Tube, International Journal of Multiphase Flow, vol. 28, pp. 927-941, 2002.
- [28] W. Yu, D. M. France, V.-K. V. Ramamoorthy, and J. R. Hull, Small-Channel Flow Boiling of One-Component Fluids and an Ethylene Glycol/Water Mixture, Experimental Heat Transfer, vol. 18, pp. 243-257, 2005.
- [29] T. N. Tran, M. W. Wambsganss, and D. M. France, Small Circular- and Rectangular-Channel Boiling with Two Refrigerants, International Journal of Multiphase Flow, vol. 22, pp. 485-498, 1996.
- [30] M. W. Wambsganss, J. A. Jendrzeczyk, and D. M. France, Two-Phase Flow and Pressure Drop in Flow Passages of Compact Heat Exchangers, SAE Technical Paper 920550, 1992.
- [31] J. R. S. Thom, Prediction of Pressure Drop during Forced Circulation Boiling of Water, International Journal of Heat and Mass Transfer, vol. 7, pp. 709-724, 1964.
- [32] R. W. Lockhart and R. C. Martinelli, Proposed Correlation of Data for Isothermal Two-Phase Two-Component Flow in Pipes, Chemical Engineering Progress, vol. 45, pp. 39-48, 1949.
- [33] D. Chisholm, A Theoretical Basis for the Lockhart-Martinelli Correlation for Two-Phase Flow, International Journal of Heat and Mass Transfer, vol. 10, pp. 1767-1778, 1967.
- [34] D. Chisholm, Pressure Gradients due to Friction During the Flow of Evaporating Two-Phase Mixtures in Smooth Tubes and Channels, International Journal of Heat and Mass Transfer, vol. 16, pp. 347-358, 1973.
- [35] M. A. Woldesemayat and A. J. Ghajar, Comparison of Void Fraction Correlations for Different Flow Patterns in Horizontal and Upward Inclined Pipes, International Journal of Multiphase Flow, vol. 33, pp. 347-370, 2007.
- [36] S. M. Zivi, Estimation of Steady-State Steam Void-Fraction by Means of the Principle of Minimum Entropy Production, ASME Transaction, Journal of Heat Transfer, vol. 86, pp. 247-252, 1964.
- [37] S. L. Smith, Void Fraction in Two-Phase Flow: A Correlation Based upon an Equal Velocity Head Model, Proceedings of the Institution of Mechanical Engineers, vol. 184, part 1, 647-664, 1969.

- [38] G. B. Wallis, *One-Dimensional Two-Phase Flow*, McGraw-Hill Companies, New York, USA, 1969.
- [39] P. A. Domanski and D. A. Didion, *Computer Modeling of the Vapor Compression Cycle with Constant Flow Area Expansion Device*, NBS Building Science Series 155, National Institute of Standards and Technology, Gaithersburg, MD, USA, 1983.
- [40] A. Premoli, D. D. Francesco, and A. Prina, *A Dimensional Correlation for Evaluating Two-Phase Mixture Density*, *La Termotecnica*, vol. 25, pp. 17-26, 1971.
- [41] G. Rigot, *Fluid Capacity of an Evaporator in Direct Expansion*, *Chaud-Froid-Plomberie*, no. 328, pp. 133-144, 1973.
- [42] J. R. Thome and R. A. W. Shock, *Boiling of Multicomponent Liquid Mixtures*, in *Advances in Heat Transfer*, edited by J. P. Hartnett and T. F. Irvine Jr., vol. 16, pp. 59-156, Academic Press, New York, 1984.
- [43] R. L. Webb and N. S. Gupte, *A Critical Review of Correlations for Convective Vaporization in Tubes and Tube Banks*, *Heat Transfer Engineering*, vol. 13, pp. 58-81, 1992.
- [44] G. P. Celata, M. Cumo, and T. Setaro, *A Review of Pool and Forced Convective Boiling of Binary Mixtures*, *Experimental Thermal and Fluid Science*, vol. 9, pp. 367-381, 1994.
- [45] J. Darabi, M. Salehi, M. H. Saeedi, and M. M. Ohadi, *Review of Available Correlations for Prediction of Flow Boiling Heat Transfer in Smooth and Augmented Tubes*, *ASHRAE Transactions*, vol. 101, part 1, paper number CH-95-12-2, pp. 225-235, 1995.
- [46] S. P. Wang and J. C. Chato, *Review of Recent Research on Heat Transfer with Mixtures – Part 2: Boiling and Evaporation*, *ASHRAE Transactions*, vol. 101, part 1, paper number CH-95-23-3, pp. 1387-1401, 1995.
- [47] S. S. Bertsch, E. A. Groll, and S. V. Garimella, *Review and Comparative Analysis of Studies on Saturated Flow Boiling in Small Channels, Nanoscale and Microscale Thermophysical Engineering*, vol. 12, pp. 187-227, 2008.
- [48] J. C. Chen, *Correlation for Boiling Heat Transfer to Saturated Fluids in Convective Flow*, *Industrial & Engineering Chemistry Process Design and Development*, vol. 5, pp. 322-329, 1966.
- [49] F. W. Dittus and L. M. K. Boelter, *Heat Transfer in Automobile Radiators of the Tubular Type*, *University of California Publications in Engineering*, vol. 2, pp. 443-461, 1930.
- [50] H. K. Forster and N. Zuber, *Dynamics of Vapor Bubbles and Boiling Heat Transfer*, *AIChE Journal*, vol. 1, pp. 531-535, 1955.
- [51] S. Edelstein, A. J. Perez, and J. C. Chen, *Analytic Representation of Convective Boiling*

Functions, AIChE Journal, vol. 30, pp. 840-841, 1984.

[52] M. M. Shah, A New Correlation for Heat Transfer during Boiling Flow through Pipes, ASHRAE Transactions, vol. 82, pp. 66-86, 1976.

[53] M. M. Shah, Chart Correlation for Saturated Boiling Heat Transfer: Equations and Further Study, ASHRAE Transactions, vol. 88, pp. 185-196, 1982.

[54] D. L. Bennett and J. C. Chen, Forced Convective Boiling in Vertical Tubes for Saturated Pure Components and Binary Mixtures, AIChE Journal, vol. 26, pp. 454-461, 1980.

[55] L. E. Scriven, On the Dynamics of Phase Growth, Chemical Engineering Science, vol. 10, pp. 1-13, 1959.

[56] M. P. Mishra, H. K. Varma, and C. P. Sharma, Heat Transfer Coefficients in Forced Convection Evaporation of Refrigerants Mixtures, Letters in Heat and Mass Transfer, vol. 8, pp. 127-136, 1981.

[57] R. W. Bjorge, G. R. Hall, and W. M. Rohsenow, Correlation of Forced Convection Boiling Heat Transfer Data, International Journal of Heat and Mass Transfer, vol. 25, pp. 753-757, 1982.

[58] D. P. Traviss, W. M. Rohsenow, and A. B. Baron, Forced Convection Condensation inside Tube: A Heat Transfer Equation for Design, ASHRAE reprint number 2272 RP-63, 1972.

[59] B. B. Mikic and W. M. Rohsenow, A New Correlation of Pool Boiling Data Including the Effect of Heating Surface Characteristics, ASME Transactions, Journal of Heat Transfer, vol. 91, pp. 245-250, 1969.

[60] A. E. Bergles and W. M. Rohsenow, The Determination of Forced Convection Surface Boiling Heat Transfer, ASME Transactions, Journal of Heat Transfer, vol. 86, pp. 365-372, 1964.

[61] G. M. Lazarek and S. H. Black, Evaporative Heat Transfer, Pressure Drop and Critical Heat Flux in a Small Vertical Tube with R-113, International Journal of Heat and Mass Transfer, vol. 25, pp. 945-960, 1982.

[62] K. E. Gungor and R. H. S. Winterton, A General Correlation for Flow Boiling in Tubes and Annuli, International Journal of Heat and Mass Transfer, vol. 29, pp. 351-358, 1986.

[63] M. G. Cooper, Saturation Nucleate Pool Boiling: A Simple Correlation, 1st U.K. National Conference on Heat Transfer, IChemE Symposium Series 86, vol. 2, pp. 785-793, 1984.

[64] V. V. Klimenko, A Generalized Correlation for Two-Phase Forced Flow Heat Transfer, International Journal of Heat and Mass Transfer, vol. 31, pp. 541-552, 1988.

[65] V. V. Klimenko, A Generalized Correlation for Two-Phase Forced Flow Heat Transfer –

Second Assessment, International Journal of Heat and Mass Transfer, vol. 33, pp. 2073-2088, 1990.

[66] D. S. Jung, M. McLinden, R. Radermacher, and D. Didion, A Study of Flow Boiling Heat Transfer with Refrigerant Mixtures, International Journal of Heat and Mass Transfer, vol. 32, pp. 1751-1764, 1989.

[67] K. Stephan and M. Abdelsalam, Heat Transfer Correlations for Natural Convection Boiling, International Journal of Heat and Mass Transfer, vol. 23, 73-87, 1980.

[68] H. C. Ünal, Prediction of Nucleate Boiling Heat Transfer Coefficients for Binary Mixtures, International Journal of Heat and Mass Transfer, vol. 29, pp. 637-640, 1986.

[69] S. G. Kandlikar, A General Correlation for Saturated Two-Phase Flow Boiling Heat Transfer inside Horizontal and Vertical Tubes, ASME Transaction, Journal of Heat Transfer, vol. 112, pp. 219-228, 1990.

[70] K. Murata and K. Hashizume, An Investigation on Forced Convection Boiling of Nonazeotropic Refrigerant Mixtures, Heat Transfer Japanese Research, vol. 19, pp. 95-109, 1990.

[71] K. Stephan und M. Körner, Berechnung des Wärmeübergangs verdampfender binärer Flüssigkeitsgemische, Chemie Ingenieur Technik, vol. 41, pp. 409-417, 1969.

[72] D. L. Bennett, M. W. Davis, and B. C. Hertzler, The Suppression of Saturated Nucleate Boiling by Forced Convective Flow, AIChE Symposium Series. 76, pp. 91-103, 1980.

[73] H. Takamatsu, A. Miyara, S. Koyama, T. Fujii, and K. Yonemoto, Forced Convective Boiling of Nonazeotropic Refrigerant Mixtures of R22 and R114 inside a Horizontal Tube, Heat Transfer Japanese Research, vol. 19, no. 3, pp. 68-82, 1990.

[74] Z. Liu and R. H. S. Winterton, A General Correlation for Saturated and Subcooled Flow Boiling in Tubes and Annuli, Based on a Nucleate Pooling Boiling Equation, International Journal of Heat and Mass Transfer, vol. 34, pp. 2759-2766, 1991.

[75] D. Steiner and J. Taborek, Flow Boiling Heat Transfer in Vertical Tubes Correlated by a Asymptotic Model, Heat Transfer Engineering, vol. 13, pp. 43-69, 1992.

[76] D. Gorenflo, Behältersieden, sect. Ha, in VDI Wärmeatlas, VDI Verlag, Düsseldorf, 1988.

[77] D. Steiner, Wärmeübertragung beim Sieden gesättigter Flüssigkeiten, sect. Hbb, in VDI Wärmeatlas, VDI Verlag, Düsseldorf, 1988.

[78] J. Weisman, The Current Status of Theoretically Based Approaches to the Prediction of the Critical Heat Flux in Flow Boiling. Nuclear Technology, vol. 9, pp. 1-21, 1992.

- [79] L. S. Tong, Boiling Crisis and Critical Heat Flux, U.S. Atomic Energy Commission Office of Information Services, USA, 1972.
- [80] D. C. Groeneveld, S.C., Cheng, and T. Doan, 1986 AECL-UO Critical Heat Flux Lookup Table, Heat Transfer Engineering, vol. 7, pp. 46-62, 1986.
- [81] D. C. Groeneveld and C. W. Snoek, A Comprehensive Examination of Heat Transfer Correlations Suitable for Reactor Safety Analysis, Multiphase Science and Technology, vol. 2, edited by G. F. Hewitt, J. M. Delhay, and N. Zuber, pp. 181-274, Hemisphere Publishing Corporation, Washington, D.C., USA, 1986.
- [82] B. P. Kiameh, Prediction of CHF in Non-Aqueous Fluids, Master of Applied Science Thesis, University of Ottawa, Canada, 1986.
- [83] Y. L. Wong, D. C. Groeneveld, and S. C. Cheng, CHF Prediction for Horizontal Tubes, International Journal of Multiphase Flow, vol. 16, pp. 123-138, 1990.
- [84] Y. Taitel and A. E. Dukler, A Model for Predicting Flow Regime Transitions in Horizontal and Near Horizontal Gas-Liquid Flow, AIChE Journal, vol. 22, pp. 47-55, 1976.
- [85] Y. Taitel and A. E. Dukler, Flow Pattern Transition in Gas-Liquid Systems: Measurement and Modelling, Multiphase Science and Technology, vol. 2, edited by G. F. Hewitt, J. M. Delhay, and N. Zuber, pp. 1-94, Hemisphere Publishing Corporation, Washington, D.C., USA, 1986.
- [86] S. C. Cheng, Y. L. Wong, and D. C. Groeneveld, CHF Prediction for Horizontal Flow, Proceedings of International Symposium on Phase Change Heat Transfer, Chongqing, China, pp. 211-215, 1988.



Energy Systems Division

Argonne National Laboratory
9700 South Cass Avenue, Bldg. 362
Argonne, IL 60439-4815

www.anl.gov



U.S. DEPARTMENT OF
ENERGY

Argonne National Laboratory is a U.S. Department of Energy
laboratory managed by UChicago Argonne, LLC